Numerical harbour simulations with the model TRIWAQ - NH

With an emphasize on the present reflective properties

J.P.P. Schmedding

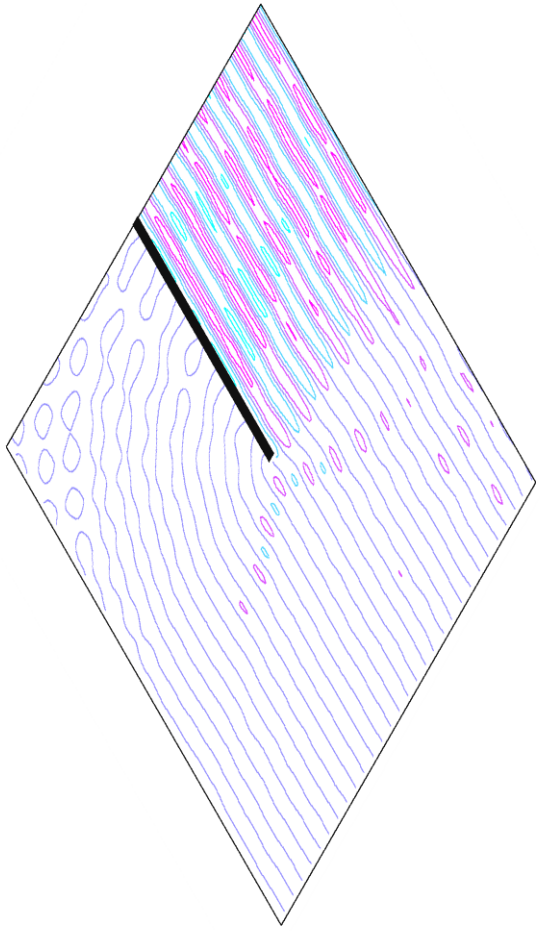

Summary

This document is the final product of the master thesis course at the section of Environmental Fluid Mechanics part of the Faculty of Civil Engineering at Delft University

The focus is on the numerical flow model TRIWAQ. It is developed as a hydrostatic free-surface flow model, which is currently being used by the KNMI and Rijkswaterstaat for predictions of water levels in the North Sea and Dutch estuaries. TRIWAQ has successfully been extended to the realm of non-hydrostatic modeling, TRIWAQ-NH, this allows the use of full Navier-Stokes equations. It has been validated to perform well for multiple processes such as dispersion and propagation.

The goal is to assess the ability of TRIWAQ-NH for harbour problems. This has not been attempted before and poses a new challenge. Before an attempt is made to simulate a harbour, methods of imposing reflection are tested. For that matter, the thesis is split in two parts.

The first part will investigate the ability of TRIWAQ-NH with respect to reflections. It will confine itself to four currently implemented open boundary conditions. It aims to provide an answer what condition is most suitable for future development into a partial reflecting boundary condition for harbour simulations. This is done by means of a literature survey, which inspects the background theory it stems from, its dependence on wave frequencies and limitations due to the angle of incidence. By means of 1 dimensional simulations the ability of each open boundary condition is tested when the non-hydrostatic method is used and will be referenced with a similar hydrostatic simulation. A monochromatic wave is used.

The first condition is called the α-value. It is based on hydrostatic theory. It is frequency dependant and only works well for nearly perpendicular incoming waves. The 1 dimensional tests show it is a difficult to calibrate this condition for full absorption when the hydrostatic method is used. Use of the α-value for the non-hydrostatic method leads to increased mean water levels and is considered unstable.
The second condition is the Riemann condition. It uses wave characteristics to create an absorbing boundary. Such a characteristic makes it depend on the angle of incidence and frequency.
The 1 dimensional tests show this condition does not achieve full absorption, but does perform rather well for both the hydrostatic and non-hydrostatic method.
The third condition is a sponge layer condition. It has been implemented in order to validate TRIWAQ-NH in previous work. In order to use a sponge, grid space needs to be extended with a certain amount of cells in which the sponge is active. At the end an open boundary is defined. Currently it is only possible to implement the sponge in the positive grid space and will only dampen velocities in that specific direction. Thus, a wave has to enter nearly perpendicular. However it is not dependant on frequencies. The 1 dimensional tests show that neither this condition is able to fully absorb. It matches the results from the Riemann condition.
The fourth condition is a gently sloping profile. The design criterion for the slope angle is based on non-breaking short waves. This method adds extra cells to the grid space and will be of the same length as the sponge layer. The slope angle is defined by one wave and is thus frequency dependant. Due to the depth changes a wave will refract; meaning it is not able to accurately simulate oblique incoming waves on quay walls. From its 1 dimensional hydrostatic simulation, it shows it is reacting similar to the sponge and Riemann conditions. The non-hydrostatic simulation shows a strong rise in mean water level. This is instability occurring due to a course grid resolution.

The second part of the thesis focuses on validating 2 dimensional non-hydrostatic simulations with TRIWAQ-NH. This is done by modelling a simplified rectangular harbour basin of constant depth. A monochromatic wave is selected. From the 1 dimensional test cases, two conditions are selected and

simulated, these are the Riemann and sponge layer condition. The last simulation has full reflective boundaries. Each is again referenced with a hydrostatic simulation.
Each simulation is considered stable once the amount of energy in the basin stays the same over time. It shows that the hydrostatic method will reach such a stable solution at an earlier stage then the non-hydrostatic method. This is directly linked to the wave propagation.

For the two absorbing conditions each simulation will make use of the open boundaries at all sides. The left and right sided boundaries will be implemented as Riemann condition in both cases, since it is not possible to implement a sponge layer in the negative direction of the grid space. This restricts implementation of the sponge to the upper or far side of the basin.
The absorbing conditions correspond to each other when the wave pattern is inspected. In general the hydrostatic model yields more erratic contour plots then the non-hydrostatic model. The use of a Riemann condition on the sides shows wiggles that are confined to the first few meters away from the boundary for the non-hydrostatic models. It is more sensitive to the angle of incidence.
Energy levels for the sponge layer are lower than the Riemann condition due to the extra term added in the impulse equation. Both yield stable solutions for hydrostatic and non-hydrostatic method.

The simulations with the closed border or fully reflective boundary have only one mechanism that allows for dissipation of energy, since friction is not present in any of the models. This is wave radiation into the outer basin.
Again differences in wave pattern are visible. Where the hydrostatic method shows a more erratic natured response and has less tops and troughs compared to the non-hydrostatic method.
The use of the non-hydrostatic method approximates the desired wave pattern much better the hydrostatic method. The hydrostatic method reaches a stable solution. From the energy levels it is seen that the non-hydrostatic method does not reach a stable level of energy. Reason is that the imposed wave forcing has a frequency that closely resembles one of the basin resonating frequencies leading to elevated amplitudes. However the algorithm of the TRIWAQ-NH is robust and able to cope with it for the duration of the simulation time.

The current use of the model TRIWAQ-NH holds practical restrictions to the implementation of open boundary conditions. When such a definition spawns a length of more than grid cell, it needs to comply with the edges of the grid. For instance, a boundary under the angle of 77 degrees is only possible by creation of a multitude of smaller open boundaries, leading to human error.

The thesis results in two recommendations. The first part covered reflections, from that segment of the thesis, it is recommended to further explore the option of a stronger and smaller grid sized sponge layer with either an open or closed boundary condition for future development as method for partial reflections.
The second recommendation is of a more practical nature and does not emerge in the work. However, the current tools available for non-hydrostatic modelling are insufficient. The smaller wave lengths require smaller time frames then the current tools provide, which is in the order of hours, days and months.

Table of Contents

Table of figures

Chapter 1: Harbours, wave processes and simulator selection

Chapter 2: Non-hydrostatic modelling in TRIWAQ

Chapter 3: Boundary conditions

Chapter 4: 1 Dimensional model

Chapter 5: 2 dimensional harbour simulations

Appendix B: The semi – infinite breakwater

Appendix C: Harbour simulation extra's

Appendix D: Terneuzen Harbour

Introduction

Background

In ancient times the Phoenicians were one of the first people to extensively trade by sea. In order to protect their vessels against waves, a secluded location was often used when they moored. Over time such a natural safe haven evolved into a harbour. These days most natural harbours have been developed. While overseas trade still requires more capacity of goods transferral. In order to accommodate for this increasing demand of capacity; harbour development in new areas is likely to be required. Since these locations will be less secluded from waves and currents, they will be more challenging engineering wise.

Let's fast forward to present days. Regularly a new harbour is built in a less protected area, where waves have a larger influence on harbour tranquillity. Safety of manoeuvring and moored vessels needs to be assessed. Economic value has increased and the hinterland needs to be protected against high water and wave loading. These reasons stress the need of predicting wave conditions inside a harbour.
The Netherlands has regulated protection of the hinterland by national act, it states that in order to assess safety of primary water defences need to be checked every five years. This leads to the need of predicting wave conditions with a certain probability of occurrence.
It becomes clear that wave prediction by modelling is an important part of assessing safety during the design cycle as well as periodic maintenance. Prediction can be done by means of physical scale experiments (in flumes) and/ or numerical modelling. Compared with scale experiments two major benefits of numerical modelling are the size of the workspace needed and the costs involved. They are pricier and take longer to setup, besides adaptation to different wave conditions is easier in a numerical model. This thesis will focus on numerical modelling of waves in harbours.

There are many wave models in existence; each has been created to simulate wave characteristics. A scale analysis can be used to determine the physical processes involved.
On a large scale; consider the ocean. In case of modelling, the wave of interest is most likely a tidal wave. Such a wave has a very long wave length. Objects that are in comparison (very) small will not be of influence to its propagation. For instance, the effect of a tidal wave on Vlissingen harbour will be an increase or decrease on the water level in its basin.
On a smaller scale; consider a propagating free-surface wind wave, travelling from deep to shallow water (typically a coastal zone). This wave might encounter a headland, where diffraction occurs. In shallow areas it can be affected by dissipation. A quay wall or dike might reflect the wave. When it is permeable, transmission of some wave energy occurs. And due to depth differences a wave can refract.
Any numerical model is an approximation of the real world. Different levels of approximation are involved, where relevant physics determine which equations need to be captured in such a model. This is the first step in validating a numerical model. Secondly, the accuracy of the algorithms used to solve the equations or approximate the solution determines the applicability. Third and last is related to coding errors in software. Thus, determining important physical processes alone do not have to lead to realistic solutions in a simulation.

This thesis will focus on the non-hydrostatic module of the TRIWAQ model; in short TRIWAQ-NH and will be applied to study feasibility of wave predictions in harbours. It is a free-surface flow model, which is part of SIMONA (SImulatie NAtte MOdellen) from the Dutch Ministry of Public Works (Rijkswaterstaat). TRIWAQ has typically been developed for use in advisory work (safety assessments e.g.) and the prediction wave heights (for the North Sea). The Royal Dutch Meteorology Institute (KNMI) and Rijkswaterstaat are two users.

Originally TRIWAQ (hydrostatic) has been developed for long waves. Generally these simulations are large scale models. Its equations, algorithms and software have all been validated for long waves that make use of hydrostatic flow.

The purpose of extending TRIWAQ to non-hydrostatic is to extend the simulation capabilities to shorter waves. It requires a change in the equations from simplified to full Navier-Stokes equations. In turn this requires a change in the algorithms and solver solutions. The performance of TRIWAQ-NH has been validated for multiple processes, such as dispersion and propagation (Zijlema, et al., 2005).

Purpose statement

The use of TRIWAQ-NH for harbour problems has not been attempted before. Its applicability to such problems needs to be assessed. This especially holds for wave reflection and the amount of wave penetration. Therefore, the aim of this thesis is twofold.

1. Implement and test TRIWAQ-NH for wave reflection against quay walls and dikes by means of a literature survey for the setup of the model and verification of results; and
2. Implement and test TRIWAQ-NH for wave penetration in a (theoretical) harbour with a simple geometry by verifying it with hydrostatic computations.

Structure of this report

Following this introduction, the next chapter will introduce multiple reasons for wave modelling of harbour areas. It will describe important physical processes and substantiate the motivation for the choice of TRIWAQ-NH. The second chapter will describe differences between the hydrostatic and non-hydrostatic method and will introduce the model TRIWAQ-NH.
In chapter 3 and 4, the first part of the purpose statement is investigated. Chapter 3 will introduce the background theory on which the presented boundary conditions are based and will end with some conclusions that may be drawn from it. Chapter 4 will show results from one dimensional tests with the described boundary conditions from chapter three. It will end with conclusions and the implications it will hold for the second part of the purpose statement.
Chapter 5 describes the setup and results of the two dimensional model and will end with additional remarks about the setup used. There by providing an answer for the second aim of this thesis.
It is followed by the conclusions found in chapter 6 and the recommendations in chapter 7.

The appendices consist of four parts. In the first appendix, the deck or input file is explained. In the second appendix simulations for a semi-infinite breakwater can be found. The third appendix holds the additional information of chapter five. The last appendix is a first attempt of modelling an existing harbour.

Acknowledgement

This thesis was written to finalize the master thesis for the study Civil Engineering at Delft University in collaboration with Alkyon Hydraulic Consultancy and Research. It was written under the supervision of Dr.ir. G.P. van Vledder and Dr.ir. M. Zijlema.
The graduation committee consists of Prof.dr.ir. G.S. Stelling, Prof.dr.ir. R.H.M.Huijsmans, Dr.ir.G.P. van Vledder, Dr.ir. M. Zijlema and Ir. M.A. de Schipper.

Chapter 1: Harbours, wave processes and simulator selection

This chapter substantiates more detailed reasons for wave modelling in harbour areas. It briefly discusses possible wave types that can be modelled for and argues which type is of interest in this thesis. With the wave type narrowed down, it allows substantiation of modelling reasons in a harbour area. In such an area many wave processes can be involved. Consequently the choice for the numerical model TRIWAQ-NH can be substantiated by referring to a few models in use, ending the chapter with its place compared to other models and reasons for investigation.

Origins of a wave for modelling purposes

A wave climate is a statistical description of observed or modelled waves over a long period of time (seasons, years, decades). For instance, it allows a prediction of a on average once in a year occurring extreme wave, that a harbour may be subjected to.
On the scale of hours a harbour is vulnerable to tidal and wind driven waves. Wind driven waves are chaotic in character and can best be described by a spectrum. It is aggregation of many possible occurring different wave components, each with its own wave period, amplitude and angle of propagation. So, it is a statistical description of wave energy in terms of frequency (in one place). Many parameters combined can describe the wave climate in a stochastic manner.
A short, locally generated wind wave has a fast varying surface elevation, whereas a tidal wave will have a slowly varying water level. The first is more important when workability and daily conditions need to be defined. The latter is used to determine extreme water levels for the once every 50 years; for example used to define dike heights.
If the harbour basin is large enough, the water level change in a basin may not be uniform. For small basins however, it is a varying a constant in the model slowly changing over time. Thus, the size of a harbour and the purpose of the model define the part of a wave spectrum that is used.

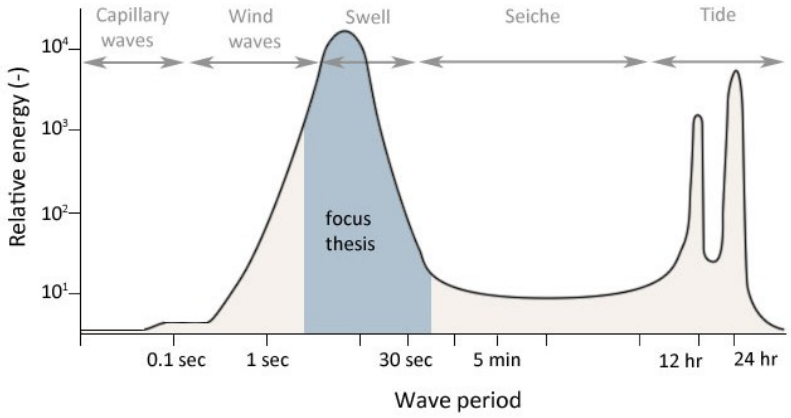

Figure 1.1 Wave classification

The focus is to test capabilities of non-hydrostatic simulations for harbours. Tidal waves are well described when a simulation uses a hydrostatic method. Roughly speaking; waves a person can see with his eyes are shorter waves. These are sensitive to vertical accelerations and need to be accounted for in a numerical model. In such a case a non-hydrostatic method is more desirable, since it is better able to account for these effects (chapter 2).
This study focuses on waves with periods in the range of 5 to 25 seconds, see figure 1.1. Waves in this range can be acquired by statistical analyses of the wave spectrum. Thus it excludes the small locally generated waves and the long tidal waves. For a wave climate this translates to an extreme condition; for example a characteristic wave that can occur once a year. From a spectrum it

“typically” translates to swell waves or n-year waves, where n is the amount of years, which require vertical accelerations to be taken into account when modelling.
Swell waves are generated by distant storms in which a chaotic wave field is created. As the waves fan out by dispersion, they order themselves by period. With longer waves outrunning the smaller ones, since length influences the propagation speed. As they become more regular, the direction becomes focused. These waves can travel very far and are also important for wave modelling in harbours because they affect the mooring safety of a large vessel.
A In (semi-) closed basins, harbours, standing oscillations of the water mass can occur. When the generating force is an external forcing, like atmospheric pressure, wind or seismic activity, these are called seiches. (Jong, 2004) If the generating force is a log wave entering through an open boundary, like a harbour mouth, it is often referred to as harbour oscillations (Rabinovich, 2009).

Throughout this thesis, a characteristic wave will be used for the simulations. It is implemented as a monochromatic wave with no variation in its direction. This is considered the dominant direction regarding geometry of the model domain. Such a monochromatic wave can either represent an extreme wave condition or a swell wave.

Modelling perspective

There are many locations that can benefit from wave modelling. One of them is ports. The purpose of a harbour is to accommodate trade of goods and people. In order to rapidly and safely transfer goods to or from shore, calm water is needed. Therefore vessel safety is important in harbour design. Vessel safety in a harbour encompasses manoeuvring, with assistance of pilots, and mooring.

Waves can enter a basin through the entrance too. Another origin of waves in a (large) basin is due to local wind. As long as these have a small period, 5 seconds or less, they are often neglected for modelling purposes, since they are not prone to induce strong reflections. However both sources are able to induce wave related processes. Disturbing the calm water and possibly endangering vessel safety.
There are several reasons for modelling waves in harbour areas. Knowledge about the local wave conditions can be used to beforehand determine downtime of manoeuvring. Currents become more influential when manoeuvring at low speeds (shown in figure 1.2 at position 1).
Another reason for modelling, is when a vessel is docked, mooring lines are used to keep it steady while waiting to load or unload (position 2 in figure 1.2). The stresses in these lines are determined by flow conditions (long waves) inside a harbour and ship size and volume.
A third reason is to assess the safety of the hinterland (position 3 in figure 1.2**Error! Reference ource not found.**). Damage due to a dike breach would spell disaster to its surroundings for humans living in the area and economic activities. This is a reason why the Dutch government has made it mandatory to check primary sea defences every five years to ensure the safety of the country and its people. Wave conditions outer seaside differ with conditions in a harbour basin, modelling will be necessary to determine extreme hydraulic conditions for the defence protection works in and around the harbour.
Standing waves can occur in a basin too. These can be referred to as harbour oscillations or seiches. To prevent this, the layout of a harbour is often a-geometrical. Regular shapes are best avoided. Standing waves can cause interruption of goods transfer or flood the lower areas of a harbour. Thus, prediction of the water level by means of modelling can be useful to determine wave conditions beforehand.

The above mentioned reasons for prediction can be summed up to one word; safety.

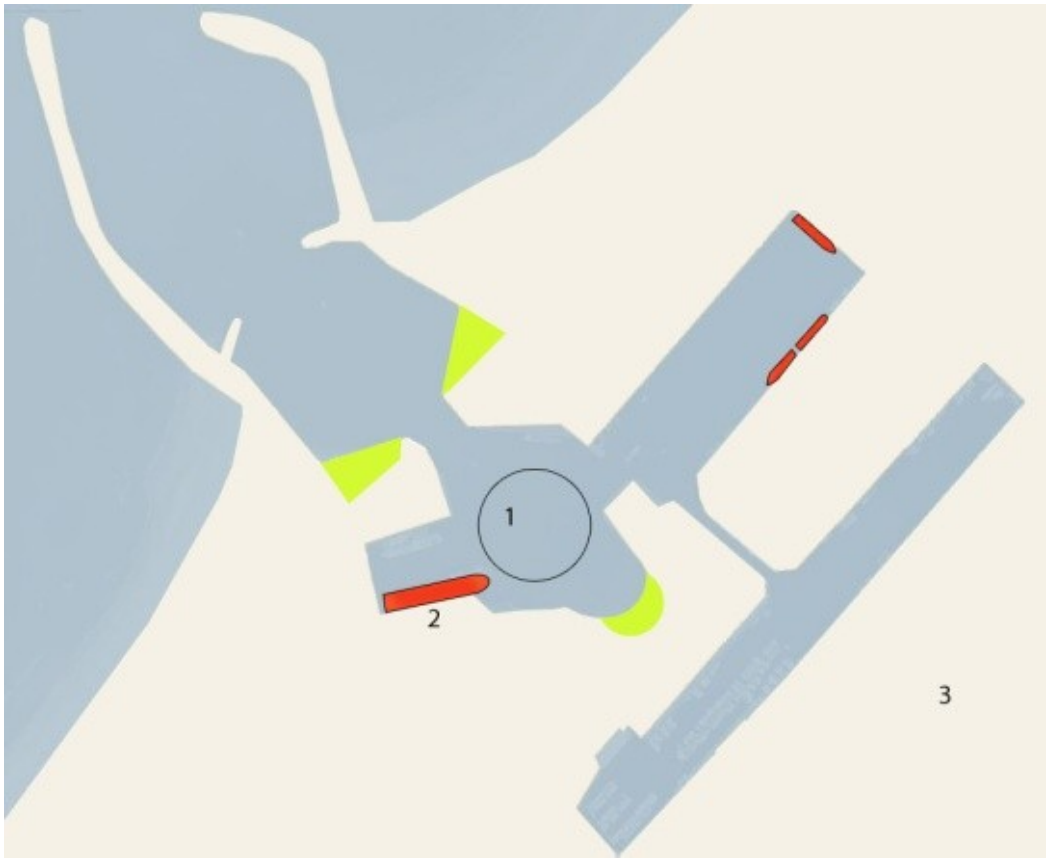

Figure 1.2 Layout of Scheveningen harbour. Numbers depict possible reasons for numerical modeling

There are two types of modelling possible; numerical modelling or physical scale modelling. Using a physical scale model requires more space and often more time to setup, thus making it more expensive. With the increasing power of computers, numerical models can now even be run on home computers. Another advantage of numerical modelling is its flexibility to quickly study different scenarios.

Concluding, numerical simulations are a powerful tool during the design stage of a harbour and in existing harbours. It is able to quickly reassess basin conditions when wave climate, basin geometry or vessel size changes.

Physical wave processes

A key aspect of harbour design deals with subduing wave penetration. While travelling they might encounter a (partially) submerged breakwater, leading to transmission (of energy). They will refract near the entrance channel and diffract around breakwaters or headlands. Waves are able to penetrate into the basin and reflect against the embankment. These are the main physical processes affecting waves in a harbour. Therefore, they are requested in any model used for harbour design.

A harbour that is exposed to a more violent wave climate may benefit from submerged breakwaters in the area of the entrance channel. These breakwaters are meant to subdue waves discarding part of the wave energy.
In many cases there is an entrance channel in front of the harbour. Due to depth differences, waves will refract (figure 1.3). This is the phenomenon where the direction of the wave changes due to depth change. The direction of the wave bends until it practically is perpendicular to the depth contour. It changes the direction of the wave front due to a lower propagation speed in the shallower water (Snel's law).

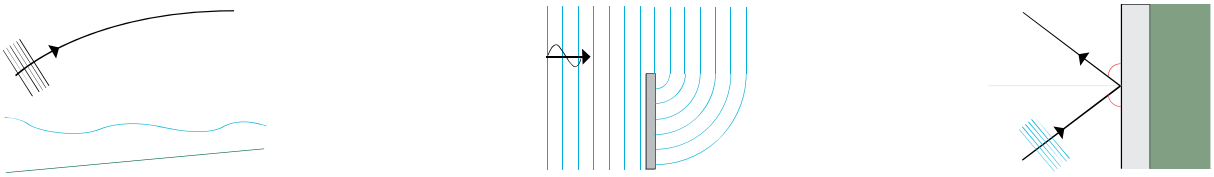

Figure 1.3 Refraction (left), diffraction (middle), reflection (right)

When the waves near the entrance of a port, there often is a head land or breakwater and diffraction occurs (figure 1.3). The water level difference between the exposed and lee side is often strong. When there is a strong gradient in the surface elevations. Diffraction is the phenomenon that reduces this gradient by a flow of energy along the crest.
It is combined with a change of the direction of the wave. If the gradient is strong enough, waves behind a breakwater can propagate parallel to it. When the breakwater is permeable, some wave energy transmits through the breakwater and the gradient between surface elevations becomes smaller. Wave transmission occurs also occurs via wave overtopping, influencing the surface elevations at the lee side.

Once waves are in the basin, they will meet quay walls and reflection will occur. The angle of incidence is the same as the angle of reflection (figure 1.3). These angles are relative to the normal of the boundary. The energy of a wave can be fully reflected, partially reflected or fully absorbed.
Reflections of quay walls require attention during modelling. A period of the propagating wave which is close to one of the eigen periods the basin, can lead to harbour oscillations. They can be determined by basin geometry (Rabinovich, 2009).
To subdue the incoming waves and their amount of reflection, beaches can be seen at the end of harbour entrances. Scheveningen harbour is such an example. These are the yellow areas in figure 1.1.
In case of breakwaters, the type influences the amount of reflection. A rubble mount breakwater will partially reflect waves. Depending on its choice of revetment the amount of reflection can be influenced. Whereas a caisson breakwater most likely gives full reflection; sometimes perforation of a caisson wall is applied in order to reduce the amount of reflection.

Selection of the model TRIWAQ-NH

A number of important aspects have been introduced, which influence the selection of a model on a conceptual basis. First, the type of wave it can handle and second, the type of processes that are expected to be encountered.
Although a numerical model is less expensive than a physical scale model, it is often not able to describe all involved processes sufficiently accurate. This has led to a wide range of numerical models, each with specific physical aspects. Therefore a careful choice has to be made.

Generally speaking, models can be divided into two categories; phase-averaged and phase-resolving models (Enet, et al., 2007). A phase-averaged model describes the surface elevation as a stochastic phenomenon. The evolution of the wave field is described by the energy balance equation. Nowadays this is implemented in discrete spectral models. Examples of these types of models are SWAN and WAM (SWAN.team). Phase-resolving models describe the surface elevation deterministic manner. They are based on momentum balance equations. These are time domain models. These can be divided into types, mild-slope models, like PHAROS, are limited in the steepness of the slope, where a nonlinear model like TRIWAQ is not. Last there are Boussinesq models, like TRITON or MIKE21 BW.

Phase-averaged models have distinct differences on a conceptual base compared to phase-resolving models. They are able to account for wind effects such that they can calculate wave growth in the area of interest. Drawback is the lack of ability to simulate diffraction.
On the other hand, phase-resolving models are able to predict diffraction, but are not able to simulate wave growth. A mild-slope model, often called diffraction-refraction model, is more suited for sinusoidal or long waves, while a Boussinesq model is more suited for non-regular or short waves. These become more significant in the coastal zone (harbours).

It is clear that not every model is able to predict each process sufficiently accurate to select one model for computations of wave conditions. So up to now, depending on the application a user has to choose between models. Coupling between phase-averaged models and phase-resolving models can overcome the drawbacks (Groeneweg, et al., 2004). This will not be further mentioned.

On an algorithmic level, phase-averaged models have the advantage in calculation time, since they are relatively fast. This is due to the fact that the grid step of the model is not strictly dependant on the wave. Drawbacks are, first, propagation of a long wave requires a non-linear correction terms. And second, wave induced flow is not directly implemented.

When simulating with a phase resolving model, the wave forcing needs to be a time series. Such a series can be discretized from a wave spectrum (figure 1.1), by cutting up the wave periods in small bins and creating a Fourier series of such a bin. The grid and time step are dependent on the wave length (or better the kh value). It makes phase-resolving models more expensive in terms of calculation time.
The main difference between mild-slope models and Boussinesq models lies in solving the balance equations. Mild-slope models neglect the advection term in the vertical and the terms of accelerations in the mass balance, making it linear models. Boussinesq models eliminate the vertical terms, but try to approximate these by means of a Taylor expansion, making it non-linear models.
The Taylor expansion leads to higher order terms, which are of some consequence. First, the third order term changes the phase speed of a wave group, leading to a change in dispersion. Second, higher order terms lead to slightly different values for potential and kinetic energy. It affects the implementation of the computer code for refraction.

Recently mild-slope models have been extended from hydrostatic to non-hydrostatic (Zijlema, et al., 2005). They aim to bridge the gap between the long and short waves (e.g. swell) or in geographical terms; these models should be able to simulate waves from deep water to coastal waters.
In previous work (Stelling, et al., 2003) (Zijlema, et al., 2005), it has been shown that TRIWAQ-NH performs well in respect to (1) the accuracy of linear wave dispersion; (2) preservation of shape; (3) the effect of shoaling and (4) refraction, diffraction and wave focussing.

For harbour response studies the amount of reflection against quays has a significant influence on its response to resonance. The proper choice of boundary conditions is essential for accurate computations of its response (Kostense, et al., 1988). It is noted that wave reflection for harbour simulations has not yet been investigated in TRIWAQ-NH, therefore this is a meaningful first step for to investigate and validate the capabilities with respect to wave propagation.

The aim is to validate the capabilities of TRIWAQ-NH with respect to wave propagation in harbours, with emphasize on its present capabilities of reflection.

The first part of this study will focus on reflective capabilities in TRIWAQ-NH. It will investigate the currently implemented open boundary conditions and assess each its ability for future development into a working partial reflection coefficient. It is based on background theory and 1 dimensional model simulations. Their response will be validated with hydrostatic simulations in TRIWAQ.

The second part of this study investigates the capabilities of TRIWAQ-NH for harbour applications. It aims to validate the capabilities with respect to wave propagation in harbours by referencing the non–hydrostatic method with the hydrostatic method. This will be achieved by replicating harbour simulation of (Isaacson, et al., 1990).

Chapter 2: Non-hydrostatic modelling in TRIWAQ

The starting point of this chapter is an explanation of hydrostatic and non-hydrostatic flow for a free-surface gravity wave. It also will define a leading indicator for non-hydrostatic modelling. It is followed by a (mathematical) description of the model TRIWAQ and its extension to the non-hydrostatic.

Hydrostatic versus non-hydrostatic wave flow

To consider hydrostatic flow, fundamental assumptions for a free-surface gravity wave (Battjes, 2002) are; (1) the fluid is stationary; (2) there is no shear stress present, which means there are no vertical velocities; (3) the viscosity is uniform; and (4) the fluid is incompressible. These four premises are needed for flow that is "little curved" or hydrostatic flow (figure 2.1). It assumes that the pressure increases linear over the water depth.

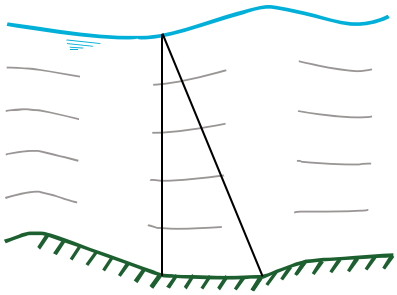

Figure 2.1 Hydrostatic pressure. Gray dashed line shows the flow field. Black line the pressure over depth

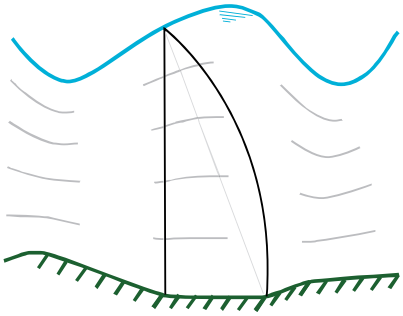

Figure 2.2 Non-hydrostatic pressure. Gray dashed line shows the flow field. Black line the pressure over depth

For non-hydrostatic model the pressure does not necessarily have to increases linear over depth. The flow lines can be (strongly) curved (figure 2.2). It allows non-uniform horizontal and vertical velocities this can be considered an advantage of non-hydrostatic modelling.
In figure 2.1 and 2.2 the difference in pressure gradient is schematized. It visualizes two different wave types as well. The hydrostatic pressure schematic resembles a non-dispersive linear wave, and the non-hydrostatic pressure resembles a dispersive non-linear wave.
The measure for dispersion is indicated by the relationship between the wave length and the water depth. The mathematical description consists of the wave number ($k = 2\pi/L$) with the total depth ($h = d + \zeta$). Where the transition between hydrostatic and non-hydrostatic is roughly at kh = 0.02.

Additionally linearity is visible in the schematizations. It is a measure of the wave steepness, the ratio between the wave length and the amplitude is an indicator. A wave is considered linear when $ka \ll 1$. Thus a steeper or non-linear wave is likely to have larger vertical velocities then a linear wave.

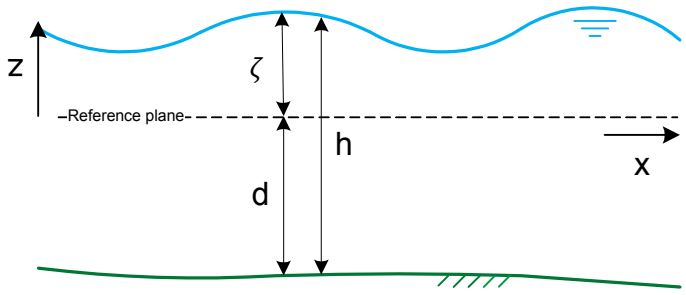

Figure 2.3 Definition of mathematical variables in the water area.

As referred to in the introduction, the TRIWAQ-NH model has been validated for dispersive linear waves (Stelling, et al., 2003) (Zijlema, et al., 2005). This thesis will also focus on this type of wave. For the use of non-hydrostatic modelling, the dispersion relationship can therefore be considered a leading indicator.

The model TRIWAQ with an extension to the non-hydrostatic

A short description of the original model environment is given. It will continue with a description of the governing equations and boundary conditions used in TRIWAQ-NH. The numerical implementation will briefly be given. An in-depth description of the background of the TRWAQ-NH model is given in (Stelling, et al., 2003) (Zijlema, et al., 2005).

TRIWAQ-NH is part of the SIMONA architecture. SIMONA stands for SImulaties NAtte MOdellen and is a platform that encompasses numerical models for wave predictions. The owner is the Dutch Ministry of Public Works.
SIMONA aims to simulate water movement and water quality. It is able to simulate both stationary and non-stationary flow. WAQUA is the 2 dimensional equivalent of the 3 dimensional TRIWAQ. Both are hydrostatic models. TRIWAQ has been expanded to the realm of non-hydrostatic modelling (Zijlema, et al., 2005).

TRIWAQ is split into multiple modules. The first module defines a way for pre-processing and can be invoked with the dos command "*waqprerun*". The second module consists of processing, memory management and data storage; it is invoked with the dos command "*waqprorun*". The last module does the post processing, is invoked by the dos command "*waqpanrun*" and allows the user to create readable files for further post processing in computer programs like Matlab.

The governing equations

In order to achieve non-hydrostatic pressure p, TRIWAQ splits the pressure into a hydrostatic component p_h, and a non – hydrostatic component, q. Atmospheric pressure is assumed to be zero. The hydrostatic pressure is dependent on the gravitational acceleration g, the distance between the free-surface ζ and the location of the reference level.

$$p = g(\zeta - z) + q = p_h + q \tag{2.1}$$

Next the Euler momentum equations are given for the 3 dimensions with velocities defined as u, v and w in respectively the x, y, z - direction.

$$\begin{aligned} \frac{\partial u}{\partial t} + u\frac{\partial u}{\partial x} + v\frac{\partial u}{\partial y} + w\frac{\partial u}{\partial z} + g\frac{\partial \zeta}{\partial x} + \frac{\partial q}{\partial x} = 0 \\ \frac{\partial v}{\partial t} + u\frac{\partial v}{\partial x} + v\frac{\partial v}{\partial y} + w\frac{\partial v}{\partial z} + g\frac{\partial \zeta}{\partial y} + \frac{\partial q}{\partial y} = 0 \\ \frac{\partial w}{\partial t} + u\frac{\partial w}{\partial x} + v\frac{\partial w}{\partial y} + w\frac{\partial w}{\partial z} + \frac{\partial q}{\partial z} = 0 \end{aligned} \tag{2.2}$$

Here frictionless flow is assumed. The continuity equation for an incompressible fluid is given by;

$$\frac{\partial u}{\partial x} + \frac{\partial v}{\partial y} + \frac{\partial w}{\partial z} = 0 \tag{2.3}$$

This leads to the kinematic conditions, which are found by integrating the continuity equation over the water depth $H = \zeta + d$

$$w_{|z=\zeta} = \frac{\partial \zeta}{\partial t} + u\frac{\partial \zeta}{\partial x} + v\frac{\partial \zeta}{\partial y} \quad 2.4$$

$$w_{|z=-d} = -u\frac{\partial d}{\partial x} - v\frac{\partial d}{\partial y} \quad 2.5$$

Ultimately the free-surface condition can be defined as;

$$\frac{\partial \zeta}{\partial t} + \frac{\partial}{\partial x}\int_{-d}^{\zeta} u dz + \frac{\partial}{\partial y}\int_{-d}^{\zeta} v dz = 0 \quad 2.6$$

Numerical implementation and solver method

The scheme of TRIWAQ-NH is edge based for pressure in the vertical (figure 2.4Figure 2.4). Leading to a more accurate approximation of the free-surface the pressure p. This is beneficial for simulations of dispersive waves. The vertical velocity w in z-direction, the horizontal velocities u and v in x-direction and respectively y-direction are located at the centre of the cell faces.
For each cell calculates of the continuity equation and the momentum equation are done. For more detailed information about the numerical scheme referred to (Zijlema, et al., 2005).

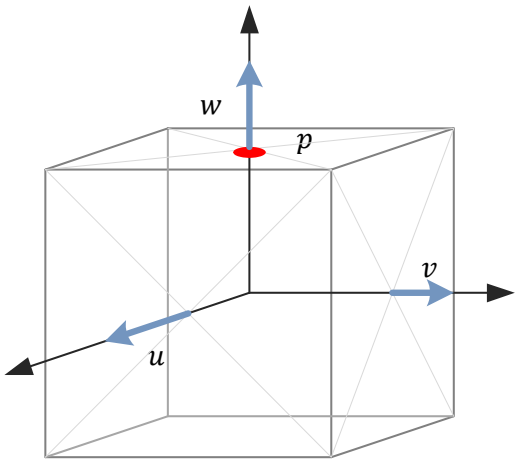

Figure 2.4 Position of variables in a grid cell. Velocities (u,w,v) and pressure p

TRIWAQ is a time-domain model. It works with time steps, where all variables from the previous time step are known. Known parameters for the next time step are: (1) the pressure at the free-surface; being zero if wind stresses are neglected; (2) the derivative of the pressure at the bottom; and (3) the vertical velocity at the bottom (being zero, since the bed is assumed impermeable).

In order to calculate a (next) time step, the overall algorithm is divided into a hydrostatic and non-hydrostatic part (figure 2.5). The hydrostatic part computes the free-surface level ζ^{n+1} and intermediate horizontal velocities u^*, v^*. Next, the non-hydrostatic step adjusts these velocities and the non-hydrostatic pressure q until the continuity equation is satisfied (for each grid cell). Ultimately obtaining $u^{n+1}, v^{n+1}, w^{n+1}$ and q^{n+1}. The next two paragraphs describe the method for solving the hydrostatic and non-hydrostatic step.
The hydrostatic calculation (figure 2.5) starts with the selection of the known variables from the previous time step. Leading to values $\zeta^n, u^n, v^n, w^n, q^n$. With these values the momentum equations are solved and u^{**}, v^{**} are obtained. With those two a correction, $\Delta\zeta$, for the water level is found, leading to $\zeta^* = \zeta^n + \Delta\zeta$ and u^*, v^*. These steps are repeated until the values ζ^*, u^*, v^* converge. Once reached the water level is set to $\zeta^{n+1} = \zeta^*$
For a new non-hydrostatic time step (figure 2.5) the non-hydrostatic pressure is set to $q^n \equiv 0$. First it solves the intermediate vertical velocity, leading to w^*. Next, the pressure is corrected with Δq,

which is obtained through a pressure correction equation, updating the pressure to $q^{n+1} = q^n + \Delta q$. Next all velocities are updated to $u^{n+1}, v^{n+1}, w^{n+1}$.

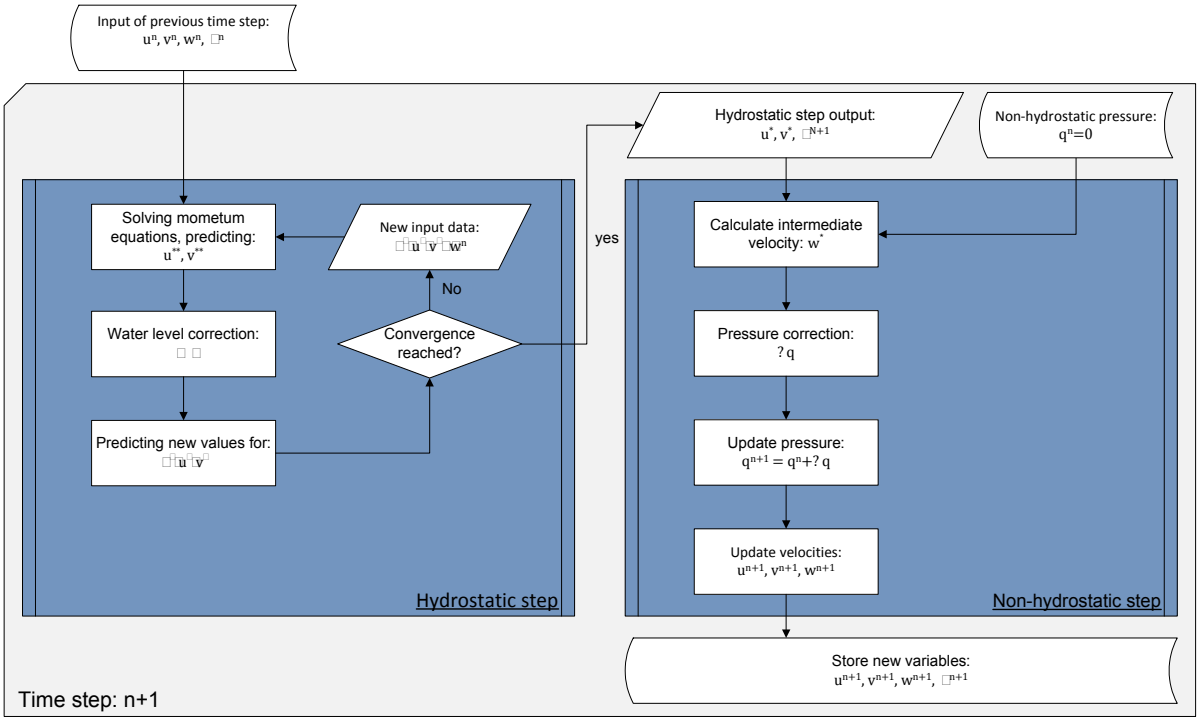

Figure 2.5 Flow scheme of variable calculation for a new time step

Chapter 3: Boundary conditions

This chapter will first discuss the wave maker boundary condition and its implementation to non-hydrostatical simulations. Next its focus will shift to the boundary conditions, providing background information on the currently implemented boundary conditions in TRIWAQ-NH.
It will provide information on implementation of three different boundary conditions in the model TRIWAQ-NH and describe possible limitations that may arise from its usage. In the next sections the background on boundary conditions is given. It will cover the wave maker condition, (partial absorbing boundary conditions and end with some conclusions that may be drawn from it.

Time domain modelling and the use of boundary conditions

TRIWAQ calculates in time steps. At the beginning of the simulation, the model domain, its initial water level and velocities are in rest.
The wave maker condition is used to approximate the real waves from outside the model domain. It is the boundary condition where a wave forcing is imposed. This wave will propagate through the domain, thereby disturbing the initial "rest". A common used method to determine what the wave forcing should be; can be found in chapter 1.
Other boundary conditions are used to approximate how the propagation wave should respond once it reaches such a boundary. The wave can (1) fully reflect and thus change its direction by 180 degrees; (2) fully absorb and thus exits the model domain or (3) partially absorb/ reflect, which is a combination of the first two. By selecting the proper boundary conditions, over time, or after a certain amount of time steps, a stable solution will occur. The total amount of energy in the model domain is used as measure. It should also lead to reoccurring wave heights and wave patterns.

The wave maker condition

At the boundary a wave maker condition has to satisfy the continuity equation. The wave forcing is implemented as a function of time $f_u(t)$ normal to boundary. The tangential velocities are set to zero.

$$\frac{\partial u}{\partial x} + f_u(t) = 0 \qquad 3.1$$

Since the momentum equation (eq. 2.2) is not solved and the non-hydrostatic pressure gradient is unknown beforehand, the wave forcing is implemented as hydrostatic. Due to these restrictions the propagation speed c can be found from the linear dispersion relationship.

$$c = \frac{\omega}{k} = \sqrt{\frac{g}{k}\tanh(kh)} \qquad 3.2$$

Where: $\omega = 2\pi/T$
$k = 2\pi/L$

With a pre-defined wave period T and wave amplitude a the velocity amplitude $\hat{u}$ can be found from linear wave theory. It requires that the amplitude of the wave is small compared to the depth of the model.

$$f_u(\mathrm{t}) = \hat{\mathrm{u}}\sin(\omega t) = \frac{\omega a}{kh}\sin(\omega t) \qquad 3.3$$

The wave maker condition is implemented as a Fourier series in TRIWAQ-NH where the velocity amplitude $\hat{u}$ and the wave period ω are required.

The (partial) absorbing boundary condition

The amount of reflection required at the boundary defines the selection of the conditions needed for implementation in a numerical model. These can roughly be divided into two extreme conditions, which are full reflection and full absorption at the boundary and all types in between; partial reflection.

When full reflection is considered the boundary is closed. The full wave should be transmitted back into the model domain. Mathematically it means that tangential stress and normal velocities are set to zero. This is also known as the free-slip condition.
An absorbing or non-reflective boundary is defined as an open border where wave propagation or flow is not disturbed. An outgoing wave should not reflect and an incoming wave must be free to travel into the model space. Mathematically it means the normal stress and tangential velocities are imposed and hydrostatic flow is assumed near the boundary, consequently the water level is prescribed (Zijlema, et al., 2005).

The approach for a partial reflective boundary is to create an open boundary condition and impose some "reflection" upon it. Or in other words, a partially absorbing boundary is created. Of interest are the properties for an outflow boundary. These conditions are based on the Sommerfeld's radiation condition.

$$\frac{\partial f}{\partial t} + Rc\frac{\partial f}{\partial x} = 0 \qquad 3.4$$

Here f represents the surface elevation and the tangential velocity component, R is a transmission coefficient. It can be interpreted in multiple ways. R can have (1) a relation to the rate of energy transfer; (2) to the wave height and its phase at the boundary or (3) to a more conventional reflection coefficient.

The next three sub sections will describe the theory behind the currently implemented open boundary conditions of the α –value, artificial dampening by a sponge layer and a method of changing a wave characteristic in a model by use of a sloping profile.

The weakly reflective properties of the α-value

The model was designed to predict water levels along the coastal zone and simulate long waves. As such the original intend of open boundaries was to minimize the model space and calculation time. Therefore absorption or non-reflection for long waves is of interest. The numerical implementation of such conditions is tedious and often leads to some reflection. Hence these boundaries are referred to as weakly reflective in TRIWAQ.

In TRIWAQ three options are given to create a (weakly) reflective boundary. These are (1) water level, (2) flow and (3) Riemann invariant conditions. For the first two conditions an additional reflection coefficient α can be implemented. This section will detail determination of the α-value and describe its theoretical applicability.

The α-value is a pre-calculated reflection coefficient, based on linear shallow water equations and does not take friction into account. The starting point in the mathematical description for the reflection coefficient is

$$\zeta + \alpha_{\mathrm{w}} \frac{\partial}{\partial t}\{U \pm 2\sqrt{gh}\} = F_{\zeta}(t) \qquad 3.5$$

This is the formulation for the weakly reflective water level boundary, making use of hydrostatic properties. Where U is depth-averaged velocity, α_w the reflection coefficient derived for the water level and $F_{\zeta}(t)$ is the desired signal at the boundary. Note that when each ζ is replaced by U it becomes the flow boundary condition, where $\alpha_w$is substituted for a flow specific reflection coefficient α_s.
From a linear 1D model a reflection coefficient R can be derived.

R for water level boundaries

$$R = \frac{1}{\sqrt{1 + \left(\frac{4\pi\alpha_{\mathrm{w}}}{T_d}\sqrt{\frac{g}{h}}\right)^2}}$$

R for flow boundaries

$$R = \frac{1}{\sqrt{1 + \left(\frac{4\pi\alpha_{\mathrm{s}}}{T_d}\right)^2}} \qquad 3.6a \text{ \& } b$$

When α_w is large R will near zero, which represents full absorption. With a high value for α-value the reflection coefficient becomes non-existent. However the larger α the longer the spin up time, since the boundary signal is not able to reach (SIMTECH, 2000). In order to choose a proper α_w. It is suggested for use;

α_w for water level boundaries

$$\alpha_w = T_d\sqrt{\frac{g}{\mathrm{h}}}$$

α_s for flow boundaries

$$\alpha_{\mathrm{s}} = T_d \qquad 3.7a \text{ \& } b$$

with

$$T_d = \frac{2\mathrm{L_b}}{\mathrm{c}} = \frac{2L_b}{\sqrt{gh}} \qquad 3.8$$

When the wave amplitude is small compared to the depth, this is one of the assumptions, then $h \approx d$. Ultimately making both coefficients solely depended on basin properties; being the depth d and the length of the basin L_b. Leading to the domain period T_d.Note that α_w and α_s are not dimensionless, respectively $[s^2]$ and $[s]$.

There are some limitations to the use of the α – value when simulating reflection for short waves in TRIWAQ-NH.
First and foremost, its formulation has been derived for 1D hydrostatic flow. Meaning, the angle of incidence for the wave needs to be nearly perpendicular and the non-hydrostatic properties are discarded at the boundary. Thus flow properties are affected, this will not be tested.
Secondly, the implementation of the α-value needs to be manually calculated and added into the simulation input file. It is therefore prone to errors.

The manual implementation of the α-value also leads to an opportunity. The domain period uses the propagation speed for shallow water c. Generally it is higher than the propagation speed for a dispersive wave. It can manually be replaced by the propagation speed;

$$c = \frac{L}{T} = \frac{gT}{2\pi}\tanh\left(\frac{2\pi d}{L}\right) \qquad 3.9$$

Drawback is that the α coefficient is not solely dependent on the basin geometry anymore. The period of the wave T becomes a variable as well; making the coefficient α specific for one monochromatic wave.

Overall the use of the excepted performance of the α - value is not applicable for non-hydrostatic simulations. Because all premises expect hydrostatic flow and are rather strict on the proper value of α.

Artificial dampening with a sponge layer

A second possibility to simulate an absorbing boundary condition is by use of artificial dampening. Using a sponge holds several advantages. First it is easy to implement and second it has good reflective properties for a wide range of frequencies, unlike the α-value. A disadvantage is, that some extra model domain is needed (Romate, 1991).

The dimensionless term κ is added to the momentum equations (eq 2.2) near the boundary for dampening.

$$\frac{\partial u}{\partial t} + \ldots + \kappa u = 0 \qquad \text{Part of equation 2.2}$$

The term for dampening has been described by (Zijlema, et al., 2005). This is a parabolic shaped term that spawns over a length L_s which stands for sponge layer length. Often a multiplicative of the wave length is used. For instance three times the wave length. The formulation for the dimensionless term κ uses $\tilde{x}$ which refers to the normalized length of the sponge layer. Where L_0 is the starting point of the sponge layer (figure 3.1). The formula for κ reads;

$$\kappa = \begin{cases} \frac{1}{4}\left(tanh\left[\frac{\sin\left(\frac{\pi(4\tilde{x}-1)}{2}\right)}{1-(4\tilde{x}-1)^2} \right] + 1 \right), & 0 < \tilde{x} < \frac{1}{2} \\ \frac{1}{4}\left(tanh\left[\frac{\sin\left(\frac{\pi(3-4\tilde{x})}{2}\right)}{1-(3-4\tilde{x})^2} \right] + 1 \right), & \frac{1}{2} < \tilde{x} < 1 \end{cases} \qquad 3.10$$

with $\tilde{x} = (x - L_0)/L_s$

At the end of the sponge layer an open boundary needs to be defined. Any of the three definitions (a water level, velocity or Riemann boundary) in TRIWAQ are possible. This thesis will use a length of three times the wave length for $\tilde{x}$. As a general rule of thumb, 20 grid points per wave length give a good description of surface elevation ζ, meaning a sponge layer uses 60 extra grid cells.

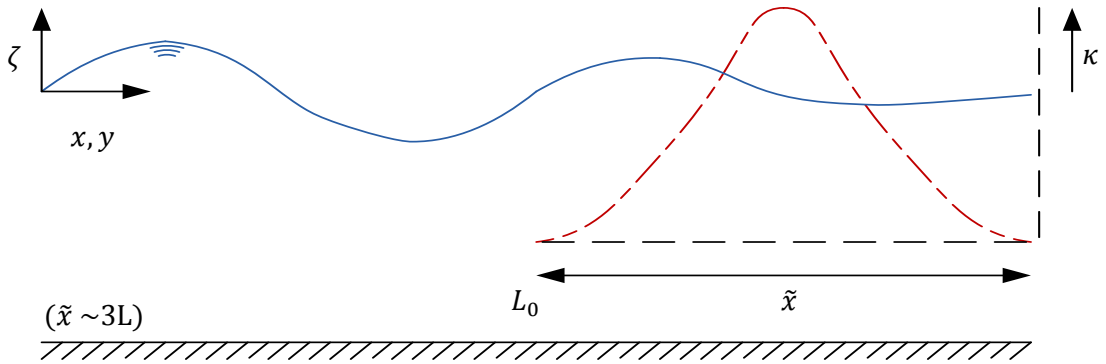

Figure 3.1 Visualization of the sponge layer and its dimensionless coefficient κ

For waves that close in with and an angle of incidence, it only dampens for one velocity direction (figure 3.3). Limiting its use to nearly perpendicular waves. Further more the usage of the sponge layer is currently restricted to the either the positive u-momentum or positive v-momentum balance equation (figure 3.2).

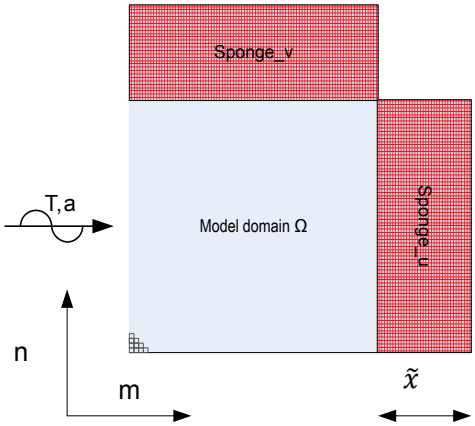

Figure 3.2 Limitations of the sponge layer positions

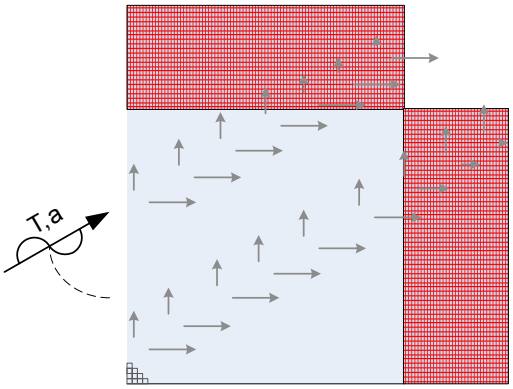

Figure 3.3 Schematization of the sponge dampening when the wave enters under an arbitrary incidence

The higher the velocity of a wave, the earlier it will notice the dampening coefficient of the sponge. By shortening the sponge layer length, the amount of wave reflection can be most likely controlled.

Presently the purpose of the sponge layer is to fully absorb waves. However, the use of a sponge layer holds some promise when a certain amount of reflection is required. The sponge layer is in fact not dependant on wave properties, like the period or amplitude. In this thesis a sponge layer length $\tilde{x}$ that equals three times the wave length is used. This does not mean that it necessarily has to be so. Also the value κ now has a hyperbolic shape. Adjustment of such a shape is likely to yield other results. And last, now the sponge layer can only be implemented with an open boundary at the end. It might be interesting to test it with a closed boundary for partial reflection purposes.

Changing depth profile

A third way to dampen waves in a model is to adjust the dispersive properties by changing the bottom profile. In the following simulations (chapter 4) a sloping bottom starts at the end of the domain. Gradually the depth will decrease until the incoming wave its dispersive characteristic has changed. It will then encounter an outlet where the wave is able to settle under its new conditions. At the end of the outlet an outflow boundary will be present.

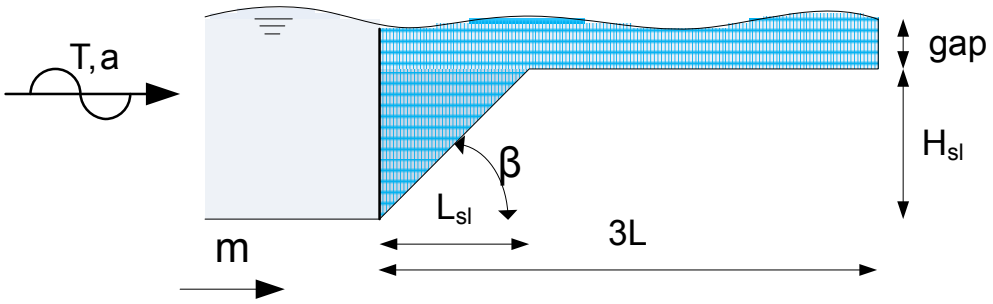

Figure 3.4 Schematic of the changing depth profile

Like with aritficial dampening, it requires additional model space, which is a arithmic drawback. Secondly, the slope angle and the grid step size determine the smoothness of the slope. The slope may turn out to angular, resulting in undesired effects in the model domain. Third, when reflection is concerned, this method is restricted to waves that travel (nearly) perpendicular to the slope. When the angle is to large, refraction is likely to occur. Once reflection is present, it will be out of phase and the wave will not relfect at the intended x, y place in space leading to a phase difference.
Advantages for using a sloping bottom profile are, it will work well for a wide range of frequencies and it is easy to implement into TRIWAQ.

For the creation of a sloping profile, short wave theory will be used (Battjes, 2001). It is designed to have a simular length as the sponge layer condition, of $3L$ (figure 3.4). The slope steepness β is defined as the maximum angle for non-breaking periodic standing waves. It is a function of the wave length (L) and the slope height h_{sl}.;

$$\beta_{max} = 0.2\tanh\left(\frac{2\pi h_{sl}}{L}\right) \quad 3.11$$

$$L_{sl} = \frac{h_{sl}}{\beta_{max}} \quad 3.12$$

At the top of the slope the outlet has multiple times the length of the wave and has a constant depth. The end of the slope uses a Riemann boundary. The gap height is defined by the $kh = 0.02$, so that the wave will meet hydrostatic requirements of the open boundary. This is the maximum value for waves before they are considered to be to dispersive. When restriction for steepness is loosened the grid step becomes much more important when a smooth slope is required.

The purpose of a changing depth profile is mainly to compare it with the sponge layer. This thesis uses a set angle of incidence. It is expected to perform well in one dimensional test where little or no reflection should be present.

Reflective capabilities of the current boundary conditions

It is the intention to test the reflective capabilities of TRIWAQ-NH. The present possibilities at and near a boundary are all more focused towards absorption of propagating wave that travels nearly perpendicular to the boundary of interest.
A distinction needs to be made between modelling objects, when wave reflection in harbours is concerned. Quay walls are (nearly) vertical. The angle of incidence is bound to be oblique at any given boundary, in complex shaped basin. Modelling reflection with a sponge layer or sloping bottom profile do not favour these conditions. It will lead to phase errors. Since the wave is able to propagate beyond the intended point of reflection. With complex geometries the extra grid space required will require nesting of the model. Unfortunately the wave signal needs to be perpendicular to the nested grid, which would make it rather tedious work. Using an open boundary with an α – value, will not have these drawbacks, but is completely calibrated for hydrostatic flow. It is highly likely stable simulations are impossible to achieve.
The second type of boundaries are the more sloping structures in harbours, like (absorbing) beaches. Not only are these often positioned at locations where the wave direction is (still) channelled.

In short, two important selection criteria are: (1) the type of reflection. Is used model going to be simulating monochromatic waves?; and (2) the angle incidence. Is the incoming wave going to come at a nearly perpendicular angle or will it oblique (due to harbour geometry)?

Chapter 4: 1 Dimensional model

In the previous chapter the theory of different boundary conditions is explained. This chapter will implement the different boundary condition types for a one dimensional simulation.
The primary aim is to show the differences and find the most suitable solution for an absorbing boundary. In part, this is accomplished by modelling each boundary condition for a hydrostatic wave and non–hydrostatic wave.

General settings and scaling principle for comparison

General settings

In the simulations, some general parameters and settings are applied. All tests will neglect bottom friction. This corresponds to one of the assumptions for which the reflection coefficient (α) was derived. Furthermore viscosity is neglected. Both terms could influence the results, making testing of reflection effects harder to interpret.

In previous simulations with the TRIWAQ-NH model it was shown, that the propagation speed for a dispersive wave deviates from exact solutions. It also showed that, simulations with two layers are more accurate in that respect. However, the shape of the wave was preserved (Stelling, et al., 2003) (Zijlema, et al., 2005).
These simulations make use of 1 layer. Main reason is the simulation time, which increases for 2 layers. For the one dimensional tests the computational time was roughly doubled. Stability of a one layered model is a somewhat easier to accomplish as well.

Scaling principle for comparison of the simulations

The simulations for the non-dispersive and dispersive wave types are scaled in a similar fashion for the space and time step as well as the duration of a run.

Scaling of the space step means that the number of grid cells per wave length is in the same order for both wave types. In general 20 points should suffice. However such a resolution is too course for the runs with a sloping profile. It is increased to approximately 300 grid points per wave. This is similar to the resolution in the third test in of (Stelling, et al., 2003), which describes shoaling over a submerged bar.
Instead of having a fixed basin length for both wave types, it is scaled to fit 4 waves in a basin. Meaning there is a small difference between grid cells per length. The scale of the basin length is the same for both the 1D and 2D models.

The time step is scaled to 20 steps per wave period. The total runtime is defined by the time it takes for a wave to travel three times through the basin will then be considered stable.
It must be noted that the version of TRIWAQ (build 0506) used, has a practical limitation. After the simulation is finished, it will have created one large data file containing all information; like ζ, u, v, w. In order to use the data, it has to be post processed with the dos command *waqpanrun*. This creates many small Matlab files for each timestep. However the dos command is capped to create a maximum of 999 files.

The 1D model

Parameters and geometry of the model

In order to test each simulation for a hydrostatic and non – hydrostatic wave, two sets of wave parameters are created. In chapter 1 the kh-value is introduced as a measure to describe the difference.

The first set of wave parameters describes the hydrostatic wave and is defined by the kh-value of 0.01. The second set uses a kh-value of 1.00 and will be used for the non–hydrostatic simulation. With the formulations given in chapter 3 these can be translated into a wave period and wave length. The first set, with kh-value 0.01, yields a wave period (T) of 122 seconds with a wave length (L) of 240 meters. The second set, kh-value 1, yields a period of 1.454 seconds and a length of 2.514 meters respectively. For both sets the wave amplitude (a) is equal to 0.0107 [m] and the depth (d) is 0.4 [m]. It has one depth layer. The mean water level is set at 0 meters.

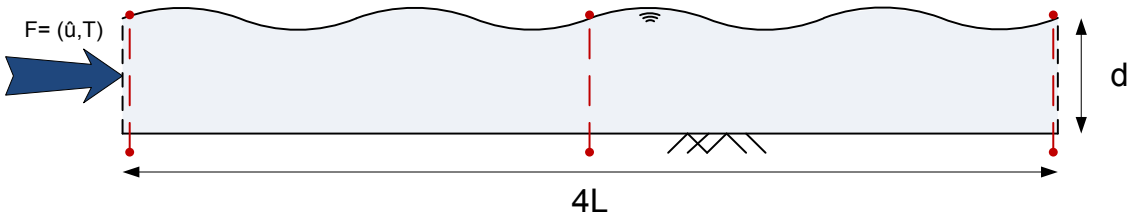

Figure 4.1 Geometry 1 dimensional of the model. Inflow is defined at the left hand side by $\hat{u}$ and T. The outflow boundary is defined at the right hand side at the black dashed line. The three red lines are the locations of the surface elevation stations.

The distance from the inflow to the outflow border is set to four times the wave length, making the basin length scale in space. It corresponds to (L_b) 960 meters and 10.08 meters respectively. At these distances the outflow boundary is defined.

Results for kh 0.01

The results shown are a snapshot in time over the length of the model. The full gray line is the mean and the dashed gray lines are the corresponding amplitude in meters to the velocity amplitude. For a fully absorbing border, the wave should propagate in between the dashed lines, where tops and troughs 'touch' the dashed lines.

On page 33, the results from figure 4.2, 4.3 and 4.4 show the propagation of the water level over the whole basin length of for three different time frames. Each figure shows four simulations. Each simulation makes use of a different boundary condition at the outflow boundary (at $x = 960$ meters). These are an α-value; a Riemann condition; a sloping profile; and a sponge layer. In the legend these are given as Alpha, Riemann; Slope; and Sponge respectively.
However, it must be noted that the sloping profile and sponge layer have additional grid cells that are not shown. The properties are described is chapter 3.

The three figures (4.5, 4.6 and 4.7), on page 34, show the water level at three different points in the basin change over time. The first water level station is at the inflow boundary. The second water level station is in the middle of the basin and the third is at the outflow boundary.
For readability of the water levels, the last 900 seconds of the simulation time is only shown. Thus spin up is not visible.

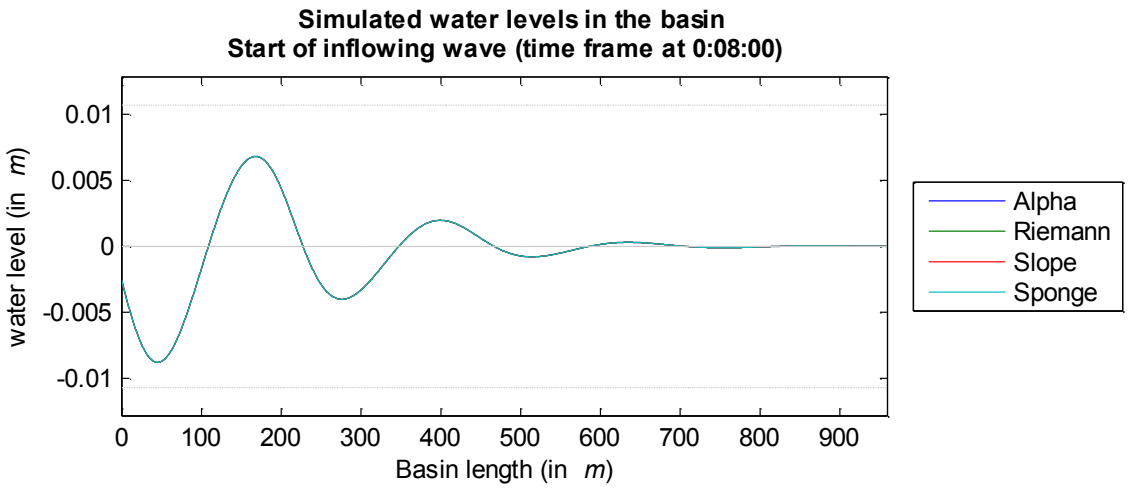

Figure 4.2 Inflow of the hydrostatic wave in the basin at the start of the simulation. With different outflow conditions. In the legend: Alpha is outflow condition using the α – value; Riemann makes use of a Riemann condition; Slope uses of a sloping profile condition; and Sponge is the sponge layer condition.

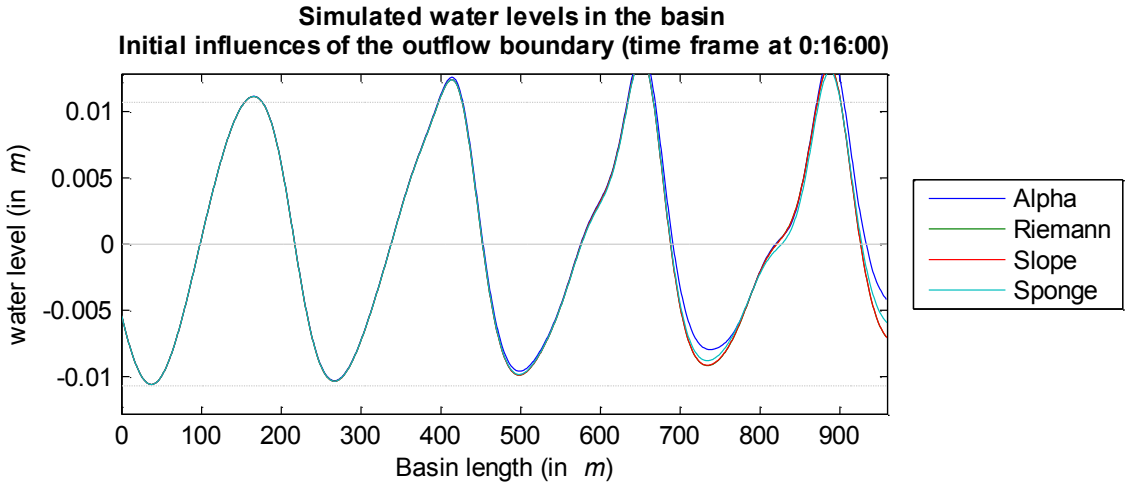

Figure 4.3 Initial influences of the boundary condition for the hydrostatic wave. With different outflow conditions. In the legend: Alpha is outflow condition using the α – value; Riemann makes use of a Riemann condition; Slope uses of a sloping profile condition; and Sponge is the sponge layer condition.

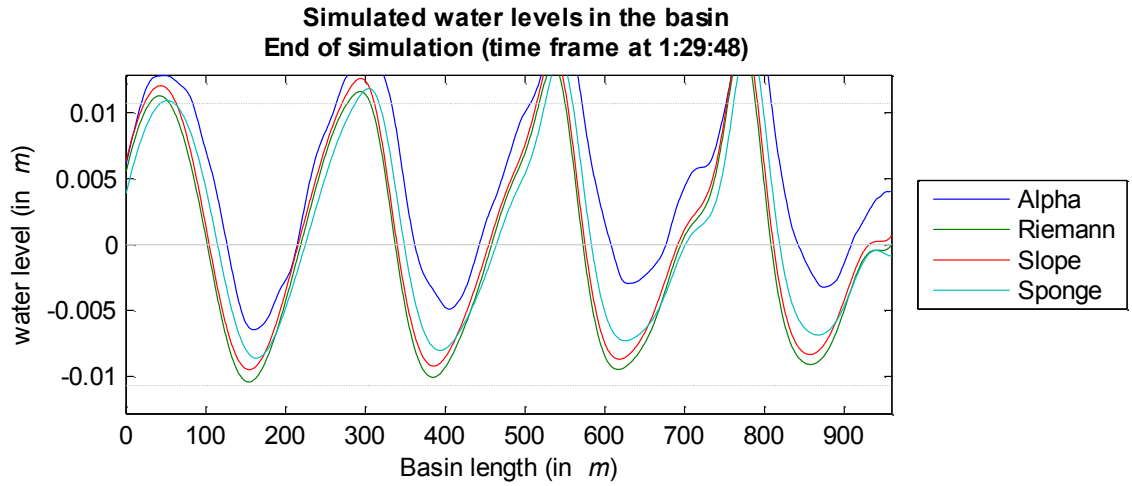

Figure 4.4 Water levels at the end of the simulation. In the legend: Alpha is outflow condition using the α – value; Riemann makes use of a Riemann condition; Slope uses of a sloping profile condition; and Sponge is the sponge layer condition.

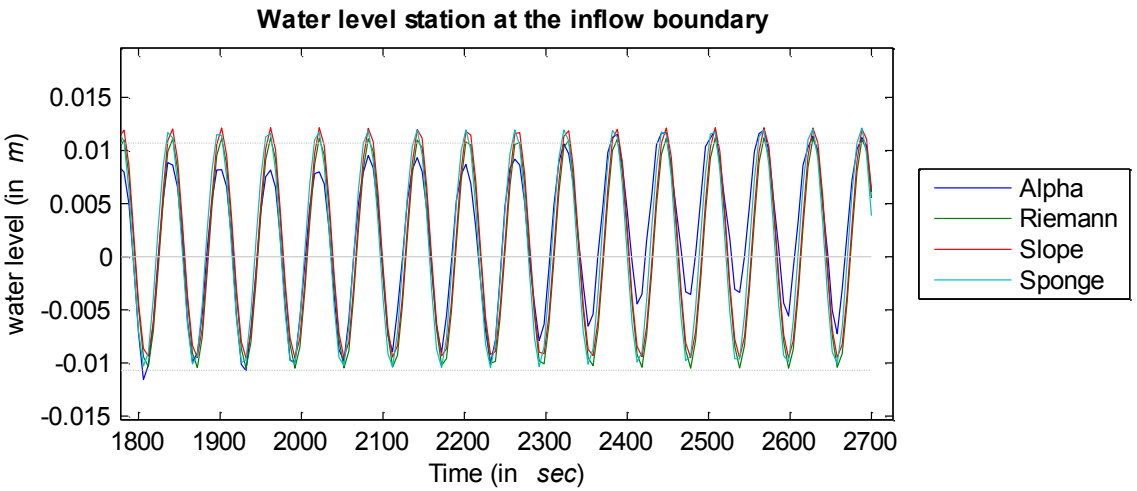

Figure 4.5 Water levels for the last 900 seconds of the hydrostatic simulations at the inflow boundary. Alpha is outflow condition using the α – value; Riemann makes use of a Riemann condition; Slope uses of a sloping profile condition; and Sponge is the sponge layer condition.

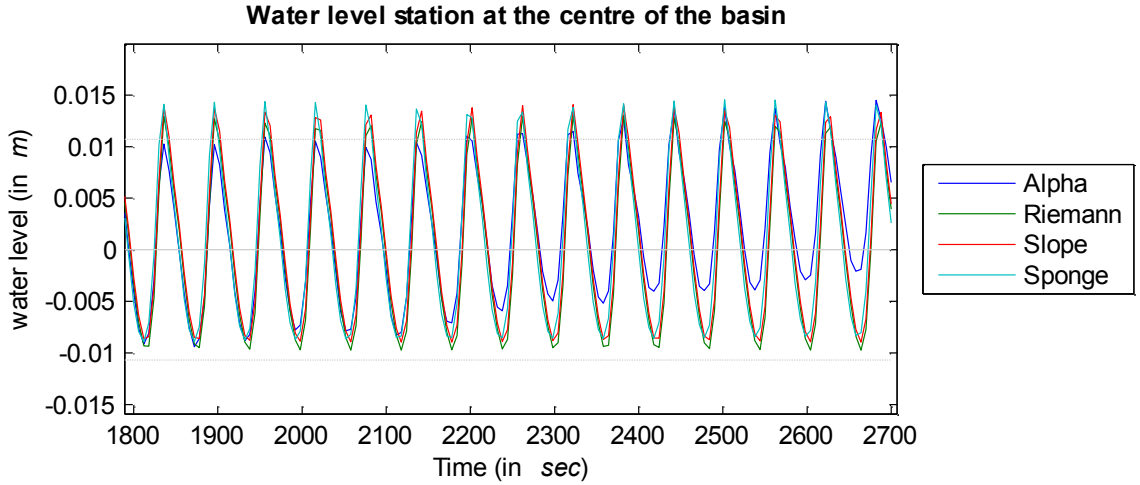

Figure 4.6 Water levels for the last 900 seconds of the hydrostatic simulations at centre of the basin. Alpha is outflow condition using the α – value; Riemann makes use of a Riemann condition; Slope uses of a sloping profile condition; and Sponge is the sponge layer condition.

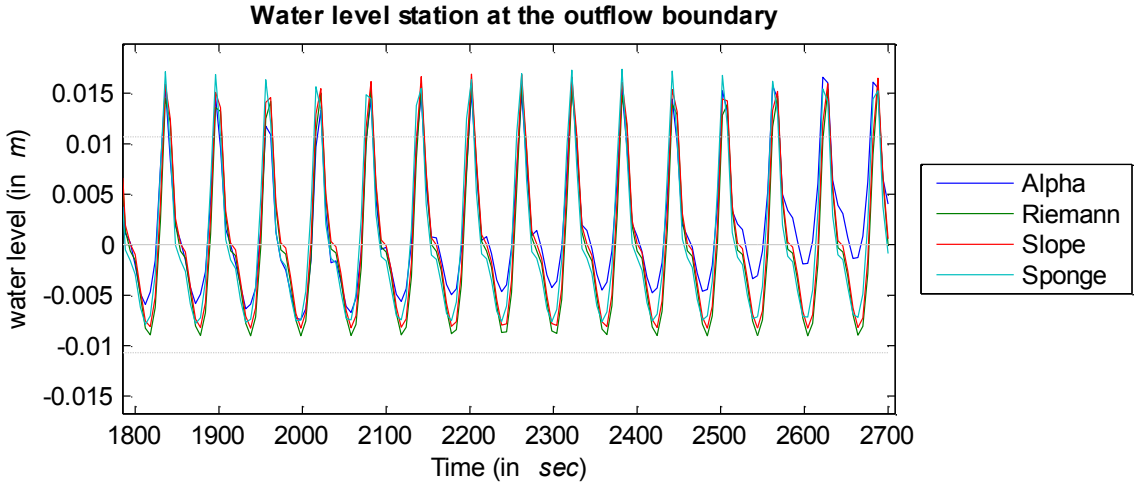

Figure 4.7 Water levels for the last 900 seconds of the hydrostatic simulations at the outflow boundary. Alpha is outflow condition using the α – value; Riemann makes use of a Riemann condition; Slope uses of a sloping profile condition; and Sponge is the sponge layer condition.

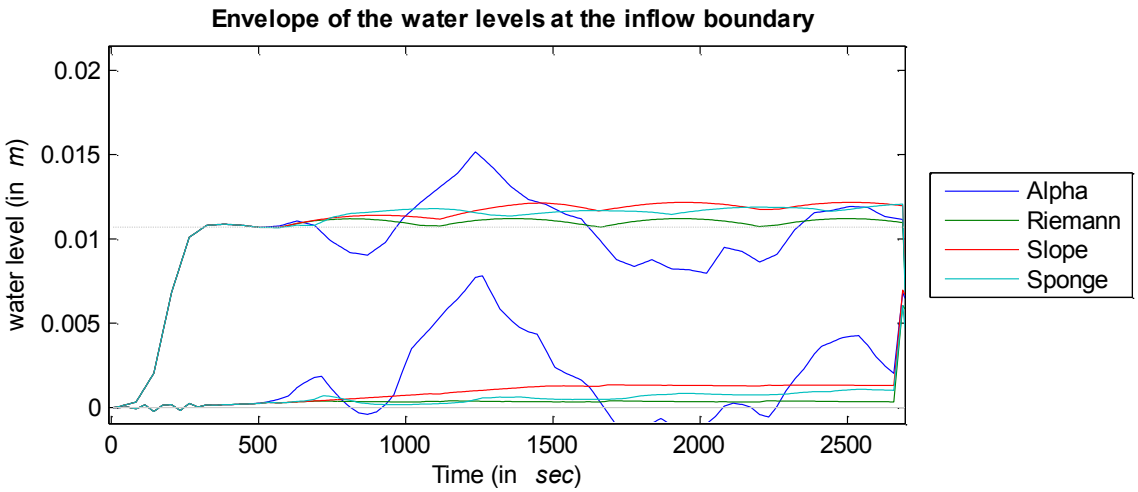

Figure 4.8 The envelope of the wave tops and mean for the hydrostatic simulations at the inflow boundary. Alpha is outflow condition using the α – value; Riemann makes use of a Riemann condition; Slope uses of a sloping profile condition; and Sponge is the sponge layer condition.

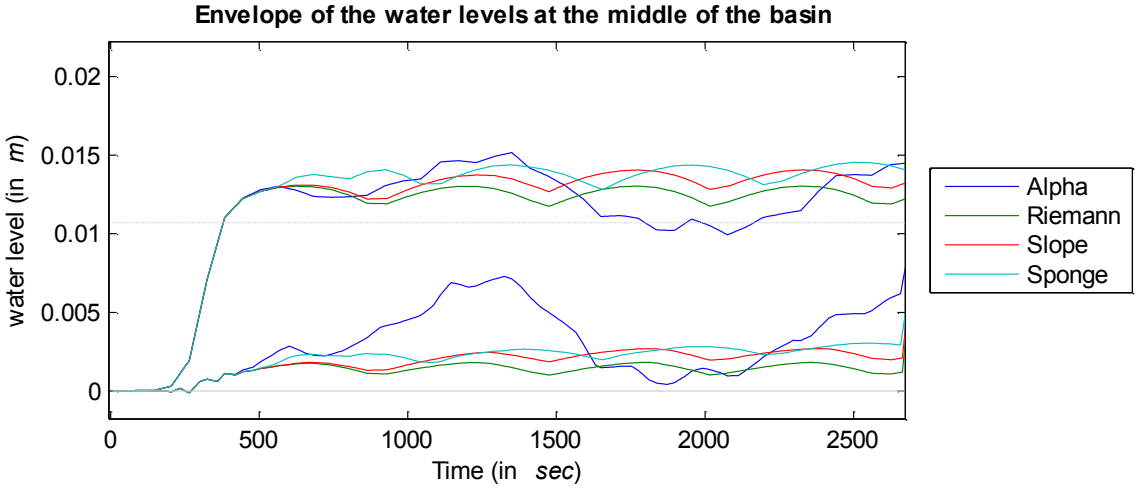

Figure 4.9 The envelope of the wave tops and mean for the hydrostatic simulations at the centre of the basin. Alpha is outflow condition using the α – value; Riemann makes use of a Riemann condition; Slope uses of a sloping profile condition; and Sponge is the sponge layer condition.

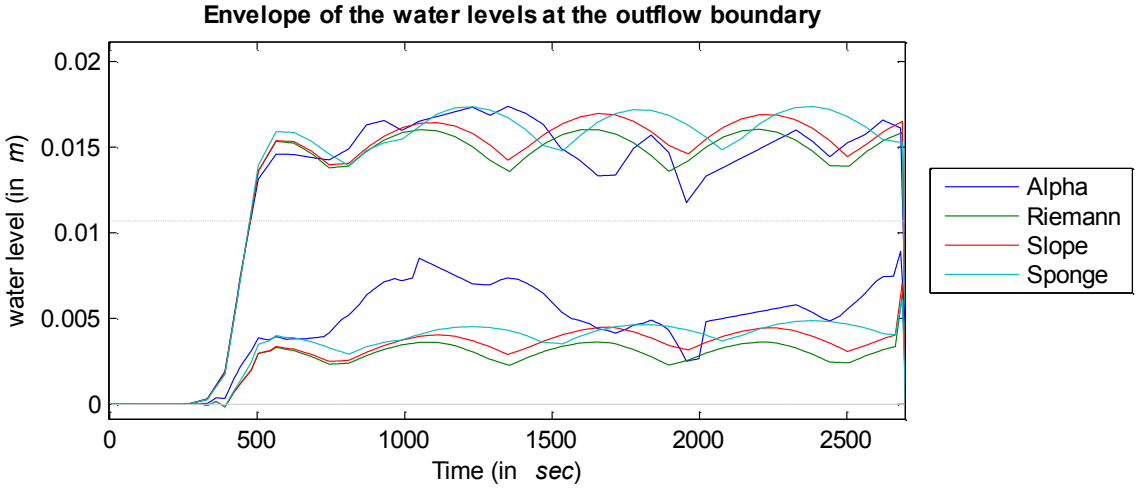

Figure 4.10 The envelope of the wave tops and mean for the hydrostatic simulations at the outflow boundary. Alpha is outflow condition using the α – value; Riemann makes use of a Riemann condition; Slope uses of a sloping profile condition; and Sponge is the sponge layer condition.

Envelopes of the wave tops and troughs are found from the results in figure 4.5, 4.6 and 4.7. The enveloping mean is averaged between the enveloping tops and troughs. This is shown in figures 4.8, 4.9 and 4.10 respectively, on page 35.
However instead of showing the last 900 seconds of the simulation, these figures show the whole simulation time. Note that only the envelopes of the tops and mean are shown. At the most right sides of each figure, the lines make a hard sudden drop to zero. This is due to the end of the simulation and the envelope ends.

Discussion of results for kh 0.01

In figure 4.2 on page 33 the gray line indicates the mean water level and the dashed gray lines indicate the wave amplitude. The influence of the velocity forcing becomes more apparent. It is at its maximum when the water level is at the mean. The model is in rest at the beginning of simulation time, meaning there are no velocities present. The derived wave height; as imposed by the forcing is not yet reached.

In figure 4.3 on page 33 the influence of the outflow boundary is minimal, since the different simulations have barely reached the outflow boundary, which has not yet had time to influence the full basin (right hand side of the figure).
The waves are not completely sinusoidal while the outflow boundary has yet to influence the wave over the basin length and friction is set to zero during the simulations. Therefore this asymmetry of the wave occurs due to geometry. Where the amount of water that passes through a grid cell (mass balance) needs to be equal for tops and troughs. Leading to a lower and higher flow velocity respectively; resulting in the asymmetry.

Figure 4.4, also on page 33, shows the water levels at the end of the simulation time. It clearly shows differences between the used outflow boundaries. The use of a Riemann boundary or a slope does not yield very different results for the water level; in the time frame. The simulation that uses of the α-value shows a rise of the water.
The pre-calculated wave length is 240 meters. This length has been predicted by the analytical solution. From figures 4.3 and 4.4 it is visible that it is matched by the simulations.

In figures 4.5 to 4.7 on page 34 a similar effect can be seen. The α-value shows a stronger water level increase then any of the other outflow conditions.
All four simulations show higher wave tops and troughs as the wave gets closer to the outflow boundary (compare figure 4.6, to 4.7 with each other). There is a water level increase at the inflow boundary of 1 centimetre and at the outflow boundary this is 5 centimetres. Thus the water level is a bit skewed. Meaning each simulation retains some water in the model. If the outflow was to be fully absorbing, this would not be the case.

From the envelopes in figure 4.10, it can be seen that the spin-up time is about 500 seconds in total. The wave reaches the outflow boundary after approximately 350 seconds and it takes approximately 150 seconds more for the water level to reach the desired amplitude.

These hydrostatic simulations are not fully absorbing, the envelopes (figures 4.8, 4.9 and 4.10, on page 35) of each simulation are a way to visualize reflection. The α-value boundary condition shows a different pattern from the other three simulations, which are more or less similar.
The patterns of the Riemann, sloping and sponge layer boundary all have a more or less parabolic shape, it signifies a standing wave with an approximate period of 500 seconds. This is most clearly seen in figure 4.10. The phase of the standing wave differs for those simulations. After inspection, it is seen that the phase difference between the sponge layer and the Riemann/ sloping profile boundary is largest. However, the sloping profile makes use of more added length to the model (which is not shown in any figures).

The difference between phases occurs due to the added model length for the sponge layer and sloping profile. When taking the Riemann boundary as measure, the length difference can be translated to a phase shift of 1.4π and 2.6π, respectively (Klopman, et al., 1999).
The amplitudes of the standing wave decrease over length; in figure 4.10 these are much higher than in figures 4.8 and 4.9. The source of the amplitude dampening is the incoming wave.

For these hydrostatic simulations with an kh-value of 0.01, the absorption of the outflow boundary is not a full 100%. The Riemann boundary is taken as measure, since this is considered to be a good theoretical outflow boundary for hydrostatic waves. It still shows some reflection.
In general the sloping profile and sponge layer do not seem to underperform in respect to the Riemann boundary.
The α-value boundary has been designed for non dispersive waves, so it should be able to perform well in these runs. However, this seems not to be the case.
Two possible reasons for this can be, it is hard to calibrate and this pre-calculated coefficient is not able to adjust to a change in wave. For instance wave asymmetry due to the geometry of a model.

Results for kh 1.00

In a similar fashion as the hydrostatic wave, previously described, simulations are made for its non – hydrostatic counterpart. The depth and length of the basin are adjusted to fit the same requirements as shown in figure 4.1.

The simulations with a sponge layer and slope both have the same added length of approximately 3 times the wave length (the added length is not shown). Additionally, the slope has been defined by equation 3.11 and 3.12, which defines the angle at 15 degrees. This is considered a mild slope.

In figures 4.11 to 4.13 on page 38, the surface elevations of different time frames in the basin are shown. Respectively the time frames considered are (1) the start of the inflowing wave; (2) an initial response of the surface elevations after the wave has hit the outflow boundary; and (3) end of the simulation time.

The three figures (4.14, 4.15 and 4.16) on page 39 show the surface elevation at different positions in the basin. These are respectively, at the inflow boundary, at the centre of the basin and at the outflow boundary.
Like with the previously presented hydrostatic simulation, these non – hydrostatic simulations only shows the last part of the simulation (15 seconds). Again, these do therefore not show the spin up and the initial response to the outflow boundary condition.

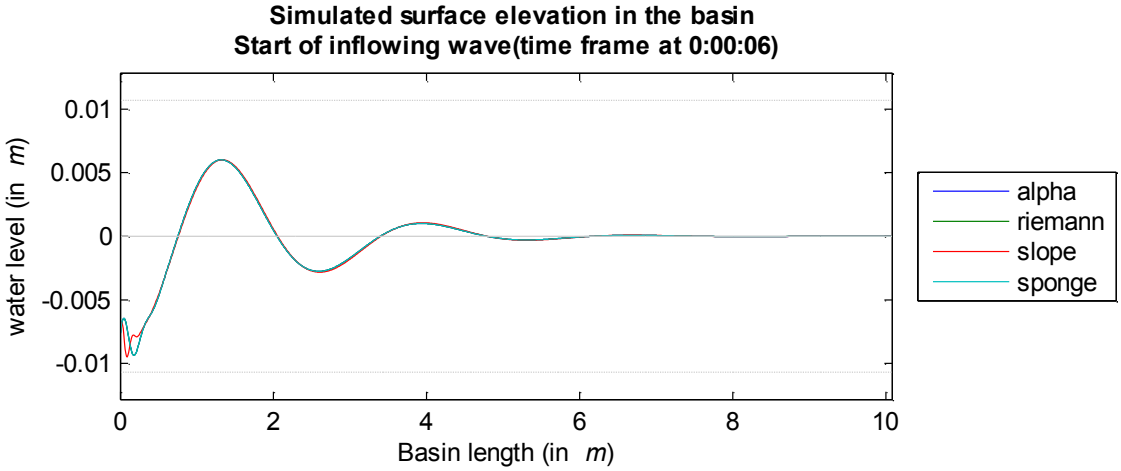

Figure 4.11 Inflow of the non - hydrostatic wave in the basin at the start of the simulation. With different outflow conditions. In the legend: Alpha is outflow condition using the α – value; Riemann makes use of a Riemann condition; Slope uses of a sloping profile condition; and Sponge is the sponge layer condition.

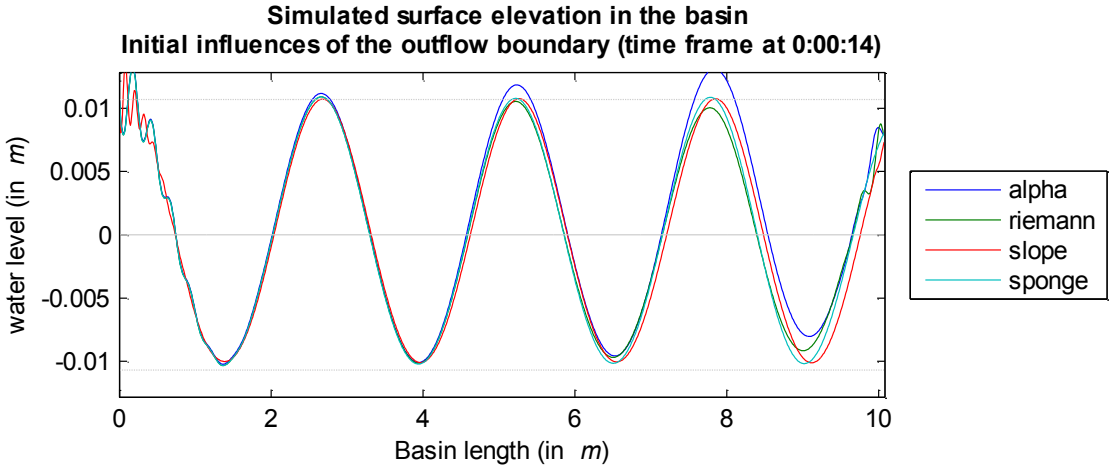

Figure 4.12 Initial influences of the boundary condition for the non - hydrostatic wave. With different outflow conditions. In the legend: Alpha is outflow condition using the α – value; Riemann makes use of a Riemann condition; Slope uses of a sloping profile condition; and Sponge is the sponge layer condition

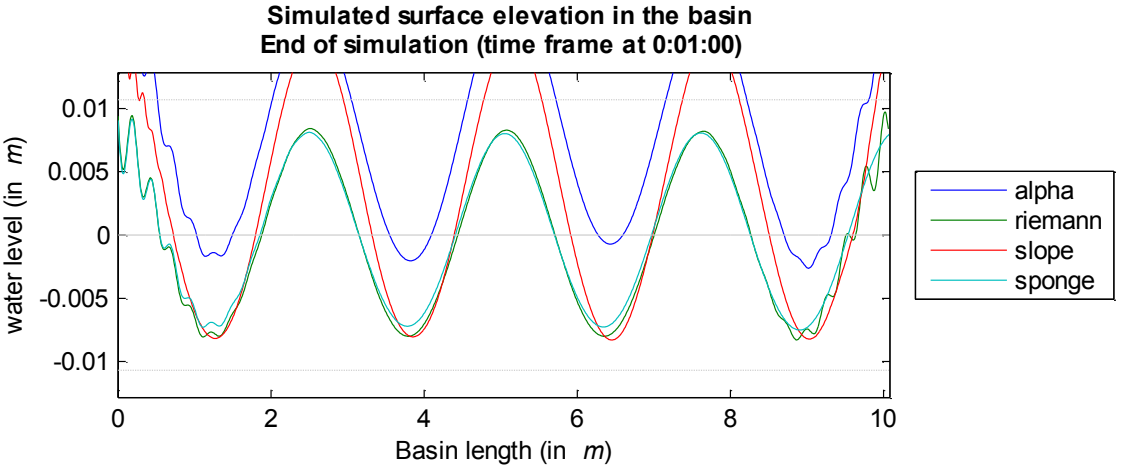

Figure 4.13 Surface elevations at the end of the simulation. In the legend: Alpha is outflow condition using the α – value; Riemann makes use of a Riemann condition; Slope uses of a sloping profile condition; and Sponge is the sponge layer condition.

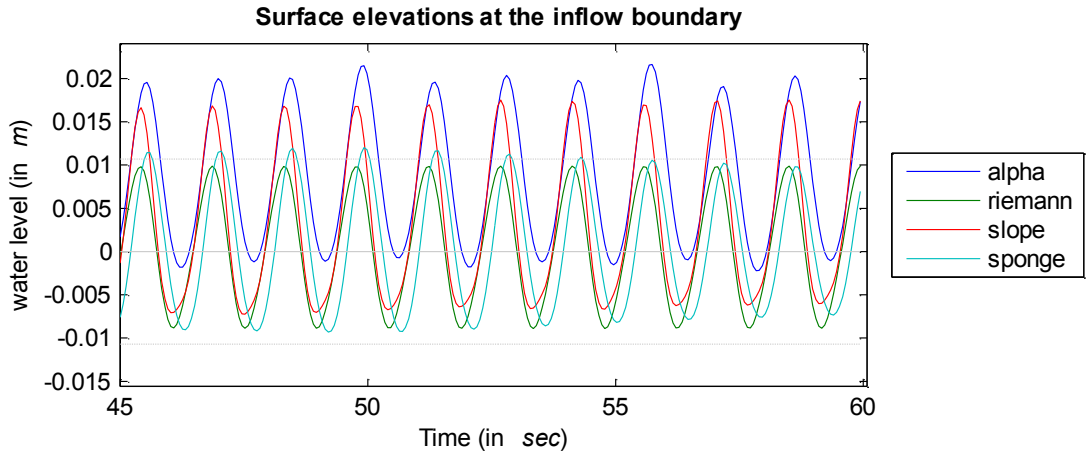

Figure 4.14 Surface elevations for the last 15 seconds of the non - hydrostatic simulations at the inflow boundary. Alpha is outflow condition using the α – value; Riemann makes use of a Riemann condition; Slope uses of a sloping profile condition; and Sponge is the sponge layer condition.

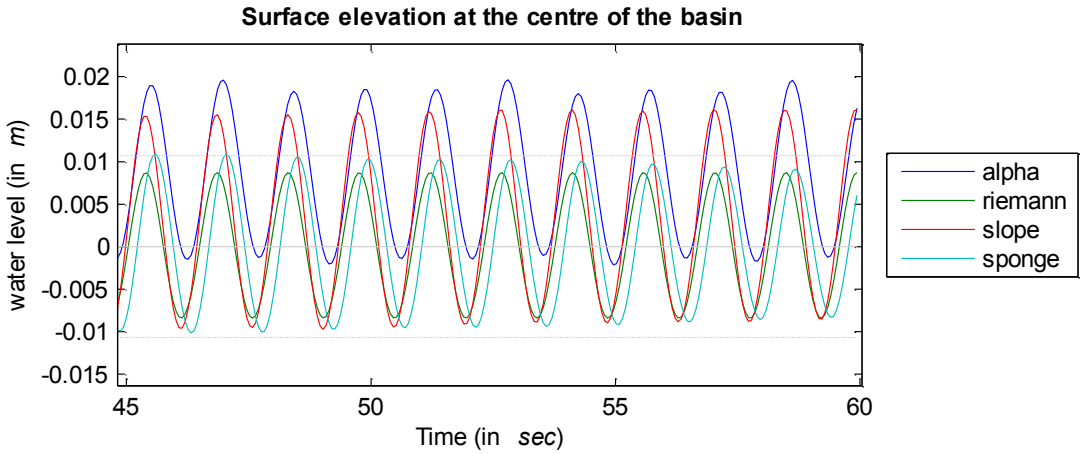

Figure 4.15 Surface elevations for the last 15 seconds of the non - hydrostatic simulations at the centre of the basin. Alpha is outflow condition using the α – value; Riemann makes use of a Riemann condition; Slope uses of a sloping profile condition; and Sponge is the sponge layer condition.

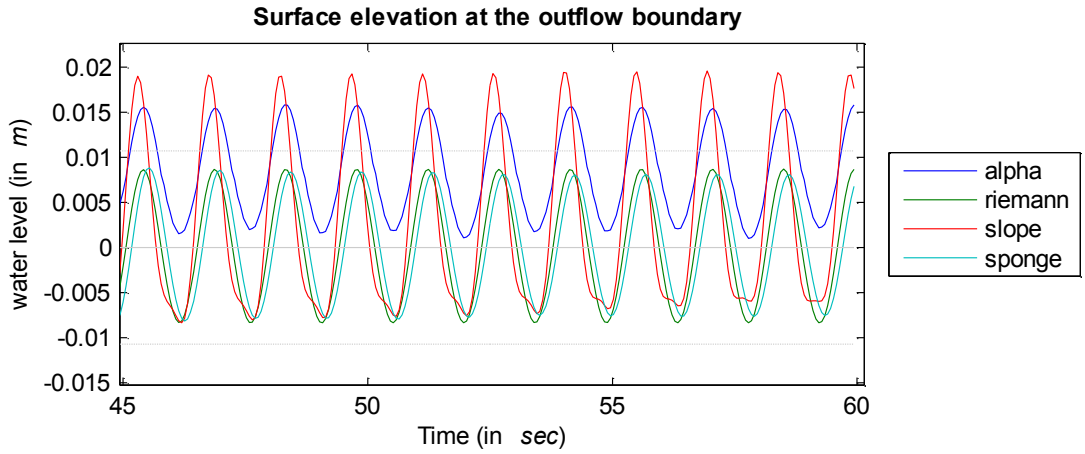

Figure 4.16 Surface elevations for the last 15 seconds of the non - hydrostatic simulations at the outflow boundary. Alpha is outflow condition using the α – value; Riemann makes use of a Riemann condition; Slope uses of a sloping profile condition; and Sponge is the sponge layer condition.

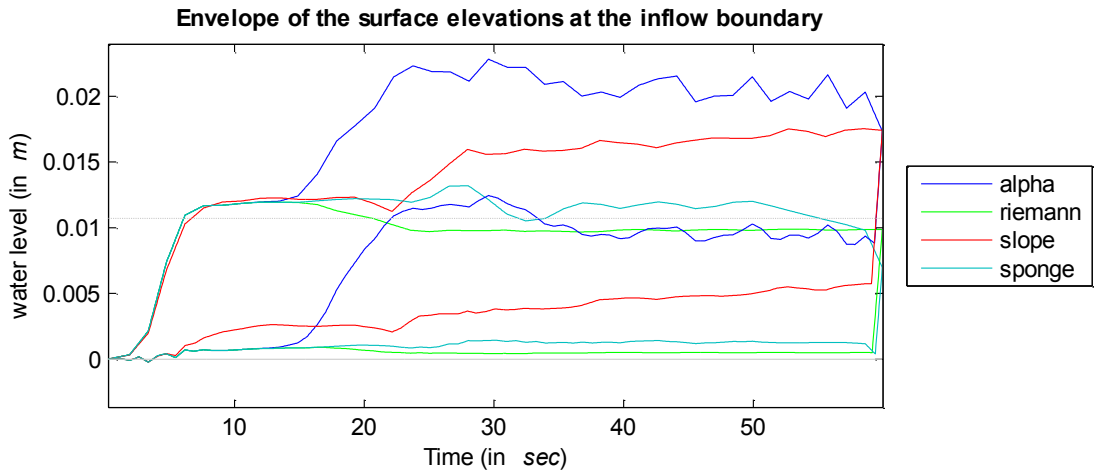

Figure 4.17 The envelope of the wave tops and mean for the non - hydrostatic simulations at the inflow boundary. Alpha is outflow condition using the α – value; Riemann makes use of a Riemann condition; Slope uses of a sloping profile condition; and Sponge is the sponge layer condition.

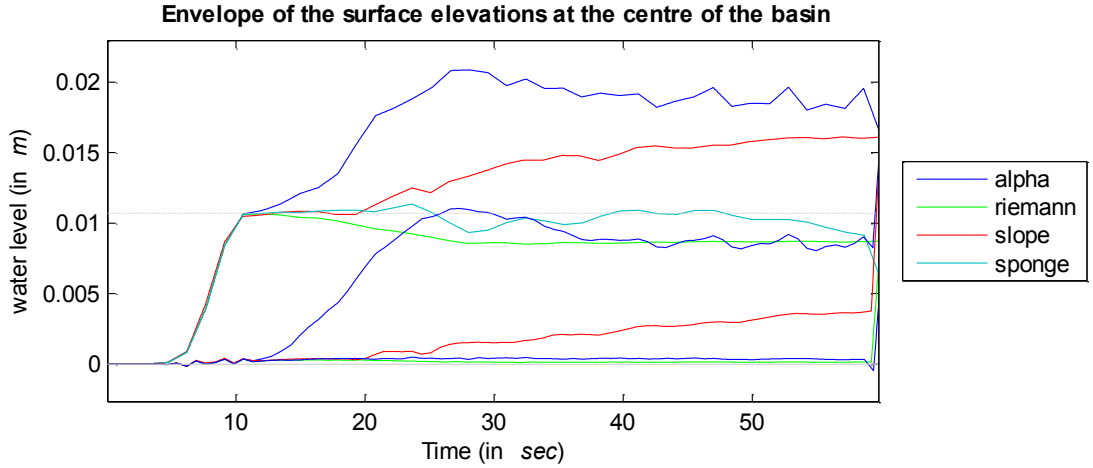

Figure 4.18 The envelope of the wave tops and mean for the non - hydrostatic simulations at the centre of the basin. Alpha is outflow condition using the α – value; Riemann makes use of a Riemann condition; Slope uses of a sloping profile condition; and Sponge is the sponge layer condition.

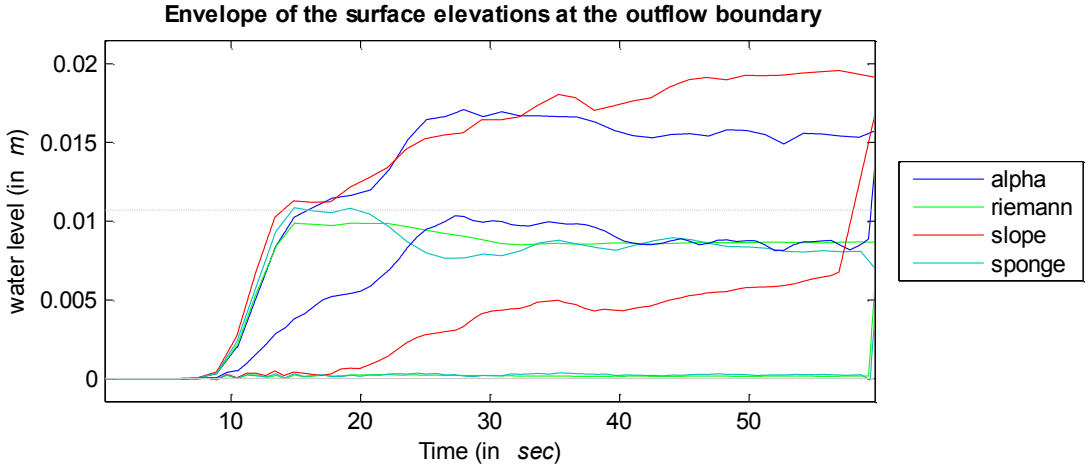

Figure 4.19 The envelope of the wave tops and mean for the non - hydrostatic simulations at the outflow boundary. Alpha is outflow condition using the α – value; Riemann makes use of a Riemann condition; Slope uses of a sloping profile condition; and Sponge is the sponge layer condition.

The figures 4.17 to 4.19 on page 40 shows the envelopes of the wave top and mean surface elevations are shown. It must be noted that at the end time of the simulations the mean always errs. This is an error in the written Matlab script due to the fact that the shown mean is calculated as the average value between a top and a trough (troughs are not shown). This is most clearly seen in figure 4.19 for the mean water level of the simulation with a sloping profile (red line).
The strong increase of the mean water level for the simulation with the sloping profile clearly shows a lack of stability, due to a course grid size which leads to ill predictions of surface elevations.

Discussion of results for kh 1.0

In figures 4.11 to 4.13 on page 38 time frames are depicted. Again the first figure shows, due to use of a velocity forcing, a sinusoidal function that does not immediately correspond to the design amplitude of the free-surface elevation, which is 0.107 meter. The outflow boundary has not yet had any effect on the wave. The results are identical, which meets expectations, since the outflow boundary has not yet had any influence.
A small error is seen at the boundary of the inflow border. Over time, it seems to expand in the direction of the wave propagation (figures 4.12 and 4.13). However, it confines itself to the first meter of the basin, which is equal to $1/10^{th}$ of the basin length.
The time frame in figure 4.12, of initial contact with the outflow boundary, starts showing slight differences. Use of the α–value (blue line) shows reflection has occurred. The wave tops and troughs are slightly heightened. While at the boundary there is no such thing visible yet. Over time the amount of water in the basin rises (figure 4.13).
For the Riemann boundary (green line) a trailing error begins to occur at the outflow boundary, which becomes better visible in figure 4.13. However, like the error at the inflow boundary, it confines itself to the first meter in front of the outflow boundary.
The sponge layer (turquoise line) has an almost perfect fit with the Riemann boundary condition throughout figures 4.11 to 4.13. However, it does not show the same trailing error at the outflow boundary.
At the initial contact with the outflow boundary, the sloping profile (red line) does not show any real differences with the sponge and Riemann simulations. At the end of the simulation (figure 4.13), the wave amplitude has increased.

Inspection of the surface elevations over time, for the three stations in figure 4.14 to 4.16 on page 39 confirm the results seen at snap shots of the time frames.
The simulation with the α-value boundary (blue line) shows an increased mean water level at all stations for the last 15 seconds of the simulation. A second change is seen in the amplitude (predefined at 0.0107 meters), which reduces near the outflow boundary (figure 4.16).
The Riemann boundary (green line) does not have an increased mean water level. However, like the α–value there is a small decrease in amplitude near the outflow boundary.
The sponge layer (turquoise line) compares well to the Riemann boundary. There is a marginal shift in wave period. Furthermore the amplitudes are a bit larger in all three surface elevation stations.
The sloping profile (red line) shows a slightly elevated mean water level. However, more prominently visible is the increased amplitude of the wave, which is visible throughout figures 4.14 to 4.16. One last difference compared to the other boundary conditions, when using a slope is seen in figure 4.16. Tops are more peaked compared to its troughs. This is due to the use of the slope.

The envelope of the tops and mean water levels (shown in figures 4.17, 4.18 and 4.19 on page 40) show the complete time lines instead of the last 15 seconds. Figure 4.17 shows it takes roughly 9 seconds before the amplitude of original design is reached. Furthermore, it shows that the selected input for the velocity amplitude gives slightly higher wave amplitude then predicted by short wave theory.
The simulation with the α-value (blue line) shows a bit of a increase in mean water levels once the outflow boundary has been reached. At approximately the 11^{th} second, after the reflected wave has

met the inflow boundary again, an extreme increase in mean water level is seen (figure 4.17). This is seen throughout the other envelopes as well. A stable solution seems to be reached after the volume of the water has increased. The wave amplitude is still the same.
The simulation with a sloping boundary at the outflow (red line) shows an increase of the water volume. This unexpected rise of volume begins ones the wave has met the slope at approximately 18 seconds (figure 4.19) and slowly starts to propagate back to the inflow boundary, increasing the water volume in the basin. This sudden jump of volume is best seen in figure 4.17 between the 22nd and 28th second.
The sponge layer (turquoise line) and Riemann boundary (green line) respond alike. The mean water level is slightly elevated at the inflow boundary (figure 4.17), while the amplitude is slightly underestimated in the simulation, when compared to the pre-calculated amplitude. The sponge yields more variable tops then the Riemann boundary. However, overall there is a good match between the results.

Implications for two dimensional simulations: expectations from theory and one dimensional simulated results

The original goal of these simulations was to assess how well the various boundary conditions were able to fully absorb incoming waves.

The α-value fails at both the hydrostatic and non- hydrostatic simulation runs. In the hydrostatic simulation, the α-value creates a resonating wave, with roughly twice the frequency of the other boundary conditions. The non–hydrostatic simulation does absolutely nothing except fill the basin.
In chapter 3 it became clear that the use of the α–value as boundary condition is based upon long wave theory. The input value for α needs to be pre calculated and manually added to the simulation input file.
Considering both simulations are one dimensional and yield results that are not nearly absorbing enough. Further exploration in the two dimensional plane will be useless. It will also be cumbersome if the model space makes use of depth changes. A recalculation of the α–value will be required.
Introduction of multiple wave periods by use of a Fourier series at the inflow boundary or by resonance in a basin due to geometry will complicate calculation of a value for α even more. The (mean) period of either must be known beforehand.
In conclusion, the results and requirements to make the α-value work for hydrostatic simulations is more difficult than expected. For non-hydrostatic simulations it is impossible, which is not strange since it was designed with low kh values in mind only. It makes full absorption very hard to acquire. Therefore it will not be further explored for the two dimensional plane. Furthermore this boundary condition seems like an unlikely candidate for partial absorbing boundaries.

The Riemann boundary condition is an absorbing boundary condition for hydrostatic waves by design. Full absorption is not acquired in the hydrostatic simulation, but comes close. For the non-hydrostatic method absorption is well approximated. This is unexpected, because the boundary condition originates from hydrostatic theory which assumes small values for kh. This requirement is not met. The reason this does work, is due to the use of one depth layer. It effectively means that the pressure over depth for both methods is in fact linear (with a correction for pressure for the non – hydrostatic method). It is suspected but not investigated here, that the use of two depth layers will significantly decrease the absorption.
This boundary condition is easiest to implement in .

In conclusion, results with a Riemann boundary condition are good for both types of simulations. This boundary condition will be further explored in the two dimensional pane. Furthermore, it seems likely to be a good candidate to be a starting point for partial absorbing boundaries.

The sponge layer boundary condition has been specifically implemented in TRIWAQ for non – hydrostatic simulations. In hydrostatic simulations it performs similar to the Riemann condition, which was expected. Obviously it was expected to perform well in the non – hydrostatic simulation as well.
In chapter 3 the limitation to imposing a sponge layer as boundary condition is described. First, it cannot currently be implemented on all boundaries. It is confined to the positive boundaries in the x - and y – plane of the grid. Secondly it requires additional grid space.
In conclusion, results are as expected, since this condition has been successfully implemented in (Zijlema, et al., 2005). This boundary condition will be further explored in the two dimensional pane. Furthermore, the sponge layer seems to be a good candidate for partial absorbing boundaries, since friction coefficient κ is relative easy to manipulate, as is the shape of the coefficient over the added length.

The sloping boundary condition performs as expected in the hydrostatic simulation. However in the non - hydrostatic simulations it severely underperforms, which is unexpected. Since, in theory, this gentle slope should alter the incoming wave from dispersive to less (none) dispersive, or non – hydrostatic to hydrostatic. Therefore results should correspond with the Riemann and sponge boundary. This is not the case.
The coarseness of the grid is likely to be at fault. In order to make sloping boundaries feasible, grid resolution has to be increased. Meaning more computational time is needed. Besides, stability of the computation has to be reassessed, making this a tedious process.
Thus in conclusion, the needed increase of resolution with the added model space length makes the use of a sloping profile very costly for two dimensional simulations and is therefore discarded. Furthermore, by adjusting the angle of the sloping boundary, partial reflection can be acquired. In this regard it holds promise, but seems mostly to be of academic value.

Chapter 5: 2 dimensional harbour simulations

This chapter will focus on 2 dimensional modeling of a theoretical harbour. The main purpose is to test how well TRIWAQ-NH performs for 2 dimensional modeling. It also tests the reflective capabilities of the Riemann and sponge layer boundary conditions inside the basin; where the propagating wave is able to meet the boundary condition under an oblique angle of incidence.
The 2 dimensional computations are based on the simulations done by (Isaacson, et al., 1990). Their paper describes a method which is able to adequately predict diffraction and partial reflection. The setup of the model is meant for a generic layout.
Reproduction of these simulations tests the capabilities of TRIWAQ-NH and is considered adequate validation for wave propagation in harbours, when compared with the hydrostatic method. Shown simulations are the two limiting cases for reflection; full reflection and full absorption.

Modeling domain of the 2 dimensional the model

The modeling domain of the harbour exists of two parts; an exterior and interior region. The water depth is constant in both therefore the wave number k is equal in both. The regions are separated by two breakwaters whose tips form the harbour entrance.
At the boundary of the exterior region a wave forcing is imposed. It is a monochromatic wave which travels orthogonally towards the interior region. Reflection along the shoreline and breakwaters in the exterior region are assumed to have no influence on the wave propagation on the interior region. This is neglected, although it may not be completely realistic.

Model setup

A fundamental layout is chosen. This is a theoretical harbour with a rectangular basin of constant depth (figure 5.1). Meaning the wave physical wave process refraction will have no influence (chapter 1). The width of the entrance is equal to the length of the wave, thus the process of diffraction is going to occur and depending on the boundary conditions used the quay walls will show reflection. From chapter 4 it follows that two types of boundary conditions are selected which will be further investigated. These are the Riemann and sponge layer condition.

The length and width of the basin are both 300 meters. For the simulations a wave with a length L of 50 meters is chosen. The depth d is set to 20 meters. The corresponding wave period T is 5.7 seconds. Its kh- value is 2.51, making this a highly dispersive wave (table 5-1).
In this study one of the limitations is the use of linear waves. Meaning $ka \ll 0$ should hold. Each simulation, for a 2 dimensional harbour case, has defined amplitude â of 0.25 meter. Converting it to the velocity forcing (û), as described in chapter 3 it yields 0.11 meter a second. It must be noted that the wave is more dispersive and less linear then in the 1 dimensional test case. This is the same setup as described in the paper of (Isaacson, et al., 1990).

General rule of thumb for numerical simulations is to use 20 grid points per wave length, which properly approximates a propagating wave. However these simulations have the wave segmented into 40 point, which results in a Δx of 1.25 meters (table 5-1).
Reasons are twofold. First, with the high dispersion value for this wave, these extra grid points will describe the shape of the wave better. Secondly, due to the symmetrical nature of the basin standing waves might occur, with different periods.

The following paragraphs will each contain two simulations each uses a different method (hydrostatic versus non–hydrostatic) and will have the same boundary conditions. Their differences will be shown by (1) a time line of the surface elevations; (2) total energy in the basin, and (3) two contour plots.

Each contour plot is a snapshot of the surface elevations; at a time frame where the total energy level has stabilized. These are intended to show differences in the wave pattern for hydrostatic and non – hydrostatic modeling. Due to the symmetrical nature of the basin, the wave pattern will be identical for the left hand and right hand side of the basin. It allows for an easy comparison between the two methods.

Wave specifications	
$T = 5.7$ seconds	$ka = 0.003$
$L = 50$ meter	$kh = 2.51$
$\hat{a} = 0.25$ meter	$\hat{u} = 0.11$ m/s

Basin specifications	
$depth = 20$ meter	
$length = 300$ meter	
$width = 300$ meter	$\Delta x = 2.5$ m

Table 5-1 Summarized wave specifications for the 2 dimensional simulations

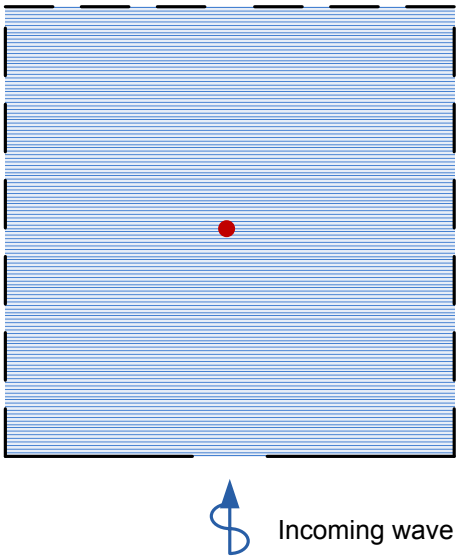

Figure 5.1 Rectangular harbour. The red dot is the centre of the basin. The dashed lines show boundary conditions that may vary per simulation.

In figure 5.1, the red dot shows the location of time line of the surface elevations. The dashed lines indicate (left, right and upper line) changed boundary conditions.

In general, stability of a simulation can be calculated/ predicted by the (Courant–Friedrichs–Lewy) CFL condition (Stelling, et al., 1999). This condition describes whether convergence for partial differential equations is reached numerically. Like those TRIWAQ-NH uses.
Each simulation has a runtime of 10 minutes (or 600 seconds). The time interval (Δt) is 0.001 minutes or 0.06 seconds. With a wave period (T) of 5.7 seconds this corresponds to 95 time frames per wave period.
With these settings for both grid (Δx) and time step (Δt), both the hydrostatic and non–hydrostatic method are stable according to the CFL condition.

The Riemann boundary

The first set of two simulations, utilizes the Riemann boundary (see chapter 3 for the mathematical background of this condition). It is implemented on all the dashed lines in figure 5.1.

In figure 5.2 the surface elevations are shown. This figure consists of three plots. The upper plot shows the surface elevations at the centre of the basin (red dot in figure 5.1)
In the upper plot, two things need to be noted. First, and most obviously, the spin–up time for the non–hydrostatic model takes roughly 2 times as long when compared to the hydrostatic method. The user can not influence this effect, since it is due to approximation differences between the two methods (see figure 2.5 on page 24). Secondly, the predefined amplitude of $\hat{a} = 0.25$ meter at the inflow boundary is not present inside the basin. There is a slight difference in amplitudes between the two methods.
In the envelope plot of the surface elevations these two differences are seen as well. The envelope shows more clearly that the amplitudes between methods differ. With the non–hydrostatic (NH)

method leading to slightly lower amplitudes, when compared to the hydrostatic (hydro) model. This is presumably the result of the pressure correction done in the NH–method.
The envelopes show a third effect for the hydro–method. The mean water level shows a small rise. This effect was also seen in the one dimensional simulations.
The third plot is a zoom of the last minute of the simulation. It shows there is no difference in wave periods between methods. Which is expected, since the period (T) is a constant for each wave at any point in time and place. Lastly, the hydro–method does not show wave asymmetry like the first set of tests of the one dimensional model.

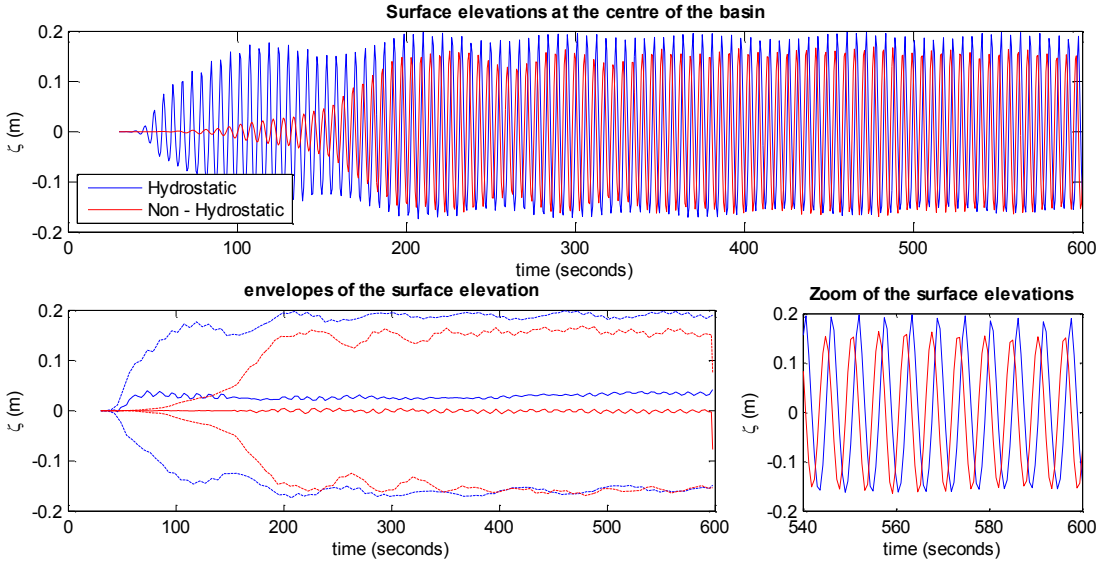

Figure 5.2 Surface elevations at the centre of the basin for the Riemann boundary

The next two figures (5.3 and 5.4) on page 47 each show a contour plot of both the non–hydrostatic and hydrostatic method. On the left hand side results of the NH–method are depicted. On the right hand side the Hydrostatic results are shown. Figure 5.3 shows the contours just after the spin–up time is finished (at 250 seconds) and equilibrium (in total energy) is roughly reached. Figure 5.4 shows contours of the surface elevations far into equilibrium.

Many differences are visible. Not only differences between the two methods, but also between the two different time frames. The latter does not necessarily give the proper impression, because contours plots are able to change rapidly per time frame. So as a word of caution, these differences are not purely due to a more advanced time frame, where equilibrium is more or less established; see figure 5.5.

Let's start with the differences between methods with respect to the propagating wave. The first thing standing out is that the amount of contours on the left hand side always seems to have the upper hand. This indicates two things. First, the non - hydrostatic method has more zero crossings per time frame. Meaning there is a difference in wave length between the two methods. This is best seen along the centerline (the dashed red line) in figure 5.3. There are six waves present for the NH–method, and almost four in the hydro–method. This corresponds to wave lengths of 50 meters and 80 meters respectively. This corresponds with the wave theory for transitional waters and shallow water.
A second observation can be made from this amount of contours. The left hand side has more condensed contour packing. Meaning the NH–method is more peaked, which is attributed to the smaller wave lengths. When following the (dashed red) centre line, the contours are equidistant. It indicates a propagating wave with no asymmetries. For the hydrostatic method this does the distances between

Contour plot with use of the Riemann boundaries

Non – Hydrostatic method *Hydrostatic method*

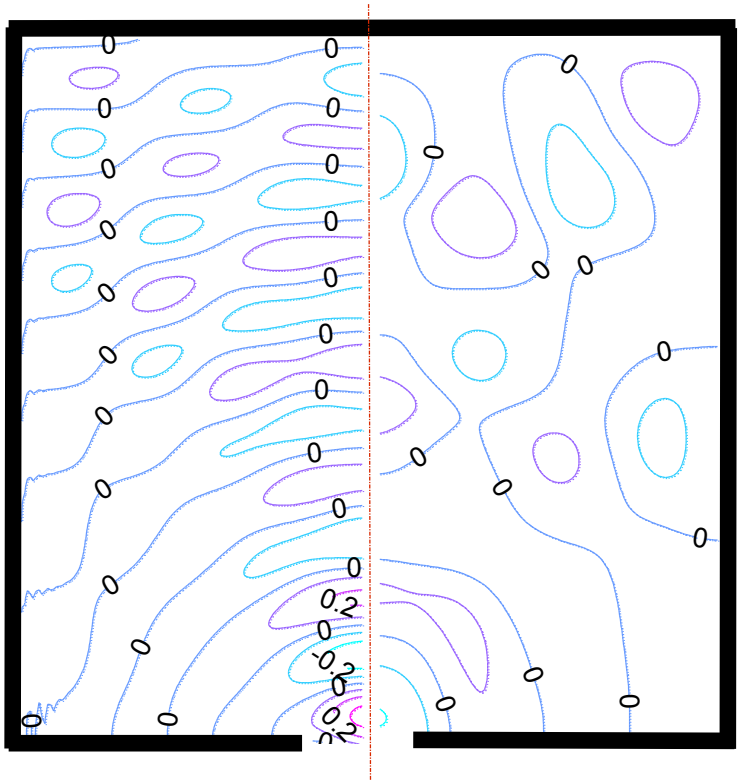

Figure 5.3 Contour plot of the surface elevations at $t = 250$ seconds for the Riemann boundary

Contour plot with use of the Riemann boundaries

Non – Hydrostatic method *Hydrostatic method*

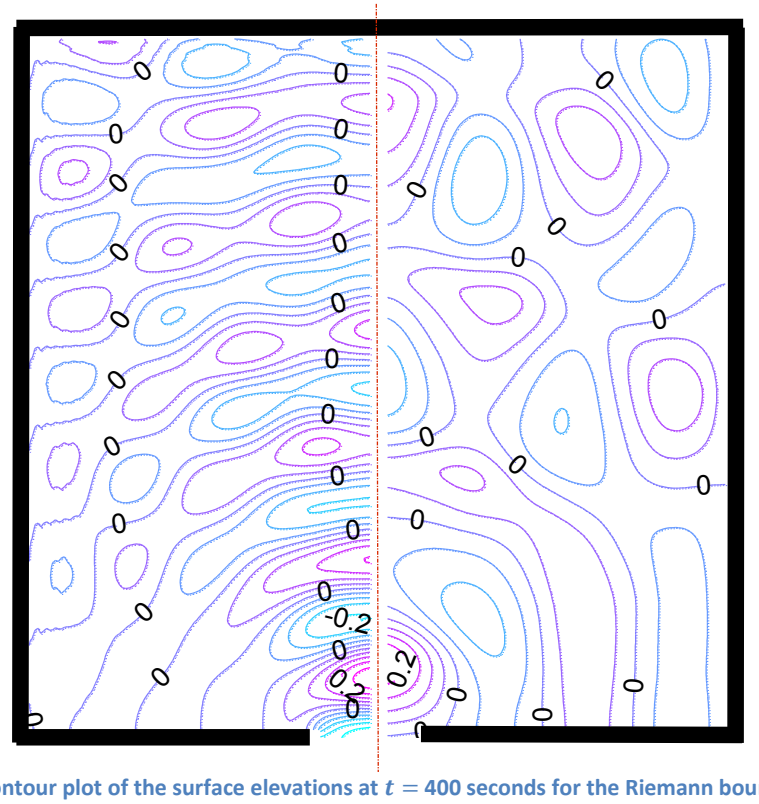

Figure 5.4 Contour plot of the surface elevations at $t = 400$ seconds for the Riemann boundary

The zero crossings are roughly equidistant in all traveling directions for the diffracting wave (best seen in figure 5.3). This is most obviously seen for the non–hydrostatic simulations. The hydrostatic method does this as well. However due to the Riemann boundary not being fully absorbing, the sides distort the picture. In a similar fashion, the upper boundary has some reflection as well. This is best seen in figure 5.3, where the lower quadrant of non–hydrostatic method does not show the closed circle contour lines. These indicate that reflection occurs. Overall these phenomena correspond with the 1 dimensional results of the Riemann boundary found in chapter 3.
A closer inspection of the side boundary for the non–hydrostatic simulation shows that the diffracted wave copes with Riemann condition, but shows errors. The contours show, wrinkles and wiggles perpendicular to the side boundary. This is seen in each figure for all contour lines, but most visible in the lower quadrant in of figure 5.3. This error seems related to the direction of the velocities, or angle of incidence of the wave, since this does not happen at the upper boundary. Furthermore this only happens for the NH–method.

Last the time evolution of the total wave energy in the harbour basin can be calculated. The method used to calculate the energy is by summation of the energy from all instantaneous amplitudes in the grid cells per time step. With the use of a curve fitting tool these instantaneous energy levels are averaged. This is shown in figure 5.5. The upper plot shows the fits, the lower plot shows the residuals of the fits.
In order to find an exponential fit for the non–hydrostatic simulation, the first 100 seconds have been ignored, as the residual plot shows. This is purely done from a practical perspective in order to make the fit.
The energy in the basin is higher for the non–hydrostatic method. Since there are “more” waves in the basin, this is expected. It also shows that the contour plot of figure 5.3 is not yet in full equilibrium state. This was also found by the missing rounded contours in the lower quadrant of the plot.

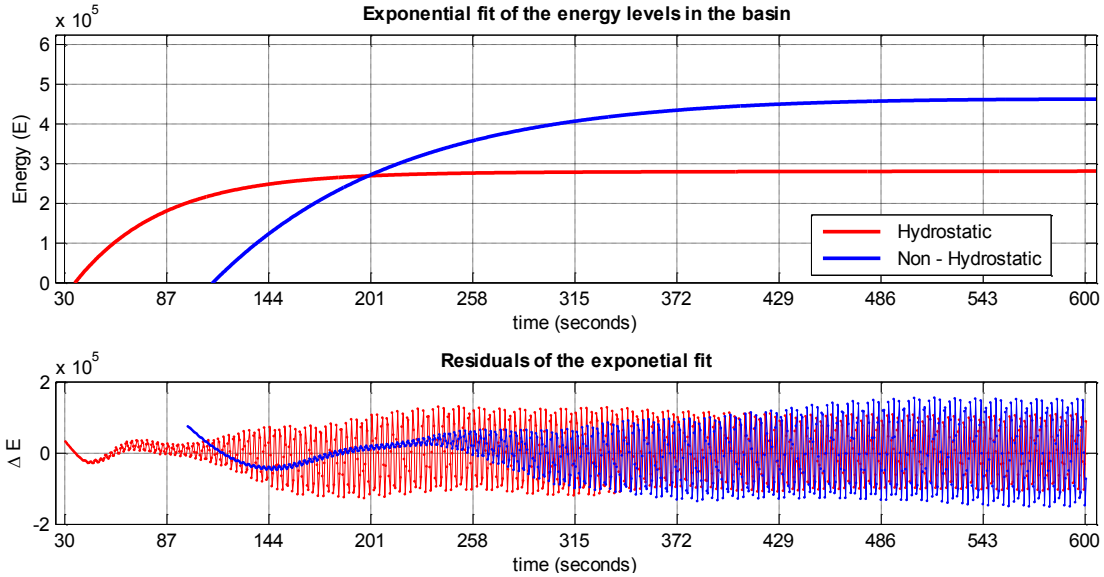

Figure 5.5 Fit of the total energy in the basin for the Riemann boundary condition

The sponge layer boundary

The next set of simulations will make use of a sponge layer at the upper boundary. Since the model TRIWAQ –NH is only able to provide sponge boundaries in the positive direction of m, n for the grid; it would mean that a second sponge could only be implemented at the right side (see chapter 3). However this would not yield the symmetrical results. Therefore the boundary conditions used at the sides are described by Riemann.

The sponge layer has a length of three times the design wave length (150 meters). This is added length to the model space (see chapter 3), which has not been added in the visualization of the contour plots (figure 5.7 and 5.8).

This paragraph will solely describe the sponge layer. No comparisons are made with the previous paragraph. This will be done in the next paragraph, which will round up the open boundary conditions.

In figure 5.6 the plots again shows the surface elevations over time at the centre of the basin (red dot in figure 5.1). The upper plot shows that spin–up time for the NH–method takes roughly over to 3 minutes or 200 seconds.

From the envelopes it is seen that the hydrostatic method shows a mean water level rise which gradually returns to the values as the NH–method has. The wave amplitudes are very similar in both methods. Although these values do not reflect the design amplitude of 0.25 meters, they are very similar.

The zoom of the last minute, shows a difference between the waves for each method. The non–hydrostatic method counts 11 troughs and the hydro–method counts 10 respectively. This difference in tops and troughs count is due to propagation speed differences between methods, which leads to a relatively different wave in time. Both methods corresponds with the design value for the wave period of (T) 5.7 seconds.

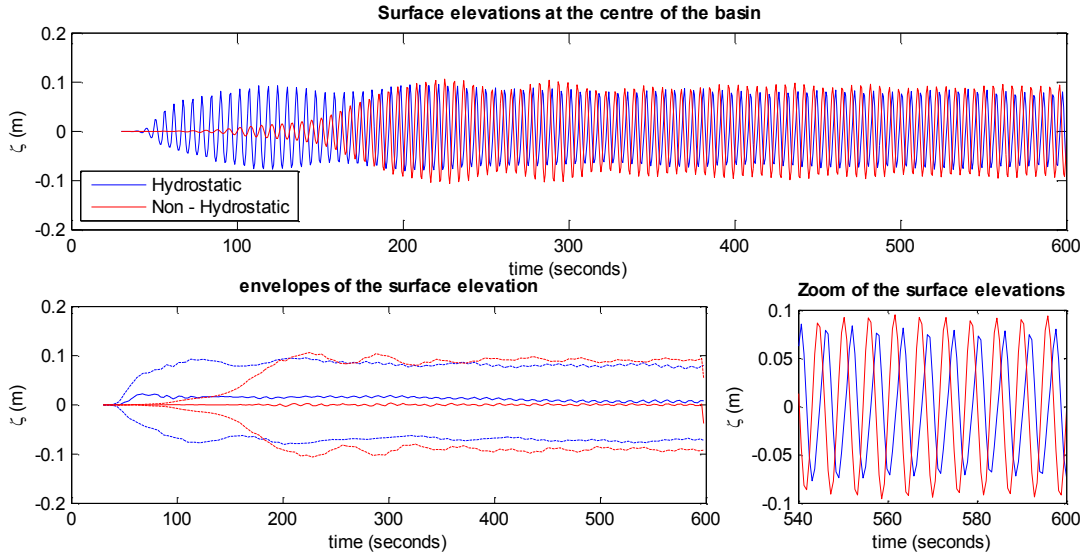

Figure 5.6 Surface elevations at the centre of the basin for the Sponge layer boundary

The next two figures (figure 5.7 and 5.8) on page 51 show the contour plots at two different time steps. These are shown at 250 and 400 seconds. First the contour lines of the surface elevation are inspected with respect to the propagating wave. After which the behavior of these lines will be regarded with respect to the sponge boundary condition.

Contour plot with use of Sponge layer boundary

Non – Hydrostatic method *Hydrostatic method*

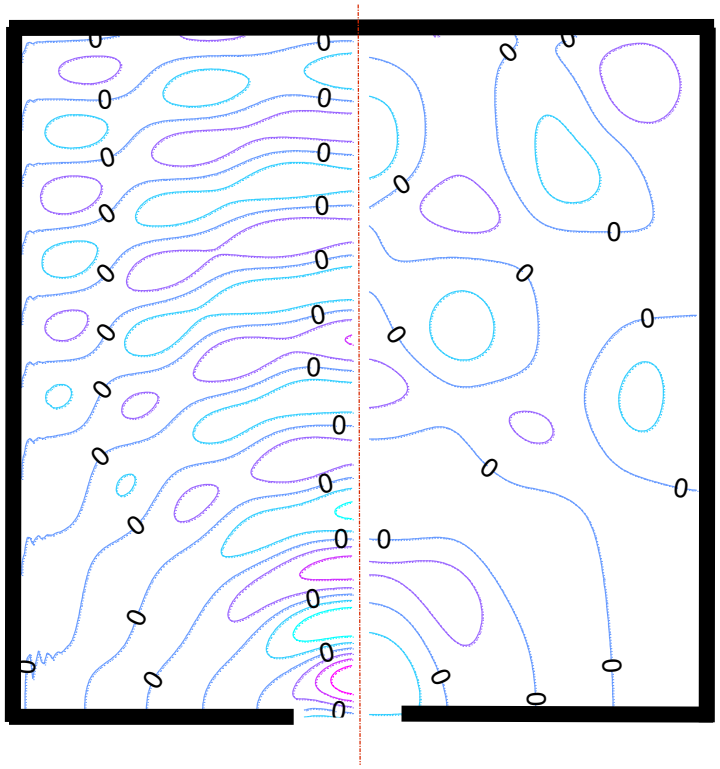

Figure 5.7 Contour plot of the surface elevations at $t = 250$ seconds for the sponge layer boundary

Contour plot with use of Sponge layer boundary

Non – Hydrostatic method *Hydrostatic method*

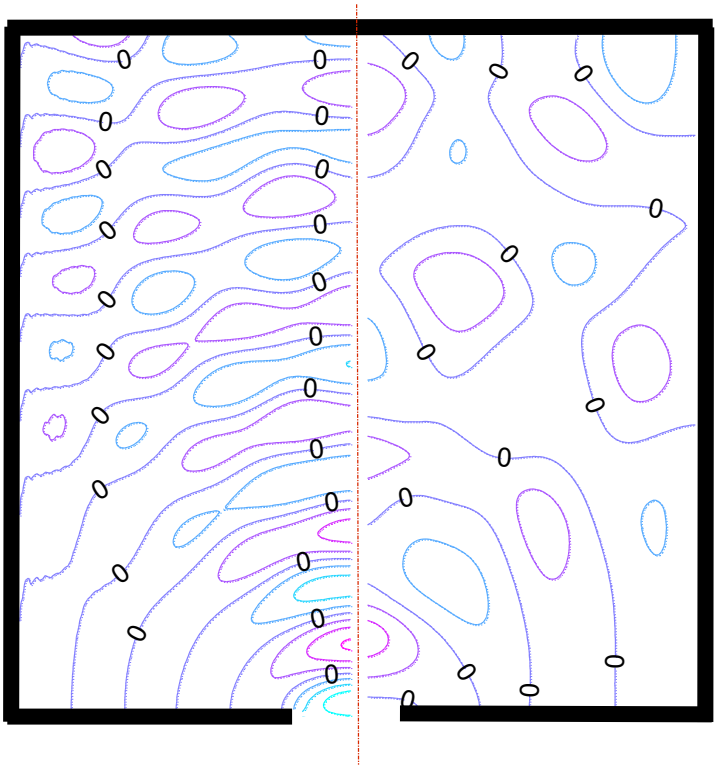

Figure 5.8 Contour plot of the surface elevations at $t = 400$ seconds for the sponge layer boundary

The first notable difference between the NH–method and the hydro–method is the amount of contour lines. When following the centerline (dashed red line), it shows more zero crossings for the NH–method. Meaning the wave length is different for both methods. There are respectively 6 and roughly 5 waves present in the basin. This corresponds with the difference in wave period from figure 5.6.
Spaces between contour lines are fairly equidistant for the NH–method. This is more or less true for the hydro–method too. This is best seen in figure 5.7, although it can be somewhat harder to envision in figure 5.8 due to reflections.

The upper boundary has the sponge layer implemented. Reflection is present in each method. However when comparing both non–hydrostatic plots, the first thing of notice is that in both contour plots the lower quadrant shows no circle like contours, meaning that the reflective wave seems to have dampened.

The side boundaries are Riemann conditions that behave the same as in the previous set of simulations. This error seems related to the direction of the velocities, or angle of incidence of the wave in the NH method, since this does not happen at the upper boundary.

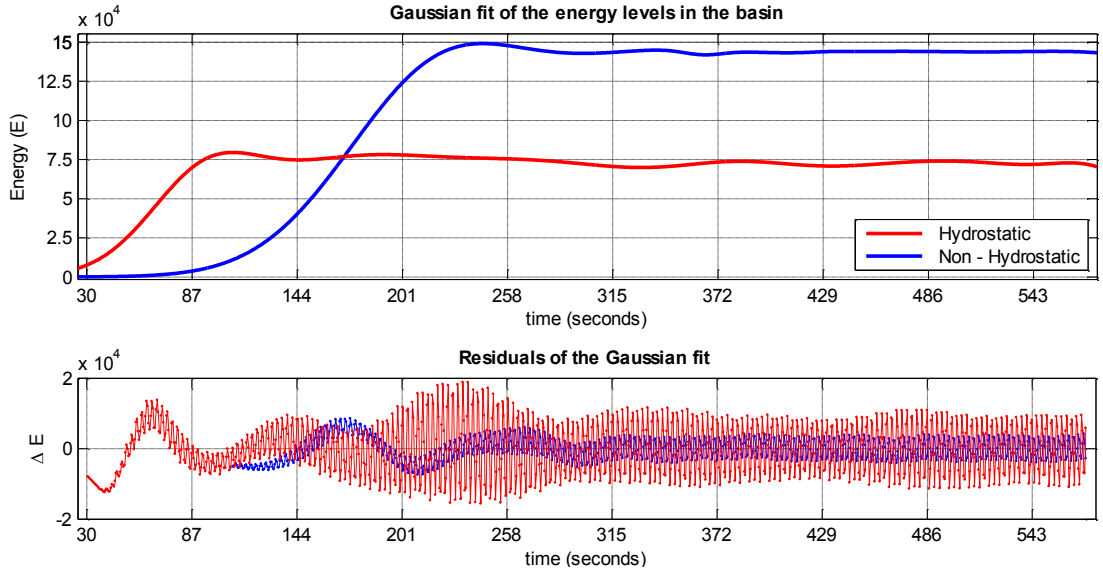

Figure 5.9 Fit of the total energy in the basin for the Sponge layer boundary condition

Figure 5.9 shows two plots, with the upper plot being a Gaussian fit of the total energy. The lower plot shows the residuals of the fit. In order to find a proper fit, the 100 seconds have been neglected from the simulation.
Note that the type of fit is different from the Riemann boundary conditions, which used an exponential fit. This is due to this small energy increase (for both methods) before stabilizing. A selection criterion for the type of fit is based on “best fit”.

For both the non–hydrostatic and hydrostatic method, there is a slight energy increase before the total energy stabilizes. Simulations are considered stable after 280 and 160 seconds respectively.
The contour plot at time frame 250 (figure 5.7) is actually at a moment where the total energy is slightly increased. It explains why there are more similarities between figure 5.7 and 5.8. The differences for the non–hydrostatic simulation show more agreement then they did in when the Riemann boundary was used.

Discussion on the Riemann and sponge layer boundary conditions

There is one design difference from the previous simulations. The upper boundary condition has changed from a Riemann condition to a sponge layer condition. Therefore any differences in the results should solely be attributed to the boundary condition.

When the surface elevation plots (figure 5.2 versus 5.6) are compared, their shapes match reasonably well. The spin up time is of the same order. Time wise, the hydrostatic simulations are roughly twice as fast, before assuming constant change in surface elevations. Revealing, expected, wave propagation differences between hydrostatic and non-hydrostatic methods.
Most notable difference between the two boundary conditions is in surface elevations. These are more dampened with a sponge layer boundary. This is due to the introduction of the extra dissipative term in the momentum balance (see chapter 3) when using a sponge layer.
An indication of the effective absorption between both boundary conditions can be found by comparing the surface elevations of each method with its respective simulations. The Riemann versus sponge layer condition results in an average amplitude difference of 56% for the non–hydrostatic simulations. Whereas the hydrostatic simulation have a 42% amplitude difference (see appendix C). In terms of effectiveness this can be interpreted as; the sponge layer is more effective for the non – hydrostatic method.

When figure 5.3 is compared with figure 5.7, most notable difference seems to be in the non–hydrostatic simulations. In the lower quadrant there are fewer contours, which might be interpreted as the basin being in a lesser developed state. However this is deceptive and cannot be proven, since contour lines are not normalized with wave heights visual differences are bound to exist. Neither is such an indication given in the surface elevations (figure 5.2 and 5.6).
For the contour plots further in time, the same criticism holds. It leads to the conclusion that there is a good overall comparison between surface elevation patterns for the Riemann and Sponge layer boundary conditions.

In all contour plots, little resemblance is found between the non–hydrostatic (left hand side) and hydrostatic methods (right hand side). As mentioned, the wave lengths and surface elevations differ, which greatly attributes to the differences in contours. This is an expected result.
Due to diffracting of the incoming wave, perpendicular velocities are present. Therefore the boundary condition at each side of the basin is imposed by a Riemann condition. It should prevent reflection of the wave and the possibility of harbour oscillations. For both methods this is the case. These effects can be seen more clearly in the hydrostatic simulations. However there is some reflection. On first inspection they seem sufficiently small to neglect.
It has already been mentioned, but the use of Riemann condition at the sides is purely motivated by the fact that a sponge layer can only be imposed on the positive m, n –axis (see chapter 3). Consequently, it would not have allowed for similar boundaries on the left hand and right hand side of the harbour entrance. This is seen as an issue on the programming level instead of simulation/ user level.

A good measure for the validity of a simulation is whether there is a state of equilibrium in the model. An exponential fit of the energy over time (figure 5.5), as was used for the Riemann boundary, is most elegant. For simulations that made use of a sponge layer (figure 5.9) it lead to some difficulties in the fit, due to the (seemingly) threshold, both non – hydrostatic and hydrostatic methods encounter.

From the energy plots three observations are made. First, there is more energy in simulations with the Riemann boundary. This is to be expected, since an extra dissipative term has been added for the sponge layer condition.

Second, when comparing energy levels of the same simulation, with a different method, there is more energy present it is non–hydrostatic form. Although amplitudes are slightly lower, there are more waves present in the basin; tipping the total amount of energy in its favour.
The percentile difference between the Riemann condition and sponge layer condition (when comparing the boundary conditions, instead of the methods) for the non–hydrostatic method is found to be 32% from figure 5.5 and 5.9. It matches to the surface elevation amplitude change of 56% from figure 5.2 and 5.6 (see appendix C). From the amplitude change of 42% previously, an energy difference of 17% is expected for the hydrostatic simulations. However, the energy difference is 26% when figure 5.5 and 5.9 are used. This is a notable difference. Since the only difference between simulations is the upper boundary condition, where it follows that the Riemann boundaries on the sides oscillations are not as small as expected and are the cause of the percentile difference.

Fully reflective boundaries

Last set of simulations is the harbour basin with fully reflective or closed boundary conditions. For clarity, this means there are no conditions imposed on the boundaries.

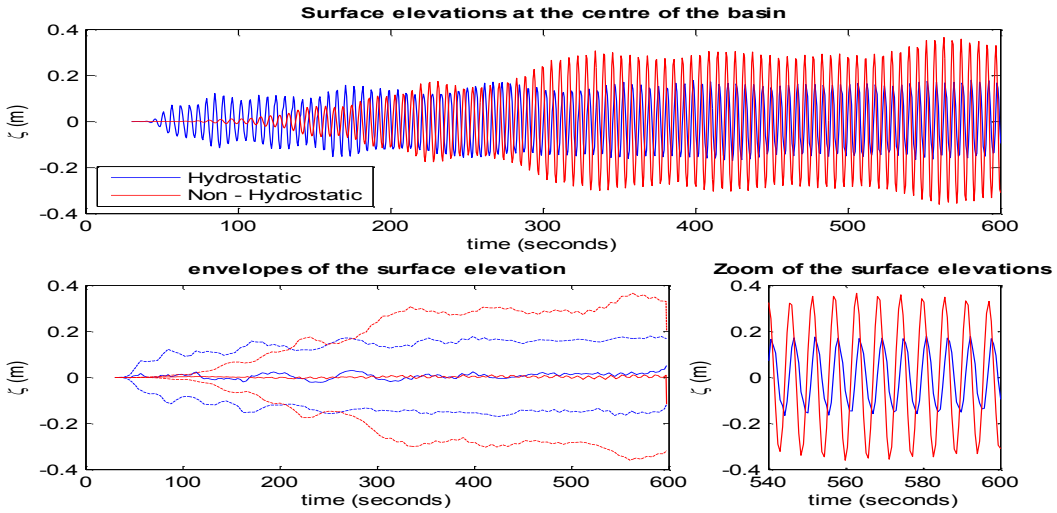

Figure 5.10 Surface elevations for fully reflective boundaries

Figure 5.10 shows the surface elevations in the center of the basin. As with previous results, the surface elevations use more time to resemble values that should occur in the non–hydrostatic method.

The first notable difference is the wave amplitude, for the hydrostatic method, the amplitude corresponds reasonably well with previous simulations. However, the wave amplitudes for the non–hydrostatic method are much higher than previously. In fact, this is the first time that the design amplitude of 0.25 meters is reached.

After 550 seconds, the non–hydrostatic method yields a concave shape for the surface elevations. It seems oscillations are starting to influence the results. Since the boundaries are fully reflective, this is not an unexpected result. In such a case this simulation should not be in equilibrium yet.

In figure 5.12 and 5.13 the contour plots are shown. According to figure 5.10 the non–hydrostatic simulation is not yet fully developed at time frame 250 (seconds). There are no large closed circle contours visible, which can be used as an indicator for reflection. For a simulation with fully reflective boundaries that has reached equilibrium, these should be visible in some sort of form. The hydrostatic simulation shows similar results to the left hand side, although it has a bit more randomness to it.

At 400 seconds (figure 5.12) patterns are emerging. The simulations have lost most of the diffracting pattern behind a headland, which should occur at some point, due to the reflections. The non–hydrostatic simulation is showing the closed circle like contours. They are switching between tops and troughs in both the horizontal and vertical. If these stay at the same position, an oscillating movement can be discerned. From this one still image, it is impossible to tell whether this occurs. In order to check for such a phenomenon, an animation has been made of multiple stills to check for such an occurrence. This is indeed what is happening. The hydrostatic simulation is showing a similar pattern more or less. Albeit being more stretched and having less amplitude.

Contour plot for fully reflective boundaries

Non – Hydrostatic method *Hydrostatic method*

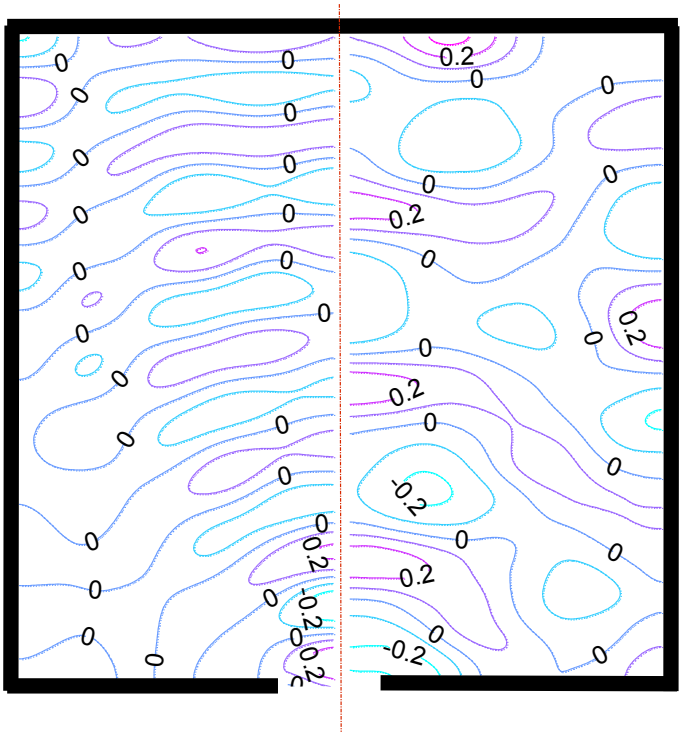

Figure 5.11 Contour plot of the surface elevations at $t = 250$ seconds for fully reflective boundaries

Contour plot for fully reflective boundaries

Non – Hydrostatic method *Hydrostatic method*

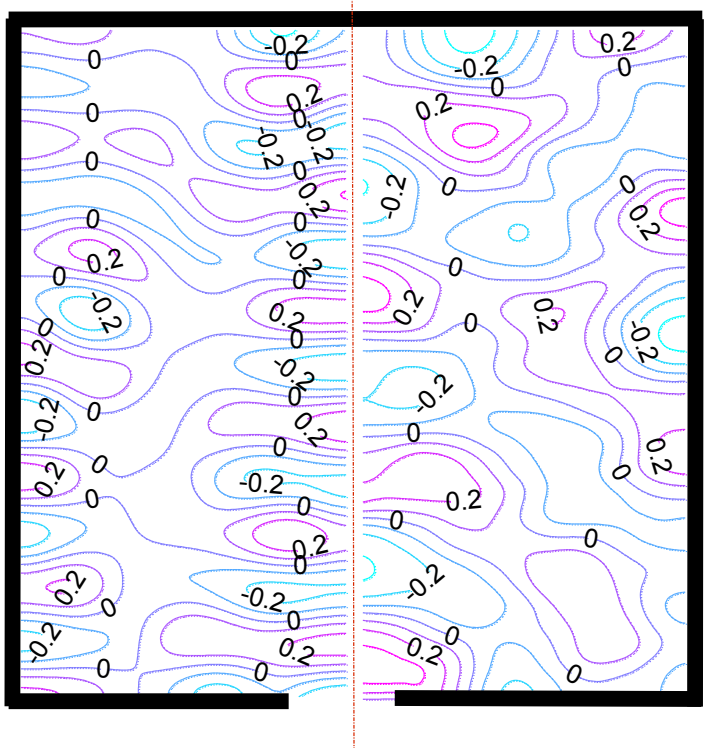

Figure 5.12 Contour plot of the surface elevations at $t = 400$ seconds for fully reflective boundaries

In figure 5.13, a curve fit of the energy levels is shown. The hydrostatic simulation has an exponential fit (red line). It shows a constant energy level in the basin after roughly 350 seconds. Thus, the contour plot shown in figure 5.11 is taken at a to early time step. After which the simulation becomes stable and performs well.

Because of the concave like envelope at the end of the non–hydrostatic function in figure 5.10 simulation time has been extended by 5 minutes (note that the residuals of the energy fit for the hydrostatic simulation end after 10 minutes).
A best fit option was used. For the non-hydrostatic simulation this is a Gaussian fit. The small hump seen at 880 seconds is likely due to the nature of the fit. This seems to be a small error to which no further value is given.
It is seen that the energy levels are still rising, meaning the simulation is not yet stable after 15 minutes of running time.

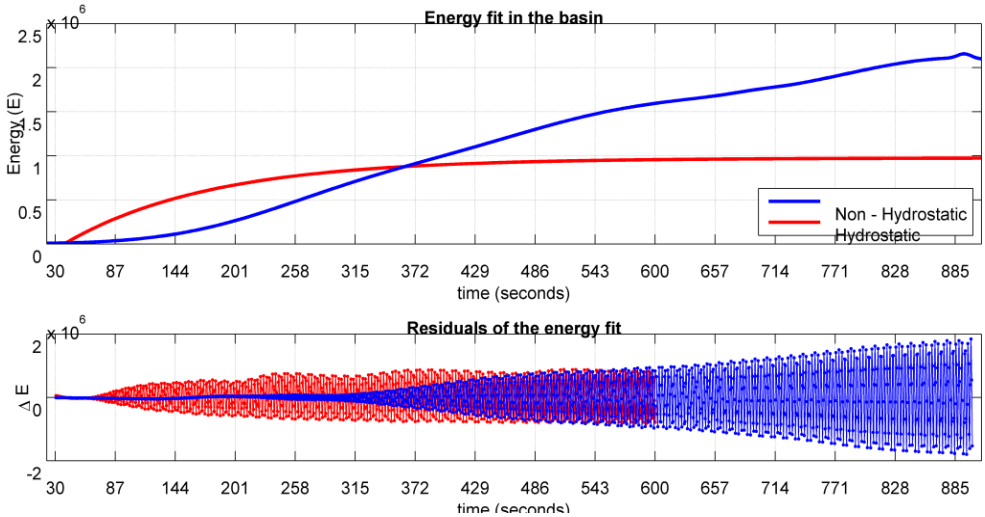

Figure 5.13 Fit of the total energy in the basin for the closed boundary condition (extended by 5 minutes)

Comments on the used geometry and further interpretation of the results

The 2D model results do not irrefutably show whether use of the non–hydrostatic module in TRIWAQ outperforms the hydrostatic simulation. An important first observation is the difference in approximation of the desired wave with identical imposed inflow conditions. This influences model behaviour with respect to reflections and consequently pattern development, energy levels and stability.
The aim of the 2 dimensional harbour simulations is to test the capabilities with the non–hydrostatic method, compare it to a similar simulation using the hydrostatic method and explain the occurring differences between model behaviours. With respect to the capabilities and comparison the 2D tests are a success. Most of the differences have been explained.

However, the energy growth and constant growth of wave amplitudes for the fully reflective boundary, non–hydrostatic simulation has not been explained. This is due to a combination between wave and the model geometry.

Friction is not implemented in the model setup. However when using a sponge layer, a dissipative term κ is introduced at certain locations. Although the Riemann boundary condition is not defined by friction, it is a dissipative term and can thus be considered to do practically the same. Difference in surface elevations between those results is minimal.

Now consider the simulations with fully reflective boundaries. This boundary condition is often referred to as a free slip surface. There are no dissipative terms introduced via either boundary conditions or friction. Therefore the only dissipative energy term available is this model is wave radiation into the outer basin. With the hydrostatic method the model finds a stable state, or energy balance, after 300 seconds. For the non-hydrostatic method this does not occur.

That important first observation about the difference in approximation of desired wave shows that the hydrostatic method calculates a wave length of 80 meters in the model, which corresponds to the shallow water theory. The non-hydrostatic simulation approximates the wave length to 50 meters and corresponds to the wave length found in transitional waters, which is closer to the truth of the model geometry, when relative depth (d/L) is considered to be a measure.
It might be noteworthy to mention that these simulations use to more extreme dispersive values then were used in (Zijlema, et al., 2005) where TRIWAQ-NH has been tested too. Here a kd - value of 2.51 was used while it was previously tested with a maximum of 1.69.

The length and the width of the harbour basin are both 300 meters, with a constant depth of 20 meters. When the last method is used, it corresponds to a wave that fits exactly six times into the basin in both length and width.
Based on theory (Rabinovich, 2009), the basin will show oscillations for certain wave periods. (see Appendix C) The 7th fundamental mode has a period of 5.7 seconds, which is equal to the imposed forcing. So oscillations should and do occur. This is the reason for the continued energy growth in the basin.
In this respect it must be noted, that the contour plot (figure 5.12) is a snapshot after 400 seconds. In that point of time, the amplitudes are roughly corresponding with the hydrostatic simulation. The residuals of the energy fit in figure 5.13 indicate that significant larger amplitudes or steeper waves should show up for a contour plot at around 800 seconds.
It can be concluded that, although the non–hydrostatic method does not show energy balance, it continues to predict surface elevations while amplitudes keep increasing due to oscillations. This is a good indication for the robustness of the algorithm.

This may not have been the best setup to test TRIWAQ-NH's capabilities, since the chosen wave forcing and geometry are going to show oscillations when the only dissipative force is radiation to the outer basin. On the other hand, this may well be a good way to show the difference between the differences in modelling methods.

With respect to the currently implemented boundary conditions and its solution to their reflective capabilities, the chosen setup is not considered ideal. The diffracting waves around the headlands make interpretation of the amount of reflection more complex. In fact from these results the only real conclusion can be both conditions are predicting a similar amount of reflection, while they are both designed to be fully absorbing more or less. This was also demonstrated in the one dimensional simulations of chapter 4. Ideally, the 2D Riemann and sponge layer tests should show a circle like diffraction around the headlands. In appendix B simulations of diffraction around a headland are shown. Which clearly and expectedly show TRIWAQ-NH is able to predict surface elevations well.

In appendix D a model of Terneuzen harbour, based on (Koop, et al., 2007), is shown. It is a quick attempt, and therefore not optimized, to simulate an existing harbour with the current bounds of TRIWAQ-NH.
The simulation shows a more practical drawback, which can be considered general drawback for phase revolving models and thus also TRIWAQ-NH. A wave forcing needs to be implemented perpendicular to the grid which in itself is not a drawback. However when combined with a less angular geometry (then the above described 2D model), where borders do not follow the edges of

the grid, then this grid has to become very dense to approximate a smooth border. If, like shown in appendix D, these are to rugged, results will show little agreement with reality.
In TRIWAQ-NH it is only possible to assign boundary conditions to borders that follow the edges of the grid or are under an acute angle of 45 degrees. Suppose a boundary condition needs to be assigned to a border under an angle of 77 degrees of the grid space. Not only does it require a heavy investment in grid density, it will also require many small entries of this condition in the input file. Since these need to be implemented manually, it will result in a very long computation time and a larger margin for human error.
Basically, the importance of good approximation for borders becomes increasingly important for simulations of local areas, like Terneuzen harbour. At present, harbour simulations in TRIWAQ-NH can be done, but are only feasible for simple and (highly) schematized harbours.

Chapter 6: Conclusions

This thesis compares hydrostatic versus non-hydrostatic modelling of free-surface waves using the model TRIWAQ-NH. It is shown that waves, propagating in transitional water depths ($1 < kh < 2.51$), are better approximated by the non-hydrostatic method, while using a single depth layer and relatively little grid cells per wave length (20 cells).
In such conditions, the non-hydrostatic method has good agreement with formulations for propagation speed and wave length found from linear (Airy) theory for transitional water depths. The hydrostatic method approximates waves in transitional water depths according to shallow water theory.

The algorithm or solving the equations in TRIWAQ-NH is robust, because: (1) it is able to calculate surface elevations for high dispersive waves (tested up to kh = 2.51); and (2) when harbour oscillations occur, with full reflective boundaries.

The suitability and adaption of four currently implemented methods for specifying boundary conditions in TRIWAQ-NH as full or partial reflection conditions was investigated. These methods are: (1) the α–value condition; (2) sloping profile condition; (3) Riemann condition; and (4) sponge layer condition.
The following aspects of specifying the boundary conditions were explored: (1) the ability to absorb for the non-hydrostatic method; (2) the dependency on frequencies; and (3) the angle of incidence.

The α-value condition is not suitable for further exploration as partial reflection condition or absorbing condition for non-hydrostatic modelling in either 1D or 2D simulations. It is shown in the 1D simulations that compared to the other boundary conditions, it underperforms for both the hydrostatic and non-hydrostatic method. This is due to the fact that, (1) the α-value needs manual calculation and (2) is very sensitive to the corresponding frequency of the wave forcing. Additionally (3) the requirement of nearly perpendicular incoming waves makes it unsuitable for partial reflections in more arbitrary 2D geometries, like harbours.

The sloping profile condition is due to practical disadvantages not suitable for further exploration as partial reflection condition or absorbing condition in TRIWAQ-NH. It is shown in the 1D test simulations that computation time increases by a factor 2 due to (1) the added grid cells in which the slope and its spillway. Also, (2) it does not perform well because grid resolution was low. For non-hydrostatic modelling of partial reflections in 2D, it holds the additional disadvantage (3) that it will not be able to predict angles of incidences well for arbitrary 2D geometries.

It is concluded that the Riemann boundary condition performs well as absorbing boundary for the non-hydrostatic method. However, it was shown that the non-hydrostatic method will show small errors in surface elevation predictions near the boundary when the incoming wave are under an obliquely angle. These do not occur for the hydrostatic method.
Compared to the α-value, sloping profile and sponge layer condition, the Riemann condition is easiest to implement and does not require enhanced grid resolution or extension of the grid, which is advantageous for computational time and for more arbitrary 2D geometries where boundary conditions might otherwise overlaps.

The fourth boundary condition is the sponge layer condition. It is concluded that this condition performs well as absorbing boundary condition for non-hydrostatic modelling and holds the greatest promise for future adjustment to partial reflective boundaries, because (1) works for a wide range of frequencies; and (2) is easy to implement.

For nearly perpendicular incoming waves, results of the sponge layer compare to the Riemann boundary condition with respect to surface elevations. However it shows a considerable amount less energy (factor 3) because the computational grid has been extended for the sponge layer, which needs length, in which the extra dissipative term κ being introduced in the sponge.
Disadvantages of the sponge layer approach are, (1) this method requires extra grid space for the for the sponge layer; and (2) presently unable to impose a sponge on any desired side of the grid (only in the positive directions of m and n).

Overall, it is concluded that the Riemann boundary condition and sponge layer condition hold the most promise for further development into absorbing and/ or partially reflective boundary conditions for non-hydrostatic modelling of free-surface waves.

Chapter 7: Recommendations

An open boundary condition was defined as a condition where waves are able to exit the model domain without reflection. The implementation and further exploration of open boundary conditions requires more attention if it is desirable to further develop it for harbour simulations. This can be split in two parts: (1) more technical issues; and (2) practical issues.

In this thesis the route to the feasibility of partial reflection by use of open boundary conditions is explored, by identifying how well the present boundary conditions are able to fully absorb.
It clearly shows the difficulty to implement truly absorbing boundary when non-hydrostatic modelling is required. It was concluded that either the sponge layer or Riemann boundary are the best candidates if boundary conditions with partial reflection when full absorption is required.

This thesis has not simulated with more than one vertical layer. However TRIWAQ-NH is able to simulate with multiple vertical layers. Therefore, it is recommended to investigate the response of the Riemann boundary for multiple vertical layers. With multiple vertical layers the pressure adjustments in the non-hydrostatic step will distort the linear pressure gradient of the hydrostatic step. When one vertical layer is used, it means that the non-hydrostatic step is mainly an adjustment to the linear pressure gradient, but pressure will still be vertical. With multiple vertical layers, the Riemann condition may well perform less, since it calculates the wave characteristic hydrostatically.

It is recommended to further develop the sponge layer condition for various reasons: (1) currently, this condition can only be imposed on the positive sides of the grid space (see figure 3.2). Expansion to the negative sides of m, n will allow the sponge layer to be imposed on all sides of the grid; (2) currently, the sponge layer is only able to dampen either in the velocity direction u or v (see figure 3.3). A layer where dampening can occur in multiple directions, will likely lift the restriction on the angle of incidence; (3) addition of a dampening coefficient for the vertical velocity w; (4) in this study the length of the sponge layer has been kept at 3 times the wave length. It is recommended test how well the sponge layer behaves with different layer lengths.
It may be feasible to create a better absorbing condition for non-hydrostatic modelling, when layer lengths are investigated in combination with (5) more configurability/ research into shapes of the damping coefficient κ, currently the shape is hard coded (see figure 3.1). This is also suggested as starting point for further creation of a partial reflection condition.

Some more practical issues arise when arbitrary 2D geometries are being modelled. Currently open boundaries cannot easily be implemented under every desired direction in the grid. Open boundaries need to follow the edges of the grid cells or cross these grid cells with an angle of 45 degrees. When creating an input file, this makes it very tedious work, with large margins of human error. It requires a specialist. Some more automation would be welcome.
Another practical issue, which has not been mentioned anywhere, is that the present tools for visualization are all designed for large scale (North Sea or estuary sized) models that are used for tidal simulations. For non–hydrostatic simulations in harbour areas, with generally smaller wave lengths and periods, these tools are unusable, due to the fact that the extend of the computational grid is in the order of meters and time in the order of seconds or minutes. They will need to be adjusted or re-developed. A first step was made towards this purpose, since all available tools were insufficient for this thesis.

Bibliography

J.A. Battjes Stroming in waterlopen [Book]. - Delft : Delft university press, 2002.
J.A. Battjes CT 4320 - Korte golven [Book]. - Delft : Delft University Press, 2001.
F. Enet [et al.] Evaluation of diffraction behind a semi-infinite breakwater in the swan wave model [Report]. - Emmeloord : Alkyon Hydraulic Consultancy & Research, 2007.
J.N. Groeneweg Near-shore wave modelling with two coupled models: swan and triton [Conference] // Conf. on coastal Eng.. - Lisabon : World Sientific, 2004. - Vols. Vol I: 868-880.
L.H. Holthuijsen Waves in oceanic and coastal waters [Book]. - Delft : Cambridge University Press, 2007.
M. Isaacson and S. Qu Waves in a harbour with partially reflecting boundaries [Journal] // Coastal Engineering. - 1990. - Vol. 14. - pp. 193-214.
M.P.C. de Jong Origin and prediction of seiches in Rotterdam harbour basins [Book]. - Delft : Delft University Press, 2004.
G. Klopman and J van der Meer Random wave measurements in front of reflective structures [Journal] // Journal of Waterway, port, coastal, and ocean engineering. - january/ february 1999. - pp. 39-45.
O.R Koop, G.Ph. van Vledder and D.P. Hurdle Golfdoordringing in de haven van Terneuzen [Report]. - Marknesse : Alkyon Hydraulic Consultancy & Research, 2007.
J.K. Kostense [et al.] Wave energy dissipation in arbitrarily shaped harours of variable depth [Journal]. - Delft : Delft Hydraulics, 1988.
LogicaCMG VORtech, Alkyon User's Guide WAQPRE. - [s.l.] : Ministry of Transport, Public Works and Water Management, 2006.
A.B. Rabinovich Seiches and Harbor Oscillations [Book Section] // Handbook of Coastal Engineering. - Singapoure : World Scientific Publ., 2009.
J.E. **Romate** Absorbing Boundary Conditions for Free Surface Waves [Journal]. - Emmeloord : Delft Hydraulics, 1991. - 99 : Vol. Jourlan of computational Physics.
SIMTECH Syllabus: Randvoorwaarden in WAQUA en TRIWAQ [Rapport]. - [sl] : Ministery of Transport, Public Works and Water Management, 2000.
G.S. Stelling and N. Booij Computational Modelling of flow and transport [Book]. - Delft : Delft University Press, 1999.
G.S. Stelling and M. Zijlema An accurate and efficient finite-difference algorithm for non-hydrostatic free-surface flow with applictaion to wave propagation [Journal] // International Journal for Numerical Methods in Fluids. - 2003. - pp. 43:1-23.
SWAN.team SWAN User manual [Online] // swanmodel.sourceforge.net. - Delft University of Technology. - 1.2. - januari 2011. - http://swanmodel.sourceforge.net.
M. Zijlema and G.S. Stelling Further experiences with computing non-hydrostatic free-surface flows involving water waves [Journal] // International Journal for Numerical Methods in Fluids. - 2005. - pp. 169-197.

Appendix A: An input example with explanation

This appendix will give a step by step explanation of the input file or deck and the input values used of the TRIWAQ model. The main purpose is to create a condensed guide, for new users. It was found that the current guide is somewhat short as it is not an easily accessible document. The user guide is vast with a lot of in-depth technical references (LogicaCMG, 2006). Many of the possible features and options are skipped in this appendix.
It starts with the identification of the experiment. This example shows the dispersive wave for the 1 Dimensional run with a sponge layer as border. It is meant to be a visualization of the way input is generated.
The input file is separated in global keywords which allow the user to set specific parameters. The first global keyword is identification. The wave type is shown in "experiment". The "modid" indicates, the run uses 1 depth layer.

```
IDENTification
  TRIWAQ
  EXPERIMENT = 'kh1'
  OVERWRITE
  MODID = 'Reflection test L1 T=1.4541 a=0.0107'
```

Global keyword: Mesh

The second global keyword is mesh. It defines the mesh size. The scales of the test are based on the test that describes shoaling over a submerged bar (Zijlema, et al., 2005). The depth used for the experiments are directly taken from it, which is 0.4 meters. In the described experiment roughly 300 grid points per wave length were used. With these given parameters the number of grid cells, "$mmax$", can be defined. It is calculated as follows:

Note: it is assumed that the wave amplitude is negligible over the total depth.

Parameters

$$kh = 1$$
$$d = 0.4\ [meters]$$
$$L/m_L \approx 300$$

Formulation

$$k = {kh}/{d}$$
$$c = \frac{\omega}{k} = \sqrt{\frac{g}{k}\tanh(kh)}$$
$$T = 2\pi/ck$$
$$L = Tc$$
$$\Delta m \approx rounded(\frac{L}{m_L})$$

Numerical result

$$k = 2.5\ \left[\frac{rad}{m}\right]$$
$$c = 1.73\ \left[\frac{m}{s}\right]$$
$$T = 1.45\ [s]$$
$$L = 2.51\ [m]$$
$$\Delta m = 0.009\ [m]$$

The basin has a length of four wave lengths. The grid step (Δm) is rounded. The number of grids cells per wave length (m_L) is not exactly 300 anymore.
This simulation uses the sponge layer. The sponge length is defined as 3 wave lengths, making the total length of the grid space 7 wave lengths.

Formulation

$$m_L = \frac{L}{\Delta m}$$
$$mmax = 7m_L + 1$$

Numerical result

$$m_l = 279$$
$$mmax = 1959$$

```
MESH
   GRID
     AREA
       ANGlegrid = 0.00
       MMAX = 1959          # Grid cells in m-direction
       NMAX = 3             # Grid cells in n-direction
       KMAX = 1             # nr of layers (meaningfull only in
                              TRIWAQ)
       LATItude = 0.00
     RECTilinear
       STEPSIZE = 0.009
```

In the grid points of interest are defined. If an open border is required, it needs to be defined in between points. In this case those are the inflow border and the outflow border behind the sponge layer.
Since this simulation has the sponge layer, additional points have been defined in front of the sponge layer. Here shown as P 124 at $m = 1121$ named "vertical wall". For a 1D simulation without a sponge or sloping border, this would be defined as $mmax$.

```
   POINTS
     P 11 = (M = 1 , N = 2    ,     NAME=' Corner (1, 1) ')
     P 14 = (M = 1959, N = 2 ,     NAME=' Corner (1121, 1) ')

     # Aditional point present
     P 101 = (M = 1 ,  N = 2     , NAME=' outer area signal')
     P 102 = (M = 6  , N = 2    ,  NAME=' outer area m+5 ')
     P 103 = (M = 11 , N = 2    ,  NAME=' outer area m+10 ')
     P 104 = (M = 16 , N = 2    ,  NAME=' outer area m+15 ')
     P 116 = (M = 561 , N = 2    , NAME=' Centre basin ')
     P 117 = (M = 1006 , N = 2   , NAME=' Vertical wall m-25 ')
     P 118 = (M = 1101 , N = 2   , NAME=' Vertical wall m-20 ')
     P 119 = (M = 1106 , N = 2   , NAME=' Vertical wall m-15 ')
     P 120 = (M = 1111, N = 2   ,  NAME=' Vertical wall m-10 ')
     P 121 = (M = 1116, N = 2,     NAME=' Vertical wall m-5 ')
     P 122 = (M = 1119, N = 2,     NAME=' Vertical wall m-2 ')
     P 123 = (M = 1120, N = 2,     NAME=' Vertical wall m-1 ')
     P 124 = (M = 1121, N = 2,     NAME=' Vertical wall ')
```

Similar to a single point, which can define a point of interest, it is also possible to define a line of interest; a curve. In this input file, the curve is defined as C1. Since this in a 1D model, there are is no need to define an enclosure.
The openings, define the open borders. Normally it is defined as a line in between 2 points. In this case it is defined as a line which starts and ends at the same point.
The bathymetry is flat and defined as a constant value of 0.4 meters.

```
   CURVEs
      C 1 : LINE ( P101, P102, P103, P104, P116, P117, P118, P119,
                   P120, P121, P122, P123, P124, ' Centre Curve ')

   BOUNdaries
      # ENCLosures
        # E = (1, 1) (1959, 1) (1959, 3) (1, 3) (1, 1)
```

```
 OPENings
     OPEN 2 : LINE ( P11, P11,      ' Wave input ')
     OPEN 4 : LINE ( P14, P14,      ' Kade ')

BATHYMetry
  GLOBAL
    CONST_Value = 0.4,
    LAYOUt = 1            # Defines the way an bathymetry input
                          file
                          # should be read by the preprocessor
```

Global keyword: General

The third global keyword is general. Here the input for physical parameters is given. It also allows the user to define if the model will be influenced by Coriolis and diffusion. For all tests these are turned off. The model scale is small for Coriolis and could influence results for border testing. This also goes for the diffusion term.

```
GENERAL
  DIFFusion
    GLOBAL
      CONST_value = 0.0
      CDCON       = 0.0
  PHYSical_parameters
    GRAVity     =    9.8130 # Gravitational constant
    WATDENsity =     1023.0 # Density for salt water
    AIRDENsity =     1.2050 # Air density
  CORIolis
    GLOBAL
      CONST_values = 0.
```

Global keyword: Flow

The fourth global keyword is flow. TRIWAQ is a time domain model. Flow lets the user set the timeframe first. In this example, the simulation may stop when wave has traveled 3 times the basin length. A wave needs at least 20 points in time to be described. This defines (Δt). The program is originally designed for long waves and requires time input in minutes.

Parameters
$c = 1.73\ \left[\frac{m}{s}\right]$
$m_L = 279$

Formulation
$L_h = 4\ L$
$T_{stop} = 3L_b/c$
$\Delta t = T/20$

Numerical result
$L_h = 10.08\ [m]$
$T_{stop} = 17.49\ [s]$
$= 0.29\ [min]$
$\Delta t = 0.073\ [s]$
$= 0.001\ [min]$

The stopping time of the model has been adjusted to 1 minute, instead of the 18 seconds that the above calculation provides. In case of a sponge or sloping bottom with outlet, the model domain is effectively larger. It should also provide for the 2D model with a foreland, which adds to the length of the model.

```
FLOW
  PROBlem
    TIMEFRame
      DATE   = '22 NOV 1980'
      TSTART = 0.00
      TSTOP  = 1
    METHODvariables
      TSTEP        = 0.001  # delta t given in minutes
      CHECKCon     = 'vel'  # Type of convergence ('vel'/'wl')
                            # default= 'vel'
      ITERCOn      = 40     # max nr of iterations for continuity
                              balance
      ITERMOm      = 2      # max nr of iterations for momentum
                              balance
      ITERACCuracy = 0.0005 # Accuracy at which convergence is
                              reached
      THETA        = 1.0    # Value for the theta method in time.
```

Drying, friction and viscosity are neglected. For the drying the same settings are used as in the test that describes shoaling over a submerged bar (Zijlema, et al., 2005).
The friction is updated in time. In order to neglect friction, its update interval is extremely high.
For viscosity, the eddy viscosity coefficient is set to zero.

```
    DRYING
      IDRYflag = 1
      DEPCrit  = 0.001
      DUPWnd   = 99999.

    FRICTion
      GLObal
        TICVal  = 9999999  # Update interval for friction
        FORMula = 'Chezy'  # Formulation to be used for friction
      UDIRec
        GLOBAL
          CONST_value = 1000.
      VDIRec
        GLOBAL
          CONST_value = 1000.

    VISCOsity
      EDDYviscositycoeff = 0.0 # default = 10.0
                               # Horizontal eddy viscosity (m2/s)
```

The forcing describes the initial state of the water in the model, its boundaries and how those boundaries are defined.
The initial state of the model is described with a constant water level, which is zero. Since there are no velocities present at the start of the simulation, the forcing used to describe the wave will start with a velocity equal to zero. Furthermore, it is a monochromatic wave. It leads to a Fourier series which uses the cosine function in TRIWAQ. In order to match the initial velocities in the model, its phase is adjusted to $\pi/2$. The amplitude of the series and its wave period are calculated:

Parameters
$T = 1.45\ [s]$
$kh = 1$
$a = 0.0107\ [m]$

Formulation
$\omega = 2\pi/T$
$\hat{u} = \omega a/kh$

Numerical result
$\omega = 43210\ [rad/min]$
$\hat{u} = 0.0462\ [m/s]$

```
  FORCings

    INITial
      WATLEVel
        GLOBAL
          CONST_values = 0.0 # water level at t = 0

    BOUNDAries
       B : OPEN 4, BTYPE='wl', BDEF ='Series', REFL= 0.0 # Kade muur
                   SAME
       B : OPEN 2, BTYPE='vel', BDEF='fourier', REFL= 0.0 # incoming
wave
                   SAME

    FOURier
      GEneral
        OMEGA = 43210.18
      SERIES
      S : P 11,              # Point sequence number
        TID = 0.0,           # Initial value at point [iseq]
        AZEro = 0.0          # Amplitude for zero frequency (m)
        AMPL  = 0.0462       # amplitude sequence of the wave (m/s)
        PHASE = 1.5707963    # Sequence of phases for N frequencies.
(rad)
    TIMESERIes
       S : P 14,             # border at the end, this is OPEN 4
         TID = 0.0           # Initial value at point [iseq]
```

Last, the checkpoints are defined under the keyword flow. Here, the points defined under “Mesh” are selected. Their values in time are written to the output file. In this example the water levels and currents for all points are selected.

```
  CHECKPoints
    LEVELStations           # water level stations
    P101, P102, P103, P104, P116, P117, P118, P119,
    P120, P121, P122, P123, P124
    CURRENTStations         # Current stations
    P101, P102, P103, P104, P116, P117, P118, P119,
    P120, P121, P122, P123, P124
```

Global keyword: Hydrodynamic

In this part the non-hydrostatic module is activated, as well as the sponge layer. The user can define the sponge layer in u-direction and v-direction. In grid direction this translates to m-direction and n-direction respecivly. This input example has the 1D model set up in the m-direction.
The sponge layer length is defined in the u-direction. It is defined as a length in meters. This corresponds to 3 times the wave length.

Parameters
$L = 2.51\ [m]$

Formulation	Numerical result
$L_{sponge} = 3L$	$L_{sponge} = 7.54\ [m]$

Note that the sponge layer only works in the non-hydrostatic module. In order to implement a sponge layer in a hydrostatic simulation, the start time of the non-hydrostatic simulation needs to be adjusted to a value that is outside the time domain of the simulation.

```
HYDRODYNAMIC
  APPROX         = 'box'
  AMOUNT_output  = 3
  SPONGE_U       = 7.54      # Length of the sponge layer in meters
  START          = 0         # Starting time of the non-hydrostatic
                             # simulation in minutes
```

Global keyword: SDSOUTput

The last keyword is SDS output. It sets the output file settings. Maps and histories can be defined, with the time of initialization. This does not have to be the same as the start of the simulation. The time step interval at which an output is stored can be changed.
All the Matlab scripts written make use of the maps output. To increase its time interval means less data will be shown. The tradeoff is disk size the output file uses. Maps output is a resource hog.

```
SDSOUTput
  MAPS
    TFMAPS = 0.00
    TIMAPS = 0.001
  HISTories
    TFHISto = 0.00
    TIHISto = 0.001
```

As a final word please note that not all the global keywords that can be defined have been used. Therefore it is stressed again, this appendix is not meant to be a manual for the setup of an input file.

Appendix B: The semi – infinite breakwater

This appendix shows results of simulation of a semi –infinite breakwater with different setups. It is based on (Enet, et al.).These simulations were made to get acquainted with the model TRIWAQ-NH. Emphasize is on the different boundary conditions that can be used. The aim of this chapter is not to compare the results of TRIWAQ-NH with the results published in (Enet, et al.).

In all simulations the wave is entering perpendicular to the fully reflective semi – infinite breakwater. The domain modeled is 1000 meters by 1000 meters with a depth of 10 meters. The axis of the breakwater is located halfway and spawns 500 meters.
The wave has a period of 8 seconds and a wave height of approximately 0.5 meters, which is the design amplitude. Since the wave forcing is given as a velocity forcing, this is not set in stone. This corresponds to a kh value of 0.88 and a ka value of 0.02. At the end of this appendix a table is presented with more specifics on the input data.
The propagation speed of the wave does not approximate the propagation speed well if shallow water theory is used to check upon the output values. Manual calculation with short wave theory is more correct. This is considered the difference between hydrostatic and non-hydrostatic modeling. Thereby allows these simulations to service as a showcase example for some of the open boundary conditions used.

The first 2 figures show the difference between hydrostatic and non – hydrostatic simulations. The hydrostatic simulation has one depth layer. For the non – hydrostatic simulations both single and two depth layer simulations are shown.

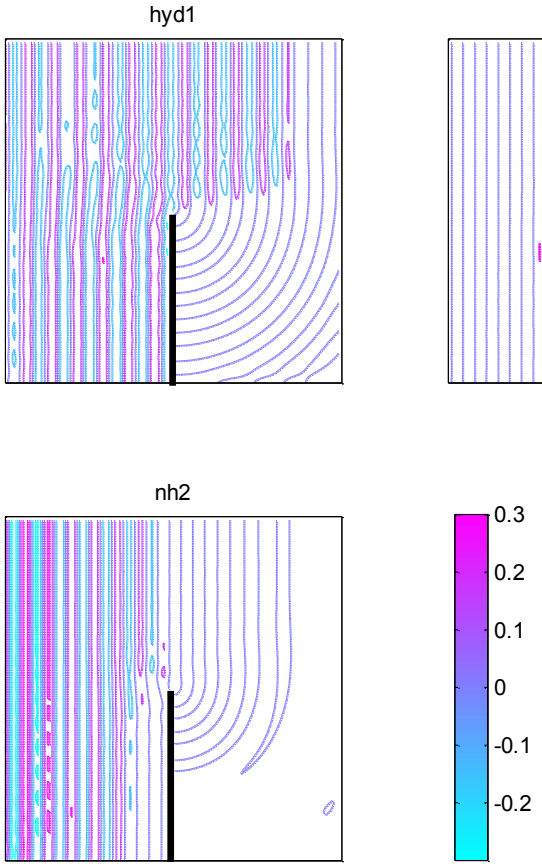

Figure B.1 Surface elevations of the simulation at 2:01 minutes. Hyd1 is the hydrostatic simulation. NH1 is the non – hydrostatic simulation with 1 depth layer. NH2 is the non – hydrostatic simulation with 2 depth layers.

The difference in wave propagation between hydrostatic and non – hydrostatic calculations is clearly shown in Figure B.1. As expected the hydrostatic simulation has a higher wave propagation than the non-hydrostatic simulations. Simulation NH1 seems to propagate slightly faster than NH2. This is expected (see chapter 3).

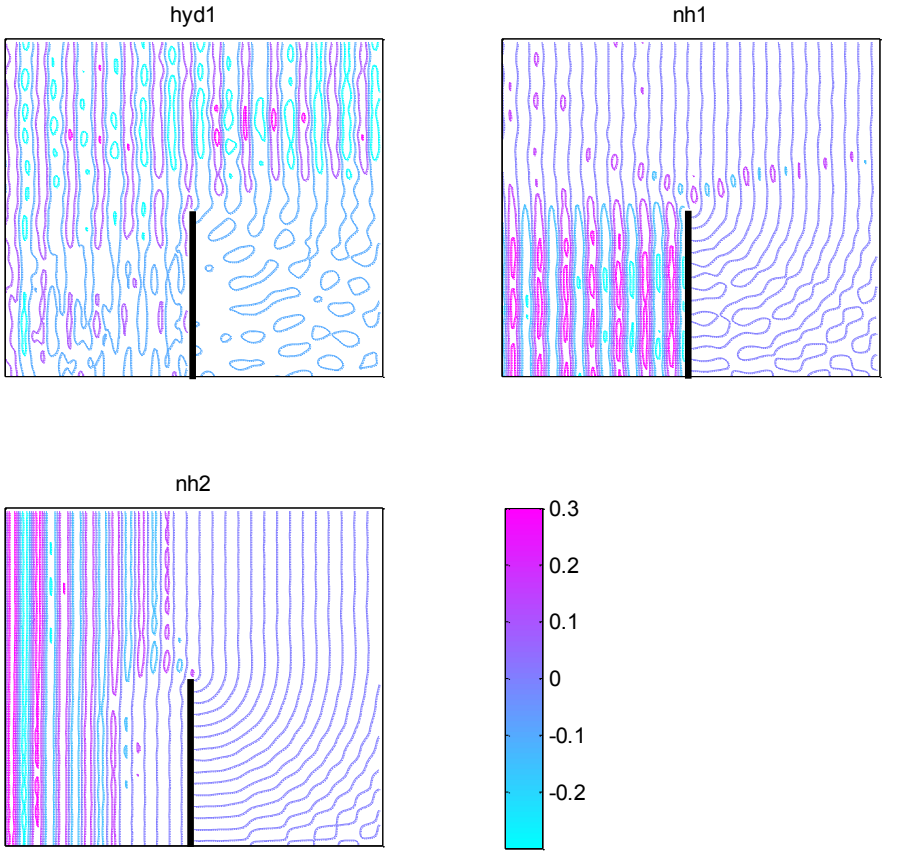

Figure B.2 Surface elevations at 7:32 minutes. Hyd1 is the hydrostatic simulation. NH1 is the non – hydrostatic simulation with 1 depth layer. NH2 is the non – hydrostatic simulation with 2 depth layers.

In Figure B.2 the influence of the boundary conditions becomes more apparent. The wave maker condition is located at the western border and uses the formulation given in Chapter 4; it is a velocity forcing prescribed by a Fourier series. This partly accounts for the fact that surface elevations are above 0.25 meter. At the end eastern boundary an open water level boundary is given.
The northern and southern boundaries are closed. This is clearly seen at the southern boundary behind the breakwater. Because it is a closed, reflection occurs. This is interfering with the diffraction pattern seen. For the hydrostatic simulation it already starts happening in Figure B.1.

In the next set of figures, non – hydrostatic simulations with one depth layer are shown, each has the same wave characteristic and the same geometry. However the boundary conditions will change. From closed to open boundaries.
With these changes the aim is to investigate two aspects of the model. First, what will happen when the open water level boundary is changed to the Riemann condition, velocity or water level condition? Secondly, how does a wave react to an open boundary, when the velocities main direction is to flow alongside the border?
One depth layer is chosen, because (1) there seems little visible difference in propagation speed with the 2 layered model; (2) The Riemann and velocity boundaries use a depth averaged velocity U, which corresponds to one layer; and (3) the computation time is less.

Riemann boundaries

In Chapter 4 background information and formulations are given on the open boundary conditions. As a small recap the water level condition and Riemann condition are given;

$$\zeta + \alpha_w \frac{\partial}{\partial t}\{U \pm 2\sqrt{gH}\} = F_\zeta(t) \qquad \text{to >>} \qquad U \pm \zeta\sqrt{\frac{g}{d}} = F_R(t) \qquad \text{Eq. B-1}$$

Differences between boundary conditions are shown in Figure B.3 and Figure B.4. In each figure, the top left is the same non- hydrostatic simulation, with one depth layer as in Figure B.1 and Figure B.2. It uses a velocity inflow boundary condition on the west side and a water level outflow condition on the east side, with $\alpha_w = 0$ and $F_\zeta(t) = 0$. All other boundaries are closed. The lower left simulation changes the western boundary to the Riemann condition, with $F_R(t) = 0$.
The top right simulation opens up an extra boundary. It is the southern part behind the breakwater. It is similarly defined as the described Riemann condition. The lower right run shows a simulation with the complete northern boundary defined as a Riemann condition.

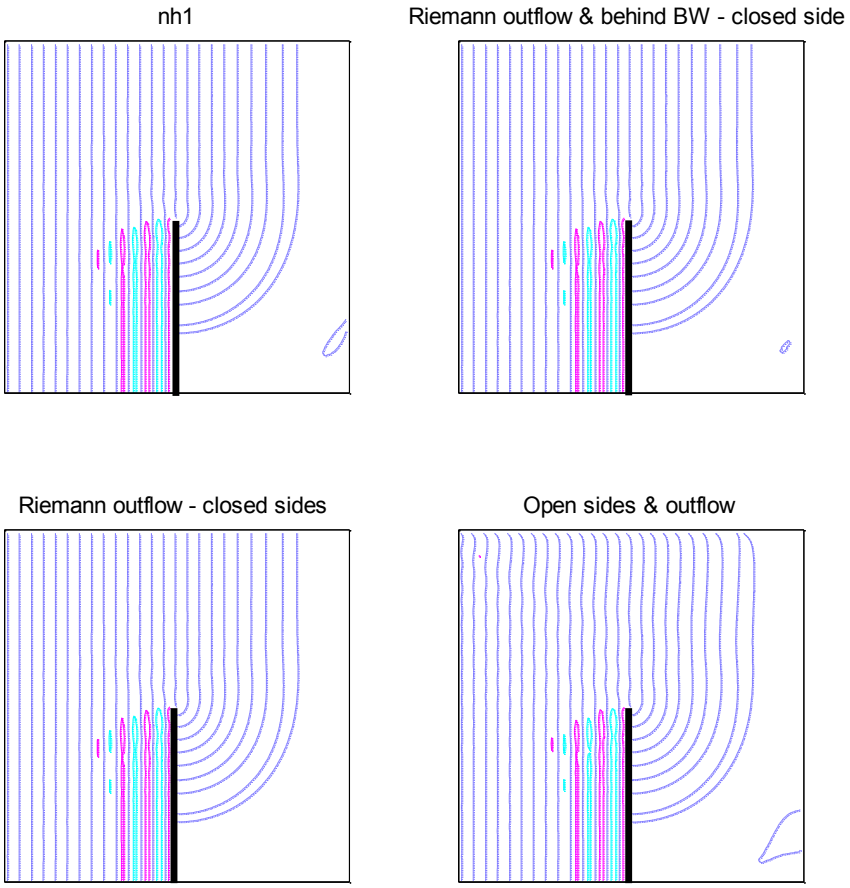

Figure B.3 Surface elevations at 2:01 minutes with Riemann boundaries.

In Figure B.3 only one difference is visible between the top left and lower left simulation. The top left shows a small disturbance separated from the visible flow field, whereas the lower left simulation does not. In itself the disturbance is insignificant, since the angle of the zero – crossing is expected. This disturbance is shown in all other simulations as well.
The lower right simulation has a distinct difference at the northern boundary with the other simulations. Some outflow seems to be present, which bends the wave slightly towards the north.

In Figure B.4 the wave field is fully developed. There seems to be no real difference between the top and lower left simulations. Choice between a Riemann and a water level condition does nothing visibly different for the results.
From the previous results it is expected that the top right simulation will perform slightly better with respect to the diffraction pattern, since there is an added open boundary. This is expectation is met. The use of an open northern Riemann boundary shows the surface elevation bending towards the north. This effect stays confined close to the boundary.

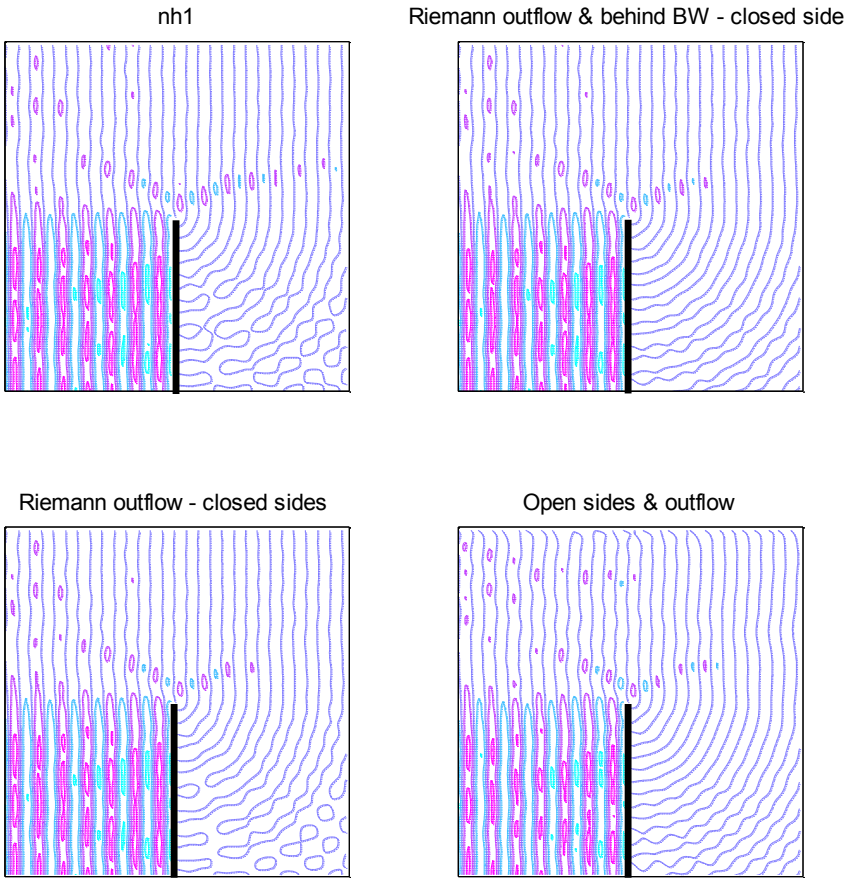

Figure B.4 Surface elevations at 7:32 minutes with Riemann boundaries

Velocity boundaries

In the next set of figures the velocity boundary is tested. This will show differences between the original, the Riemann boundaries with respect to their locations and their effectiveness over time. The velocity boundary is given by;

$$\mathrm{U} + \alpha_s \frac{\partial}{\partial t}\{U \pm 2\sqrt{gh}\} = F_s(t) \qquad \text{Eq. B-2}$$

Here U is the depth averaged velocity, the reflection factor α_s is set to zero and $F_s(t) = 0$ too.
Figure B.5 shows no real differences between all the different boundary conditions. Their resemblance to Figure B.3 is good too. So for as long as there is the wave is not fully developed there is no visible difference between a Riemann of flow condition.
Figure B.6 shows the developed wave field. There are two distinct differences. First, the use of a velocity boundary clearly affects the diffraction pattern behind the semi – infinite breakwater negatively. Second, wave tops are higher in the upper half of each simulation. Additionally unlike the Riemann condition, the wave front does not bend slightly to the northern boundary.

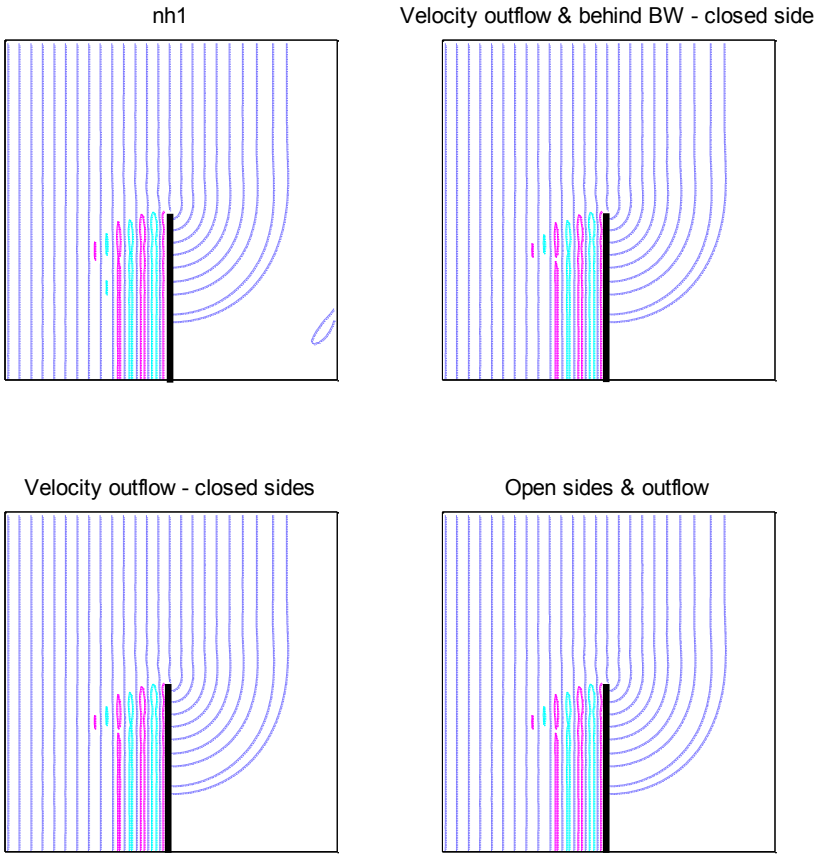

Figure B.5 Surface elevations at 2:01 minutes with velocity boundaries.

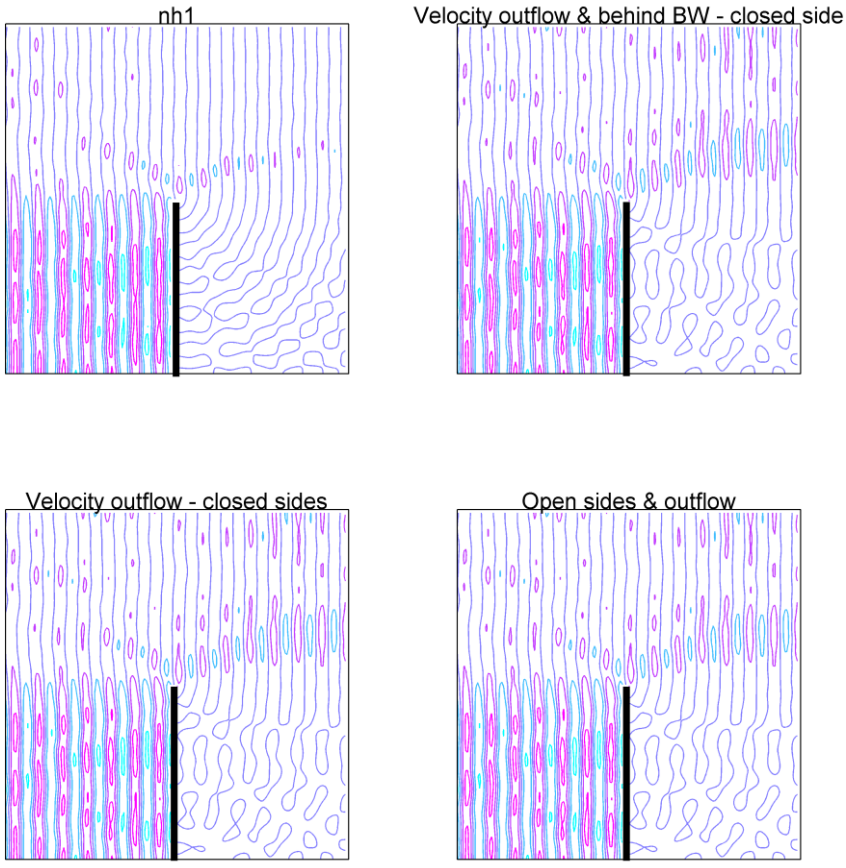

Figure B.6 Surface elevations at 7:32 minutes with velocity boundaries.

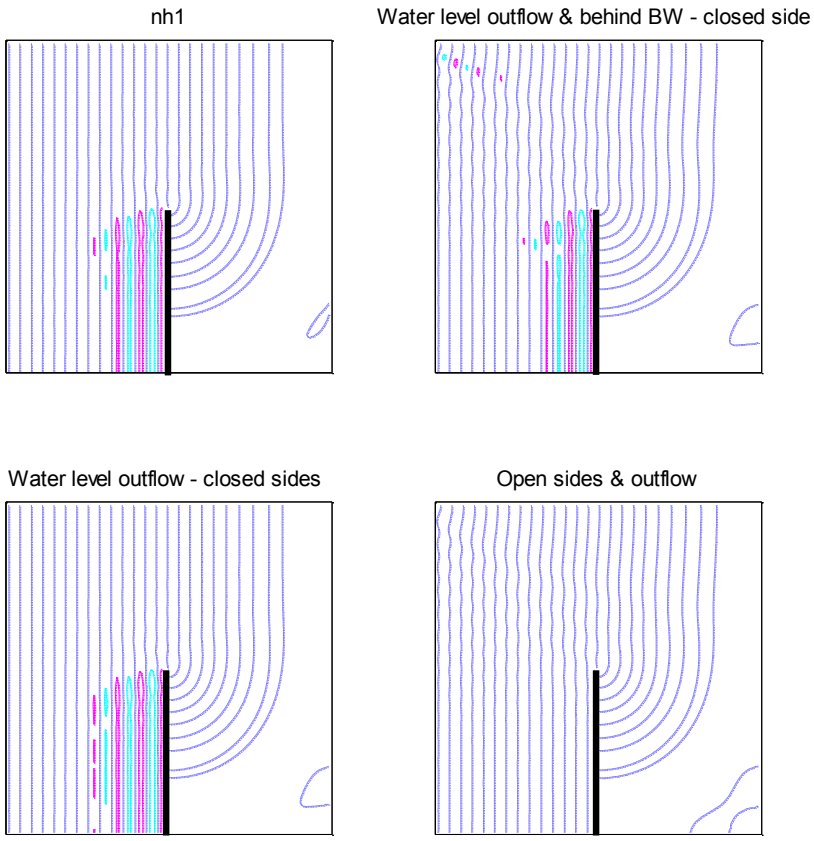

Figure B.7 Surface elevations at 2:01 minutes with water level boundaries.

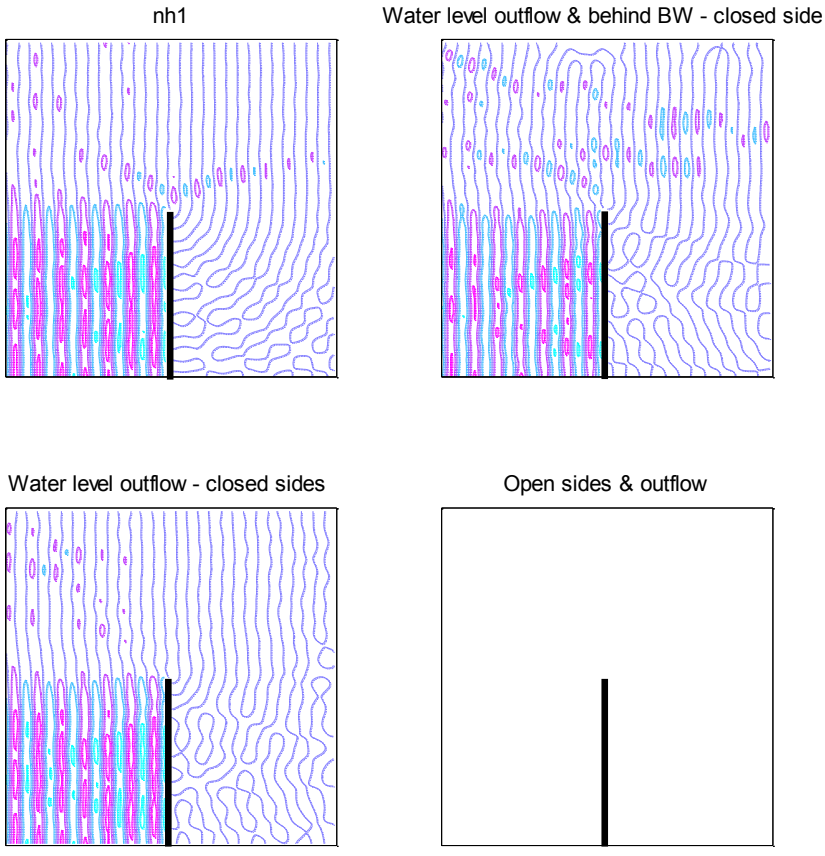

Figure B.8 Surface elevations at 7:32 minutes with water level boundaries.

Water level boundaries

For a complete comparison, of all the easily implemented boundary conditions, the water level boundary is inspected as well. It is referred to as water level boundary, since the derivation is based on long waves. See Figure B.7 andFigure B.8.
As with the Riemann boundaries a small wave is seen behind the breakwater and at the boundary in front of the wave train during the initial phase of the simulation (Figure B.7). With an open northern side the wave train seems to be a bit more anxious, but does not seem to have a large error influence (yet).
When the wave field is fully developed, again errors occur in the diffraction pattern (Figure B.8). This error is most likely the reason for the surface elevation patterns at the upper part of the simulation in with one open side.
Note that the simulation with three open boundaries has a blank field after 7 minutes and 32 seconds. This simulation became unstable after 5 minutes and 7 seconds. It stopped its simulation.

Discussion

Three types of boundary conditions have been compared. The selection of a boundary condition has influence on the diffraction pattern behind the semi – infinite breakwater and the wave propagation along the upper part of the simulation.

The water level boundary is not able to accurately simulate diffraction. The surface elevations which are free of the propagating wave at 2 minutes (Figure B.7) are presumed to be the result of reflection. The use of multiple water level boundaries behind the breakwater leads to instability of the simulation.
An open northern water level boundary with a wave velocity under a high angle of incidence does not seem to have an influence near the boundary.

The velocity boundary condition is slightly better at predicting the diffraction pattern behind the breakwater then the water level boundary. Since there is no visible difference between the closed and open velocity boundaries in that respect (Figure B.6), the use of a velocity outflow seems to be the cause.
Not only does the velocity outflow influence the diffraction behavior, it affects the wave heights for the passing wave (upper part of the each simulation in Figure B.6) as well. Opening the side boundaries does not seem to affect it.

The Riemann boundary performs best with respect to the diffraction pattern. By opening up the southern boundary behind the breakwater with a second Riemann condition, the pattern increases in predicted accuracy.
The use of an open northern Riemann boundary leads to some outflow; the wave slightly bends towards the boundary.

Wave specifications		**Geometry specifications**	
$T = 8$ seconds		$depth = 10$ meter	
$L = 71$ meter	$kh = 0.88$	$length = 1000$ meter	
$a = 0.25$ meter	$ka = 0.02$	$width = 1000$ meter	$\Delta x = 5$ m

Table B-1 Numerical values used for each model.

Appendix C: Harbour simulation extra's

Riemann and sponge layer

Simple calculation of differences in percentages

This part describes how the percentage differences have been quantified. It will use the red dot from figure 5.1 as single point of reference. Its averaged amplitudes are taken. This gives an estimate of the energy level.

The next ζ values are averaged values taken from figure 5.2 and 5.6 and are taken by visual observation. Here the percentage differences are calculated by sponge layer values over Riemann values. The relationship between percentile differences of the surface elevation amplitudes (Δâ) and percentage of energy difference (ΔE) is in the order of $E \sim f(a^2)$

fig 5.2 - Riemann	**measured**			**calculated**	
(in meters)	*ζmax*	*mean*	*ζ min*	*H*	*â*
NH	0.15	0	-0.17	0.32	0.16
Hyd	0.19	0.002	-0.17	0.36	0.18

fig 5.6 - Sponge	**measured**			**calculated**	
(in meters)	*ζmax*	*mean*	*ζmin*	*H*	*â*
NH	0.09	0	-0.09	0.18	0.09
Hyd	0.08	0.01	-0.07	0.15	0.075

Percentile differences between Riemann and Sponge		
	Δâ	*ΔE*
NH	56%	32%
Hyd	42%	17%

$$\Delta\hat{a} = \frac{\hat{a}_{Riemann}}{\hat{a}_{sponge}}$$

$$\Delta E \simeq \Delta\hat{a}^2$$

Table C-1 Wave heights quantified from figures 5.2, 5.6 and its resulting energy levels

With these simple quantifications of energy differences and the averaged energy levels from figures 5.5 and 5.9 a quick verification is possible. Generally speaking the non – hydrostatic method leads to higher energy levels. Reason behind this is described in chapter 5.

fig 5.5 & 5.9 – Total averaged energy in the basin			
	Riemann	*Sponge*	*ΔE*
NH	4.70E+05	1.50E+05	32%
Hyd	2.90E+05	7.40E+04	26%

Table C-2 Energy levels quantified from figures 5.5, 5.9 and comparison of the energy levels

From this comparison of energy differences, it becomes obvious that the energy difference between sponge layer and Riemann conditions for the non – hydrostatic method match. However, they don't for the hydrostatic simulation.

Responsiveness of the sponge layer

The contour plots from figure 5.7 and 5.8 which are shown in chapter 5, are capped. At the upper boundary the sponge layer starts. Its internal response is shown in the next set of figures. Figure C.1 corresponds with the same time frame as figure 5.7 in chapter 5. Respectively Figure C.2 corresponds with figure 5.8.

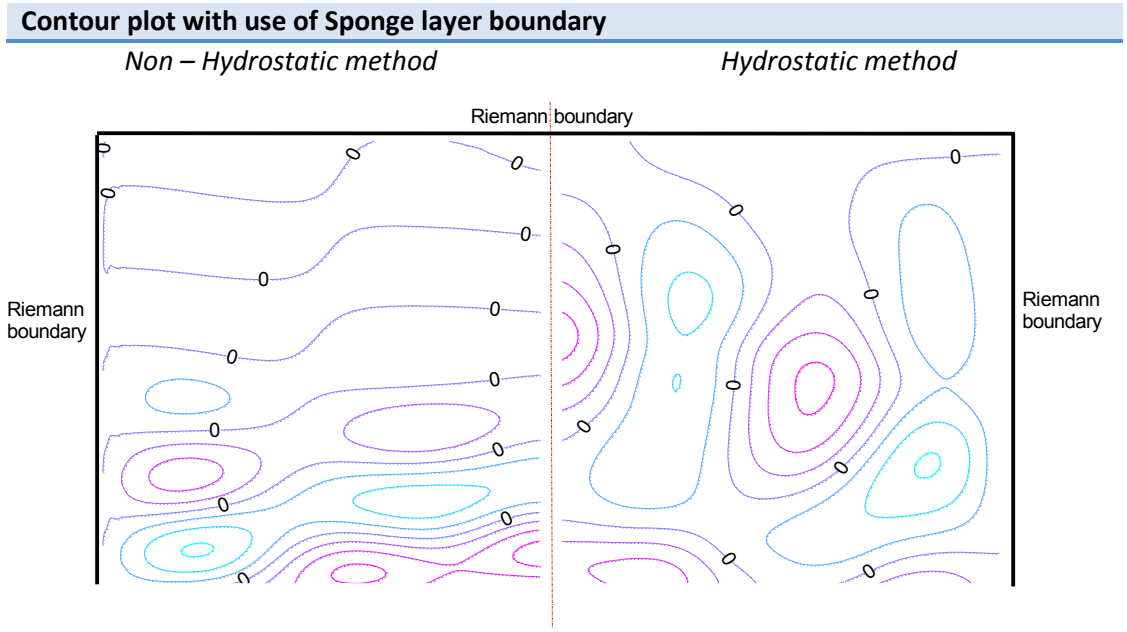

Figure C.1 Contour plot of the surface elevations at $t = 250$ seconds in the sponge layer boundary

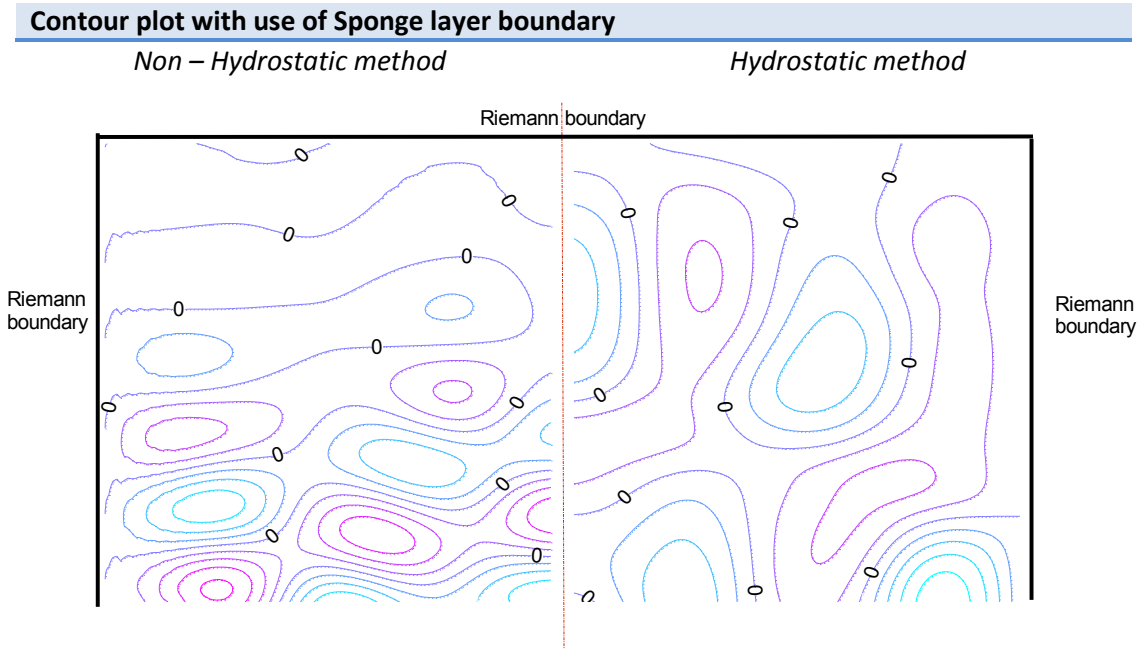

Figure C.2 Contour plot of the surface elevations at $t = 400$ seconds in the sponge layer boundary

Both figures give a good indication of the effectiveness of a sponge layer for hydrostatic and non-hydrostatic methods. In chapter 3, figure 3.1 shows the strength of the dimensionless coefficient κ. The hydrostatic method shows dampening best in figure C-2. In the center of the plot, a top seems to be missing. The wave pattern is not really affected.
The sponge was implemented for dampening with the non-hydrostatic method. This clearly shows. Halfway the surface elevations suddenly dampen. It is noted that the surface elevations disappear, with amplitudes that do not increase. This is exactly at the spot where the dimensionless coefficient κ is at its highest.

A last remark is on the wave and the angle of incidence. In chapter 3 it is stated that the sponge layer only dampens in either u or v direction. In this case it only dampens in u-direction. These simulations are not extreme test cases and keep in line with the premises of nearly perpendicular incoming waves. The dependency on the angle of incidence has not been further investigated by means of tests.

Because the dampening is done in the impulse balance equation and affects the velocity u and v, below a quiver plot with the normalized velocity direction is shown at the end of the simulation.

Contour plot with use of Sponge layer boundary

Non – Hydrostatic method *Hydrostatic method*

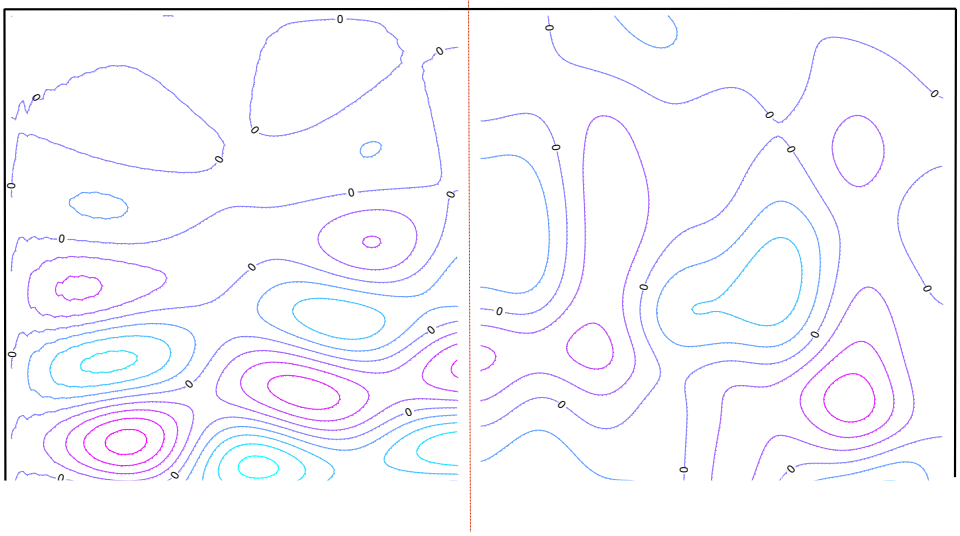

Figure C.3 Contour plot of the surface elevations at the last time step

Quiver plot of the velocities inside the sponge layer

Non – Hydrostatic method *Hydrostatic method*

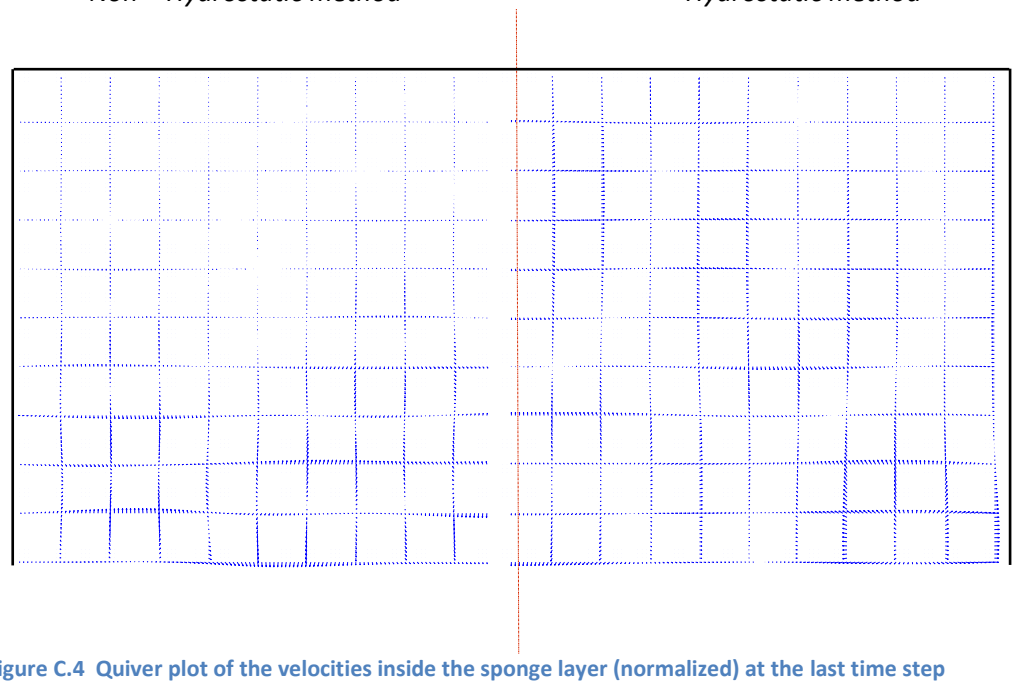

Figure C.4 Quiver plot of the velocities inside the sponge layer (normalized) at the last time step

Oscillation periods

The full reflective case in chapter 5 shows increasing amplitudes. The origin behind this increase lies in harbour basin oscillations. The driving force behind harbour oscillations is the incoming wave. Its main restoring force is wave radiation into the outer basin.
The oscillatory periods depend on basin geometry. A formulation for these periods can be found in (Rabinovich, 2009) and is given by;

$$T_n = \frac{4L_b}{(2n+1)\sqrt{gd}} \qquad n = 0,1,2,\ldots \qquad \text{Eq. C-1}$$

Where the basin length or width is L_b, g is the gravitational acceleration, d is the basin depth and n is the order of the oscillatory period. In Table C-3 the first 10 fundamental periods are shown.

Periods of harbour oscillations (in seconds)										
n	0	1	2	3	4	5	6	7	8	9
T_n	85.67	28.56	17.13	12.24	9.52	7.79	6.59	5.71	5.04	4.51

Table C-3 Modes of oscillation periods

On a side note, the zeroth order is often referred to as the Helmholtz mode or pumping mode.
The 7th order period is the almost spot on the period of the wave forcing used in the model. Due to the selection criterion of hydrostatic versus non – hydrostatic, the model results in chapter 5 are bound to give different results. However, from this table it is concluded that the non – hydrostatic method yields more realistic results. Since oscillations should in fact occur.

Appendix D: Terneuzen Harbour

This appendix will show the use of the non-hydrostatic method for a real case; Terneuzen harbour. It is derived from the(Koop, et al., 2007). The aim of this appendix is to produce a small showcase of the current capabilities of TRIWAQ-NH for an existing harbour.
The original intent of (Koop, et al., 2007) was to check whether diffraction plays a role for the Terneuzen harbour. It was tested by comparing calculations made by the model SWAN with calculations with the model PHAROS for one wave condition.

Boundary conditions

Inflow conditions

The parameters used at the inflowing boundary condition are;

Parameter	Value
H_{mo}	$2.38\ meter$
T_p	$7.15\ seconds$
Main wave direction	$325^0 N$
Depth	$20\ meters$
L	$80\ meters$
kd	1.69
ka	0.1

Table D-1 Parameters for the wave forcing

The depth corresponds with the PHAROS conditions in the appendix Diffraction in Terneuzen harbour figure 2.2, bathymetry used in PHAROS computations.

From table D-1 the kd-value is high enough, according to chapter 3, to select a non-hydrostatic model.

Reflection coefficients

The TRIWAQ model is kept in line with the PHAROS simulation and it's intend. All reflection coefficients are set to zero, since the original purpose of the study was to isolate effects of diffraction in the basin for comparison with the SWAN model. A second reason was the treatment of wave energy that differs between those two models.
Additionally, TRIWAQ currently implements reflection in models by flagging a border as open boundary. Open boundaries can only be implemented on the edges of grid cells. This is a more advanced geometry then the rectangular harbour basin described in chapter 5. Thus, the original intent of the simulations in (Koop, et al., 2007) do not impose restrictions in that respect.

Physical and numerical processes

In PHAROS the following settings were used to discard some physical phenomena. This is done in the model TRIWAQ aswell;

- Bottom dissipation is not included;
- Wave breaking is not included;
- Reflection of obstacles was set to zero in PHAROS; TRIWAQ has removed the obstacles;
- Refraction effects were removed thanks to a flat bottom.

Computation grid

The computational grid is a simple rectangular grid, with a grid size of 2.5 meters. The border of the harbour is created by manually drawing over the edges from the aforementioned figure 2.2 in (Koop, et al., 2007), see Figure D.1.
The rectangular grid for TRIWAQ-NH is rotated, in order to satisfy the need that an incoming wave is perpendicular to grid edges, since it is not possible to impose a wave forcing under an angle of incidence.

The difference between grid setups between PHAROS and TRIWAQ is that it was created with ACE/gredit (Oregon Graduate Institute, 1993) and is a triangular grid versus a manually created rectangular grid.

The red crosses in Figure D.1 are output locations of wave heights in PHAROS and SWAN. These are found in table 2.2 and 3.3 respectively from the appendix of (Koop, et al., 2007).

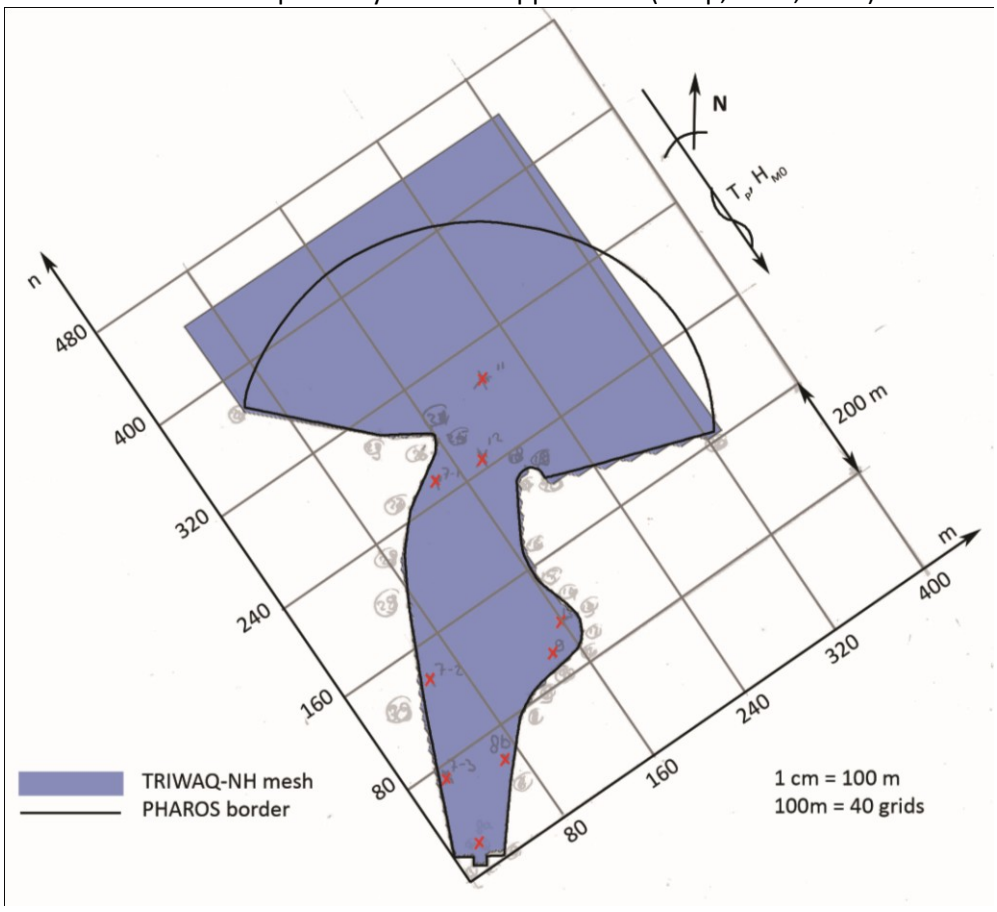

Figure D.1 Creation of TRIWAQ-NH grid for Terneuzen harbour

Multiple simulation settings for TRIWAQ

The oval like boundary is not created for TRIWAQ as can be seen in Figure D.1. The borders at the sides of the foreland are altered for the non-hydrostatic simulation.

In total there are four simulations (1) a hydrostatic simulation; (2) a non-hydrostatic simulation with a Riemann boundary condition at $m = 322$; (3) a non-hydrostatic simulation with Riemann boundaries at $m = 61$ and $m = 322$; and (4) a non-hydrostatic simulation with a sponge layer that starts at $m = 322$ which extends the grid in the m-direction to 597 grids, again corresponding to 3 wave lengths.

Results

For all 4 simulations, fits of the energy levels are shown in Figure D.2 additionally a surface elevation plots are shown in figure D.3, D.4, D.5 and D.6. The PHAROS and SWAN wave heights are taken from table 2.2 and 3.3 in (Koop, et al., 2007) and shown in the first two columns of Table D-2. Accordingly the four simulation settings are shown. The locations can be found in figure D.1.

The wave height values in the table below are acquired by generating a cumulative sinus fit with five signals. The average height from that fit is selected by manual observation.

Output location	Wave height values [m]					
	PHAROS	SWAN	Hyd	NH Riemann	NH Riem2	NH sponge
7-1	0.67	0.42	0.9	1.4	0.9	1.0
7-2	0.77	0.75	1.1	3.0	2.1	1.2
7-3	0.69	0.78	0.8	0.9	0.8	0.9
8A	0.66	1.00	0.5	2.4	4.0	1.0
8b	0.76	1.00	0.7	1.0	1.9	0.7
9	0.73	0.93	1.2	1.2	1.6	0.9
11	2.43	2.40	2.1	0.7	2.3	2.4
12	2.18	2.27	2.1	2.1	2.2	3.2
13	0.53	0.53	0.7	1.2	0.9	0.6

Table D-2 Surface elevations for multiple simulations in TRIWAQ-NH compared with Pharos and SWAN

The results in Table D-2 show a good comparison between the model PHAROS and the hydrostatic method in the model TRIWAQ.
The non-hydrostatic method for the model TRIWAQ shows a few interesting results. Both simulations using one or two Riemann boundaries show elevated wave heights at point 7-2, 8A and 13. The last two points are the more exposed spots of the harbour for the incoming waves. The first point is likely to be due to reflection.
The non-hydrostatic simulation with the sponge layer shows a comparable result to the hydrostatic simulation.

The energy fit shown in Figure D.2 needs some explanation. In general, the simulations seem stable. These fits are averaged exponential fits of the instantaneous surface elevations. It again shows similar results as the results from chapter 5, where the energy levels for the hydrostatic method are lower than the energy levels for the non-hydrostatic method.
It is important to note the energy level for the sponge layer. This fit is completely different. This has two causes. First of all, this is the only simulation that was run for 16 minutes instead of 12; where 12 minutes correspond to time step 999 and minute 16 to time step 1399.
Due to the current inability of the post processing program for TRIWAQ to create more than 999 Matlab files, the selection criterion changed a bit. The last 999 frames were chosen. Thus for the sponge this means, values for time step 401 (4^{th} minute) to 1400 (16^{th} minute) are know. For all the other simulations the surface elevations of the 0^{th} to 12^{th} minute have output.
Overall, this means the energy fit of the non-hydrostatic simulation with use of a sponge layer should be discarded, since it does not have the first four minutes of data which highly affects the exponential fit. To further substantiate this believe, it is noted that in chapter 5 energy levels of sponge layer simulations all have a elevated energy level first. Then slightly drops to become a constant, which is the reason for the drop of the energy level in Figure D.2. Lastly, in chapter 5 the exponential fit for the sponge layer simulation was not used.

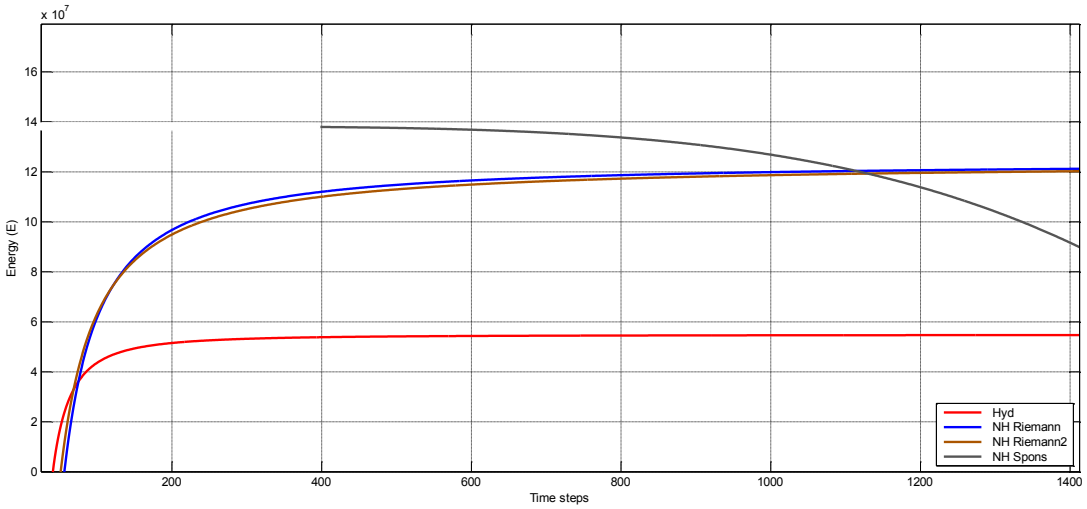

Figure D.2 Energy levels for the TRIWAQ simulations

On the next few pages figures of the surface elevations for the TRIWAQ simulations are shown for the last possible time step.

This gives definite proof of the fact that of the currently implemented open boundary conditions, non work well and the sponge layer boundary works best for non-hydrostatic simulations.
However, as there is often an outer and inner basin for these harbour models, it seems good practice to refine the above conclusion somewhat for the non-hydrostatic simulations.

The open boundaries at the outer basin are underperforming. Where the hydrostatic method seems to produce clear results and shows effects of diffraction very well. This is not the case for the non-hydrostatic method. It followed from Appendix B that it is known TRIWAQ-NH is able to account for such a physical process. Depending the out flowing boundary used. Thus this is a pure failure of the outflow boundary condition not working properly. In appendix B, the effect of such a failure was seen best in figure B.6 and B.8. The effect shown there is also seen here, figures D.4, D5 and D.6 on a wider scale.
The inner basin is of course affected by such failure at the outer basin. Its hydrostatic wave pattern in figure D.3 however is a bit choppy. When the wave pattern of the non-hydrostatic simulation with the sponge layer is inspected in figure D.6, it shows a likely pattern development. In that respect it is too bad the other two non-hydrostatic simulations are only 12 minutes long.

There is one last factor that needs to be reflected upon; the size of the harbour entrance. In these simulations, it is as wide as the basin width. In chapter 5 this is harbour mouth is the size of one wave length, both being two extremes.
So, although the failing of the open boundary conditions at the outer basin influence the conditions at the inner basin here for the Terneuzen harbour, that influence is negligible in chapter 5.

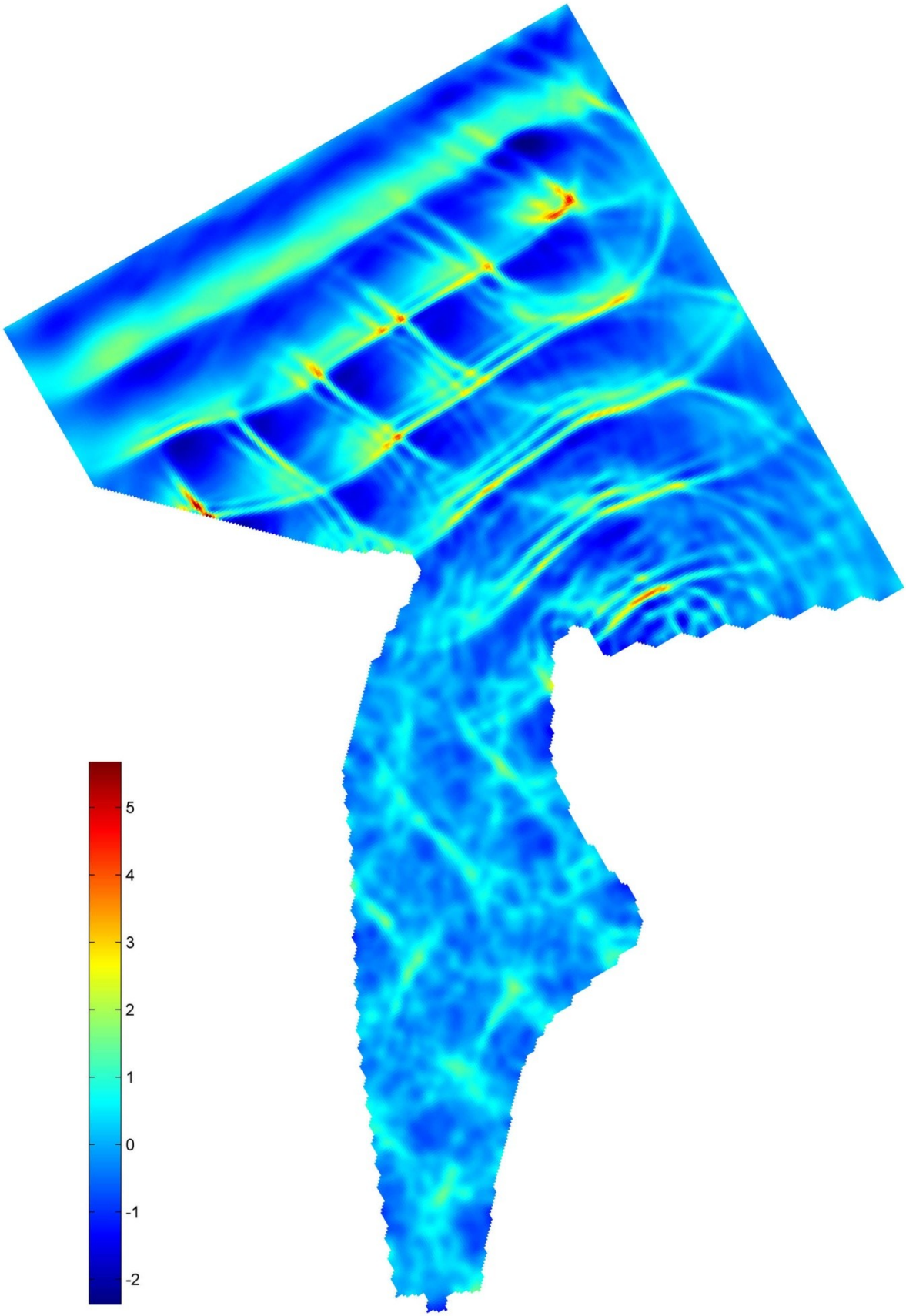

Figure D.3 Surface elevations after 12 minutes for the hydrostatic simulations in TRIWAQ

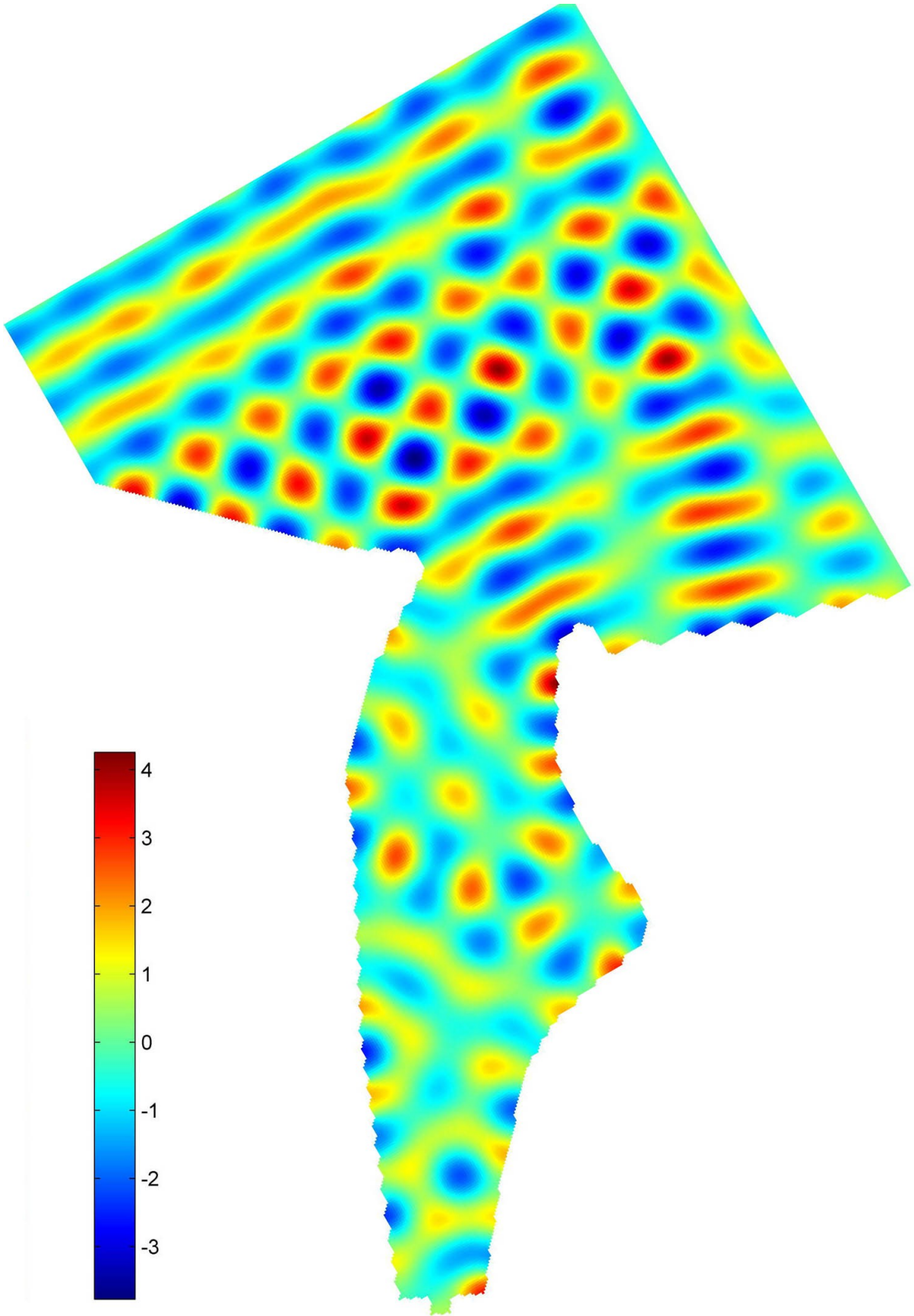

Figure D. 4 Surface elevations after 12 minutes for the non-hydrostatic simulations in TRIWAQ with a Riemann boundary at the right side

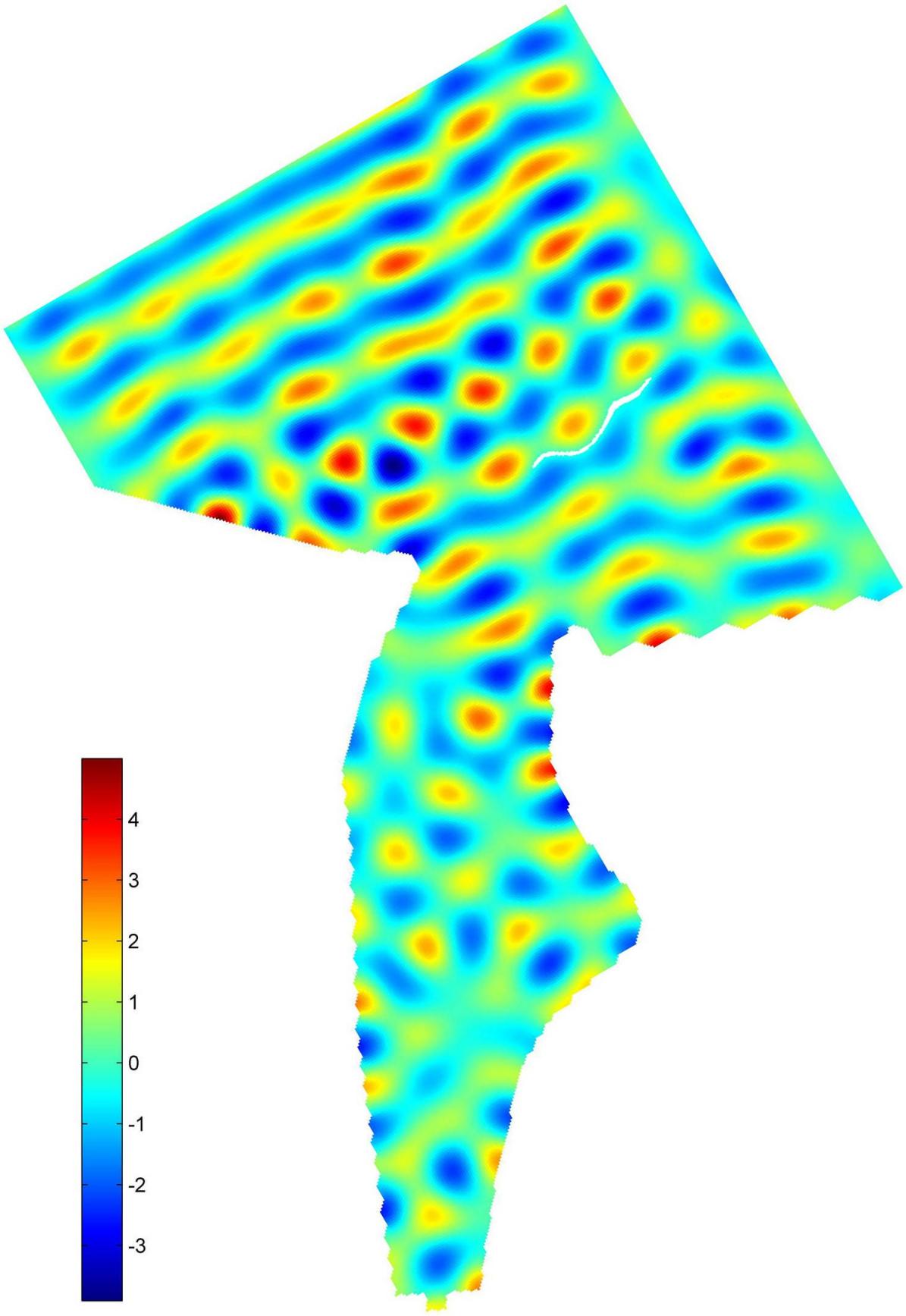

Figure D. 5 Surface elevations after 12 minutes for the non-hydrostatic simulations in TRIWAQ with a Riemann boundary at the right side and left side

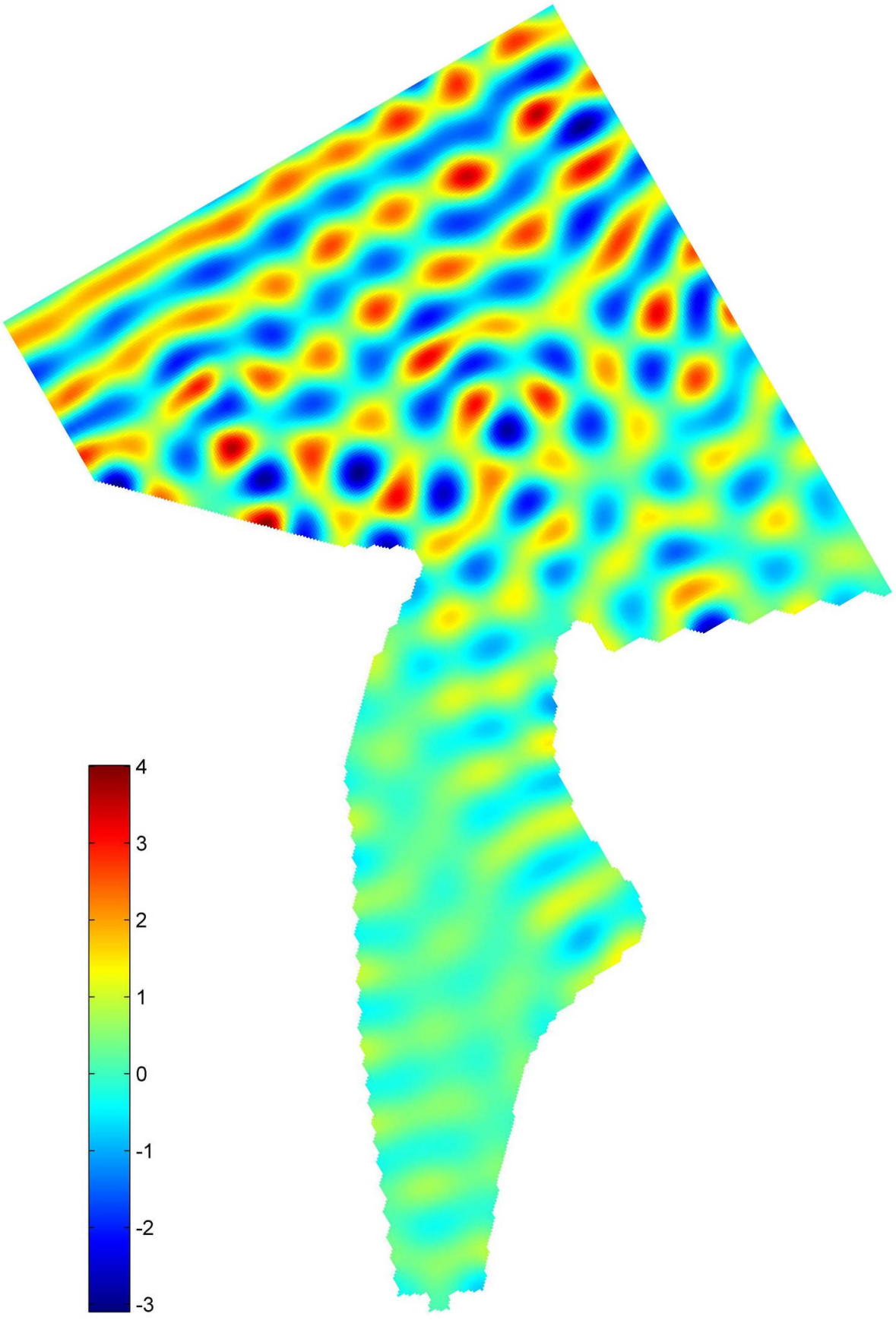

Figure D. 6 Surface elevations after 16 minutes for the non-hydrostatic simulations in TRIWAQ with a sponge layer boundary at the right side